UNIVERSITÀ DEGLI STUDI DI TRIESTE

XXVIII CICLO DEL DOTTORATO DI RICERCA IN

NEUROSCIENZE E SCIENZE COGNITIVE
-INDIRIZZO NEUROBIOLOGIA-

DENDRITIC TRAFFICKING OF BRAIN-DERIVED NEUROTROPHIC FACTOR mRNA AND NEURONAL ATROPHY

Settore scientifico-disciplinare: Scienze Biologiche
BIO/06 ANATOMIA COMPARATA E CITOLOGIA

DOTTORANDO
ANDREA COLLIVA

COORDINATORE
PROF. WALTER GERBINO

SUPERVISORE DI TESI
PROF. ENRICO TONGIORGI

ANNO ACCADEMICO 2014 / 2015

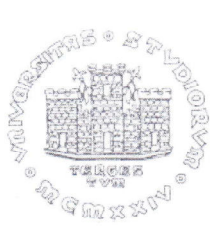

UNIVERSITÀ' DEGLI STUDI DI TRIESTE

XXVIII CICLO DEL DOTTORATO DI RICERCA IN

NEUROSCIENZE E SCIENZE COGNITIVE
-INDIRIZZO NEUROBIOLOGIA-

DENDRITIC TRAFFICKING OF BRAIN-DERIVED NEUROTROPHIC FACTOR mRNA AND NEURONAL ATROPHY

Settore scientifico-disciplinare: Scienze Biologiche
BIO/06 ANATOMIA COMPARATA E CITOLOGIA

DOTTORANDO
ANDREA COLLIVA

COORDINATORE
PROF. WALTER GERBINO

SUPERVISORE DI TESI
PROF. ENRICO TONGIORGI

ANNO ACCADEMICO 2014 / 2015

INDEX

RIASSUNTO

Il trasporto e la traduzione nei dendriti di specifici trascritti è un meccanismo alla base di processi quali plasticità sinaptica, rimodellamento delle spine e sviluppo neuronale. E' stato dimostrato che l'mRNA del fattore neurotrofico cerebrale (BDNF) è trasportato nei dendriti in seguito a stimolazione neuronale. Il BDNF ha una struttura genica molto complessa nei roditori, con undici varianti di splicing nella regione non tradotta al 5' (5'UTR) che si saldano alternativamente ad una sequenza codificante (CDS) comune che contiene due siti di poliadenilazione diversi che danno luogo a due isoforme nella regione non tradotta al 3' (3'UTR). Queste varianti hanno una distribuzione spaziale diversa nei neuroni, permettendo una fine regolazione della loro espressione. La CDS di BDNF codifica per un segnale di trasporto dendritico costitutivo riconosciuto dalla proteina legante l'RNA (RBP) Translin. Inoltre i diversi esoni al 5'UTR agiscono come segnali per la ritenzione nel soma oppure sono permissivi per il trasporto nei dendriti del mRNA. Le isoforme 3'UTR regolano il trasporto dei trascritti in risposta ad attivazione neuronale.

In questo studio abbiamo approfondito i meccanismi del trasporto dell'mRNA di BDNF e nello specifico è stata analizzata la capacità delle sequenze al 5'UTR di modificare il trasporto dell'mRNA della proteina fluorescente verde (GFP) espressa come gene reporter in neuroni di ratto. Solo tre (esone 2a, 2b e 2c) delle undici varianti sono state in grado di promuovere in modo costitutivo il trasporto di questo mRNA, mentre i restanti trascritti sono risultati ininfluenti in quanto hanno mostrato una distribuzione simile a quella della sequenza GFP. L'analisi bioinformatica delle sequenze degli esoni 2 ha evidenziato ipotetici siti di legame per ELAV-like proteins (ELAVLs) e Pumilio-2, delle RBP coinvolte nel traffico e nella stabilità di mRNA. Successivamente abbiamo caratterizzato l'interazione tra i due 3'UTR dell'mRNA di BDNF e tre diverse famiglie di RBPs coinvolte nel traffico degli mRNA neuronali: le proteine leganti l'elemento citoplasmatico di poliadenilazione (CPEBs), le ELAV-like proteins (ELAVLs) e le proteine dell' X-fragile. L'interazione tra esse e l'mRNA di BDNF è stata dimostrata attraverso esperimenti di cross-linking ed immunoprecipitazione su lisati di tessuto cerebrale. Inoltre abbiamo caratterizzato il grado di colocalizzazione *in vitro* tra le diverse RBPs e l'mRNA di BDNF visualizzate attraverso ibridazione *in situ* fluorescente e immunofluorescenza. Questo studio ha

confermato l'associazione delle diverse RBPs ai trascritti di BDNF, evidenziando un profilo di colocalizzazione eterogeneo per le diverse proteine delle tre famiglie di RBPs analizzate.

L'espressione di BDNF è alterata nella sindrome di Rett (RTT), una sindrome del neurosviluppo causata ad una mutazione sul cromosoma X del gene *MECP2* che colpisce 1 femmina ogni 10.000 nate. Dato che BDNF è coinvolto nello sviluppo e nel mantenimento dei dendriti e delle loro spine, abbiamo ipotizzato che nella RTT vi potesse essere una possibile alterazione della regolazione di questo mRNA. Per questo motivo, abbiamo analizzato la distribuzione del RNA messaggero del BDNF nei dendriti apicali di neuroni ippocampali di un modello murino della RTT (topo MeCP2$^{-/y}$). L'RNA messaggero del *BDNF* è meno abbondante nei dendriti dei neuroni MeCP2$^{-/y}$ sia condizioni basali che dopo stimolazione neurotrofica con BDNF e NT3.

Ipotizzando nel meccanismo patogenetico della RTT un'alterazione dei livelli di RBP abbiamo voluto verificare la presenza di difetti nell'equilibrio dei granuli ribonucleoproteici (RNP). Servendoci di colture neuronali primarie ottenute dal topo MeCP2$^{-/y}$ abbiamo analizzato la distribuzione, l'espressione e la dimensione di tre classi di RNP: i granuli di trasporto (GT), i granuli di stress (GS) e i processing bodies (PB), scegliendo come marcatori di questi granuli rispettivamente le proteine Staufen1, TIA-1 e Dcp1a. I livelli proteici totali dei tre marcatori sono risultati pressoché inalterati in lisati proteici di colture ippocampali di animali sani (WT) o mutati. Tuttavia i livelli di Dcp1a lungo i dendriti apicali dei neuroni MeCP2$^{-/y}$ sono risultati inferiori. Successivamente abbiamo caratterizzato la dimensione e l'intensità dei diversi granuli identificati dai tre marcatori in immunofluorecenza in dendriti apicali di neuroni ippocampali MeCP2$^{-/y}$. I PB sono risultati di uguali dimensioni ma meno densi nel loro contenuto di Dcp1a, confermando i risultati della precedente analisi. Inoltre la stimolazione con BDNF ha indotto una diminuzione della densità dei PB nei neuroni WT ma non in quelli MeCP2$^{-/y}$. I TG e i granuli positivi per TIA-1 sono risultati simili nei neuroni MeCP2$^{-/y}$ rispetto a quelli dei neuroni WT in assenza di stimoli o dopo stimolazione neurotrofica. Diversamente, gli SG assemblati in risposta a stress ossidativo nei dendriti di neuroni MeCP2$^{-/y}$ sono risultati di dimensioni maggiori rispetto a quelli del WT, mentre i TG MeCP2$^{-/y}$ sono risultati meno densi, suggerendo un alterato rimodellamento di questi granuli nel modello MeCP2$^{-/y}$. Ulteriori analisi hanno confermato che il livello di interazione tra TG e SG risulta esacerbato in seguito a stresso ossidativo in neuroni MeCP2$^{-/y}$, mentre l'interazione

tra PB e SG risulta pressoché inalterata. Infine abbiamo valutato se vi fosse un'alterata associazione dell'mRNA di *BDNF* con SG e PB che potesse giustificare i bassi livelli di questo trascritto nei dendriti. L'RNA messaggero di *BDNF* è risultato debolmente associato ai due tipi di RNP, anche se il pattern di colocalizzazione di questo trascritto con SG e PB è risultato alterato in neuroni MeCP2$^{-/y}$. Le diverse alterazioni dendritiche riguardati l'RNA messaggero di *BDNF* e i diversi tipi di granulo presi in esame lasciano supporre che un'alterata omeostasi delle particelle ribonucleoproteiche possa essere alla base dell'atrofia neuronale nella RTT.

Infine abbiamo tentato di recuperare il fenotipo atrofico nei neuroni RTT attraverso un trattamento farmacologico con Mirtazapina, un antidepressivo in grado di aumentare i livelli di BDNF nel ratto e che è stato recentemente dimostrato essere in grado di recuperare deficit morfologici nel cervello di topi RTT. Attraverso l'utilizzo di un modello per lo studio *in vitro* dello sviluppo neuronale abbiamo trattato i neuroni ippocampali di topo MeCP2$^{-/y}$ con Mirtazapina in maniera cronica (9 giorni) o acuta (3 giorni), andando in seguito a misurare la complessità dell'arborizzazione dendritica. Il trattamento cronico permette un recupero totale dei deficit nei neuroni MeCP2$^{-/y}$ concernente sia la lunghezza totale che le ramificazioni dei dendriti. Diversamente il trattamento più breve si è dimostrato solo parzialmente efficace, con un recupero della lunghezza totale ma non della complessità delle ramificazioni. In futuro questo modello potrebbe risultare utile per lo studio dei meccanismi molecolari alla base dell'atrofia neuronale e di possibili terapie farmacologiche per il suo recupero nella RTT.

ABSTRACT

Trafficking and local translation in neuronal dendrites of selected transcripts is a mechanism underlying synaptic plasticity, spine remodeling and neuronal development. It was previously demonstrated that *brain-derived neurotrophic factor* (*BDNF*) mRNA is targeted to dendrites in an activity dependent manner. BDNF has a complex gene structure that in rodents, gives rise to eleven different variants in the 5' untranslated region (5' UTRs) which are alternatively spliced to a common coding region (CDS) having either a short or long 3'UTR region due to the presence of two different polyadenylation sites. BDNF variants have a different spatial distribution in neurons, allowing a fine regulation of BDNF expression. It was previously shown that BDNF CDS encodes a constitutive dendritic targeting signal recognized by the RNA binding protein (RBP) Translin. Moreover, different exons could act as signals for soma retention or are permissive for dendritic targeting of BDNF mRNA. The two 3'UTRs regulates the activity-dependent targeting of BDNF transcripts.

In this study, we investigated the mechanisms underlying the BDNF mRNA trafficking under normal conditions and in a disease characterized by neuronal atrophy: the Rett syndrome. In particular, we analyzed if the different 5'UTRs sequences were able to modify the cell sorting of the reporter Green Fluorescent Protein (GFP) mRNA expressed in transfected hippocampal rat neurons *in vitro.* We found that only exon2 variants (exon2a, b and c) can actively promote a constitutive dendritic targeting, while all other variants are uninfluential and displayed a distribution similar to GFP mRNA reporter alone both in basal or stimulated conditions. Bioinformatic analysis of exon2 5'UTR sequences revealed putative binding sites for Embryonic Lethal Abnormal Vision-like proteins (ELAVLs) and Pumilio-2 RBP which may be potentially involved in mRNA trafficking and stability.

Then, we focused our attention on the characterization of the RBP families required for BDNF 3'UTR activity-dependent targeting. In particular, we investigated the interaction between endogenous BDNF mRNA and the cytoplasmic polyadenylation element binding proteins (CPEBs), the Embryonic Lethal Abnormal Vision-like proteins (ELAVLs) and the Fragile-X Mental Retardation Protein (FMRP). Physical interactions between these RBPs protein families and the 3'UTR of BDNF mRNA were verified by Cross Linking Immunoprecipitation (CL-IP) assays on brain lysates. Moreover, we assessed the grade of colocalization *in vitro* by fluorescent *in situ*

hybridization for endogenous BDNF mRNA coupled to immunofluorescence for the different RBPs families. This study confirms the association of these proteins to BDNF transcripts highlighting a heterogeneous level of colocalization with the different RBPs investigated.

BDNF expression is altered in Rett syndrome (RTT), an X-linked neurodevelopmental disorder affecting 1:10.000 females. RTT neurons display general neuronal atrophy, with reduced dendritic arborization and spinogenesis. Since BDNF is required for dendrites and spine development and maintenance, we investigated the regulation of BDNF mRNA in RTT. We found that *BDNF* mRNA distribution in apical dendrites of cultured hippocampal neurons of MeCP2$^{-/y}$ mice is altered, suggesting that an alteration in RBPs regulating mRNA homeostasis might be involved. Accordingly, we investigated if a dysregulation in ribonucleoprotein particles (RNPs) was involved in the altered BDNF distribution in RTT neurons. To this aim, using primary neuronal cultures from MeCP2$^{-/y}$ mice, we analyzed the *in vitro* distribution of three classes of RNP: transporting granules (TG), stress granules (SG) and processing bodies (PB). Staufen1, Tia-1 and DCP1a were chosen as specific markers to describe RNP distribution, dimension and labeling intensity.

We found no significant alteration in the total protein level in lysates of hippocampal cultured neurons. However a deficit of Dcp1a along dendrites was detected. Then, we characterized RNPs in MeCP2$^{-/y}$ neurons upon neurotrophic stimulation or during oxidative stress induced by sodium arsenite. Dcp1a processing bodies resulted less dense in their protein composition with respect to wild type. Moreover, BDNF stimulation did not induce disassembly of PB as occurs in wild type neurons. TG and TIA-1 granules displayed similar intensity and dimensions at basal levels or after neurotrophic stimulation. However, MeCP2$^{-/y}$ neurons nucleate larger SG and less dense TG upon oxidative stress, suggesting an altered RNP remodeling. Exacerbated docking of TG on SG during stress of MePC2$^{-/y}$ neurons confirmed this hypothesis, while TG and P-bodies showed normal interaction levels. Finally, we assessed if an altered association of *BDNF* mRNA with SG or PB could be the mechanism behind the decreased *BDNF* mRNA levels in MeCP2$^{-/y}$ neurons. We found a poor association of this transcript with SG and PB. However, the pattern of colocalization with PB was significantly different in MeCP2$^{-/y}$ neurons as compared to wild type neuronal dendrites, suggesting an improper *BDNF* mRNA turnover in this compartment. The observed alterations in the composition of the granules in MeCP2^{-}

$^{/y}$ cultured neurons suggest that an altered BDNF mRNA homeostasis could be involved in the mechanisms of neuronal atrophy in RTT.

Finally, we tried to rescue neuronal atrophy *in vitro* by treating cultured neurons with Mirtazapine, an antidepressant that is known to increase BDNF levels in rats and that was recently demonstrated to rescue neuronal atrophy in the brain of RTT mouse. Using a well characterized *in vitro* staging for the study of neuronal atrophy we treated MeCP2$^{-/y}$ cultured neurons with Mirtazapine chronically (9 days) or acutely (3 days) and we evaluated if a rescue of dendritic arborization occurred. We found that dendritic atrophy of RTT neurons was fully rescued after chronic treatment with Mirtazapine, while shorter treatment resulted in a partial rescue of the dendritic complexity. Further studies using this model could be helpful to discover the molecular mechanisms underlying RTT neuronal atrophy and its morphological rescue by mirtazapine.

INTRODUCTION

1. mRNA trafficking and local protein synthesis in dendrites

1.1 Localization of mRNA in cellular compartments

Localization of mRNA in different cellular compartments is an highly evolutionary conserved mechanisms present in different organisms and cell types. Sorting and local translation of mRNA allow cells to optimize gene expression of specific transcripts where massive quantity or gradient of target protein is needed (Martin and Ephrussi, 2009). Best characterized mRNAs that are asymmetrically distributed in the cells encode for proteins that exert their function in a spatial dependent manner. *Ash1* mRNA in budding *Saccharomyces cerevisiae* is selectively sorted into cortex daughter cell during late anaphase to allow mating type switching (Long et al., 1997). During embryogenesis of *Drosophila Melanogaster* specific gradient of morphogens are achieved by the localization to the anterior pole of *bicoid* mRNA and to the posterior pole of *oskar* and *nanos* mRNAs (Johnstone and Lasko, 2001). In vertebrates, similar mechanisms are involved in the sorting of *Vg1* transcript into *Xenopus* oocites for the determination of the vegetal pole in which cell will be committed to endodermal and mesodermal fate (King et al., 2005; Yisraeli and Melton, 1988). The sorting of mRNAs encoding cytoskeleton proteins is a well conserved and characterized mechanisms among different cell types. *β-actin* mRNA specific localization in fibroblast lamellipodia is crucial for cell motility (Kislauskis et al., 1994), while in developing neuron this mRNA and those of *Tau1* are transported to distal growth cones of axons that navigate following chemical gradients of chemofactors and neurotrophins (Lin and Holt, 2007; Litman et al., 1993). Dendritic trafficking and local translation of specific mRNA, such as *Arc, CamKIIα* and *Brain-derived neurotrophic factor,* in mature neurons play a pivotal role in the regulation of development and plasticity events (Martin and Zukin, 2006; Sossin and DesGroseillers, 2006) and will be discussed later.

The major advantages for sorting mRNA to subcellular compartments consist in energy saving (a single mRNA could be local translated several times before being depredated), fast response to stimulation (local protein synthesis products are ready

to be used without the need to be transported) and correct localization of the translated proteins, achieving gradients formation and high protein levels (Martin and Ephrussi, 2009).

Beyond previous evidence on local specialized mRNA, recent studies revealed that the spatial sorting of mRNAs involves thousands of transcripts in different species and cell types.

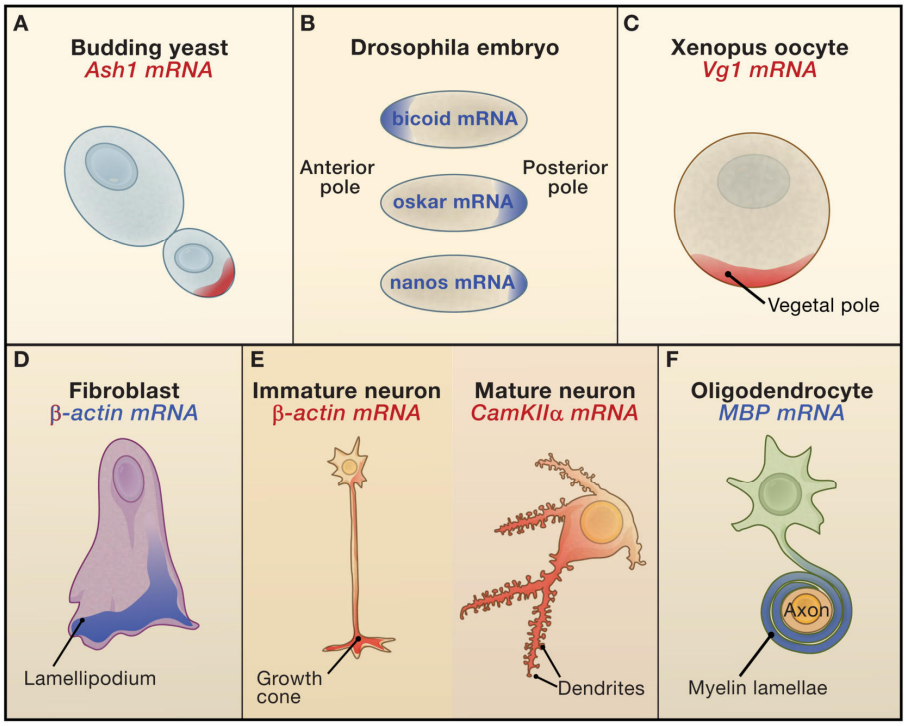

Fig. 1: mRNA localization examples in different cellular types. From Martin and Ephrussi, 2010.

High throughput *in situ* hybridization of 3370 mRNAs in fruit fly demonstrated that over the 70% of these transcripts are spatially regulated in specific compartments (Lecuyer et al., 2007). In mammals several neuronal mRNAs have been found enriched in neuronal processes of CA1 neuropil, with more of 2500 transcripts isolated (Cajigas et al., 2012). Moreover, different studies demonstrated that distinct subsets of transcripts are selectively enriched in axon and growth cones during different development phases and injury status (Gumy et al., 2011; Taylor et al., 2009; Zivraj et al., 2010). The abundance and the variety of transcripts selectively transported in specific cellular compartments strongly supports the hypothesis that mRNA localization is a common regulatory mechanisms present in almost all organisms and cell types.

1.2 *Cis*-elements

After the discovery that transcripts could be asymmetrically distributed within cell, many efforts have been done in order to elucidate the mechanisms. First studies on Drosophila oocytes, using a systematic mutational approach, identified a 625 bp region in the 3' untraslated region (3'UTR) of *Bicoid* mRNA which contained several elements required for localization (*bicoid* localization elements, BLE) (Macdonald et al., 1993). Moreover, mutations that alter primary sequence but not stem loop structures of BLE, bound by Staufen RNA-binding protein (RBP), did not affect *Bicoid* localization (Ferrandon et al., 1997). Clustered targeting elements in coding sequence and 3'UTR with stem loop secondary structure regions have been successively identified in different cell types and organisms. In yeast *ASH1* mRNA asymmetric distribution is driven by three localization elements in the coding sequence and one overlapping coding sequence and the 3'UTR. Each sequence has a stem loop secondary structure and it's sufficient alone to induce the localization of mRNA; however, the clusterization of the four element together increase the targeting of mRNA (Chartrand et al., 2002), suggesting that multiple elements recruit different RBPs that act by forming complexes to promote transcript localization (Martin and Ephrussi, 2009).

In neurons, many transcripts encoding for cytoskeleton proteins or synaptic plasticity regulation were targeted to distal segments of dendrite (Doyle and Kiebler, 2011). β-*actin* mRNA retains a targeting mechanism conserved among different species and cell types. In chicken fibroblasts and myoblasts a 54 nts element in its 3'UTR, named "zipcode", is recognized by the zipocde binding protein 1 (ZBP1) and mediates its localization in lamellipodia (Kislauskis et al., 1994; Ross et al., 1997). The same conserved mechanism regulates localization of β-*actin* mRNA in axonal growth cones (Tiruchinapalli et al., 2003).

Many other neuronal transcripts, such as *MAP2, Arc, GluR1* and *2, NR1* and *PKMς,* display dendritic targeting elements (DTEs) in their coding sequence or 3'UTR. It's worth noting that one mRNA retains often multiple DTE. This may account for a strengthening of localization signal, refined multistep localization mechanism or for a differential response to different stimuli (Xing and Bassell, 2013). However, the

physiological significance of this has to be further investigated. A well characterized mechanisms of localization by multiple DTE was described in *myelin basic protein* (*MBP*) mRNA. The coding sequence encode for a 11 nts DTE called A2RE (bound by heterogeneous nuclear ribonucleoprotein A2) that is sufficient for the localization of *MBP* mRNA in oligodendrocytes processes, but not for the localization in the myelinating compartment which is mediated by RNA localization signal (RLS) in the 3'UTR (Ainger et al., 1997).

In neurons, the *calcium calmoduline kinase IIα* (*CaMKIIα*) mRNA displays a complex DTE pattern. CamKII/Ng dendritic localization element (CNDLE), localized in nts 28-56 of 3'UTR, induces dendritic localization of the mRNA, while a larger element downstream the latter has a dominant negative effect on its targeting that is relieved upon depolarization (Mori et al., 2000). Another 1200 nt long DTE were found in the 3'UTR (Blichenberg et al., 2001), while two different cytoplasmic polyadenylation elements (CPE) were found to induce transport and translation of this mRNA (Huang et al., 2002). The importance of these sequences has been demonstrated using transgenic mice lacking the *CaMKIIα* 3'UTR, which displayed impaired long term potentiation maintenance (Miller et al., 2002). Moreover, an Y binding sites for Translin RBP in the coding sequence is required for dendritic trafficking (Severt et al., 1999). Recently, a very similar mechanism has been characterized for *brain-derived neurotrophic factor* (*BDNF*) mRNA localization in dendrites. Translin binds to *BDNF* coding region and induces a constitutive dendritic targeting (Chiaruttini et al., 2009). 3'UTR harbors distinct DTE elements bound by CPE binding proteins (CPEBs), ELAV-like proteins (ELAVL) and Fragile-X related proteins (FMRPs). 3'UTR short isoform trafficking is induced by depolarization or neurotrophin-3 (NT-3) stimulation and is mediated by ELAVL2 and 4 and CPEB1 and 2. Long isoform targeting is repressed by FMRPs binding to G-quartet structure and by ELAVLs binding in the central region of 3'UTR. BDNF treatment reliefs repression signal and induce the dendritic localization of the mRNA mediated by CPEB1 (Vicario et al., 2015).

In conclusion, several mRNAs share *cis*-elements and localization mechanisms among different organisms and cell types. The different "RNA signatures" given by multiple DTE allow a fine regulation of localization during development or in response to different stimulation.

1.3 *Trans*-acting factors : RNA binding proteins

RNA molecules are always associated to heterogeneous classes of RBPs, starting from transcription to the following steps of mRNA processing, which include stabilization, localization, translation and final degradation. RBPs bind to *cis*-elements contained in untranslated regions (5' and 3' UTR) or in coding sequence and may assemble to form larger structure: the RNA granules (Liu-Yesucevitz et al., 2011).

The role of RBPs in central nervous system development and plasticity has been deeply investigated. More than 300 different RBPs are expressed during early development of the nervous system in vertebrates. Several studies demonstrated how failure in the interaction of RBP with *cis*-elements results in impaired localization of selected transcripts in neurites (Huang et al., 2003; Zhang et al., 2001). RBPs contain one or more domain for binding of RNA with a broad range of specificity among the different classes of proteins. RNA recognition motif (RRM), K homology domain (KH), zinc finger and double strand RNA binding domains (dsRBP) are some of the most representative domains present in RBPs (Lunde et al., 2007). Moreover, the presence of protein-protein interaction domains, such prion-like domain and glycine-rich domains, facilitates the assembly of RNA granules, recruiting different *trans*-factor sharing common interaction domains (Wolozin, 2012). Once assembled RNA granules regulate the fate of mRNA: capped mRNA can be stabilized and stored translationally-silenced in stress granules (Kedersha et al., 2000); non-translating mRNA could be recruited in processing bodies where decapping enzymes, exonuclease, deanylase and silencing RISC complex regulate silencing or degradation of selected transcripts (Kiebler and Bassell, 2006); transporting granules localize mRNA in subcellular compartments where is locally translated (Martin and Ephrussi, 2009). Given the several implications of RBP in RNA homeostasis, it is not surprising that mutations in genes encoding for RBPs (*Fmr1, TDP-43, FUS, SMN1, ATX2*) cause some of the well known neurodevelompental and neurodegenerative disorders (Lukong et al., 2008). Below, are reported some of the most representative RBP families involved in mRNA localization, stabilization and translation in neurons:

Staufen: Staufen has been identified as the *trans*-acting factor necessary for *bicoid, oscar* and *prospero* mRNA localization in *Drosophila* oocytes (St Johnston et al., 1991). Two homologues exist in mammals, Staufen1 and Staufen2, with the first widely expressed in all tissues while the latter mainly expressed in brain (Monshausen et al., 2001).

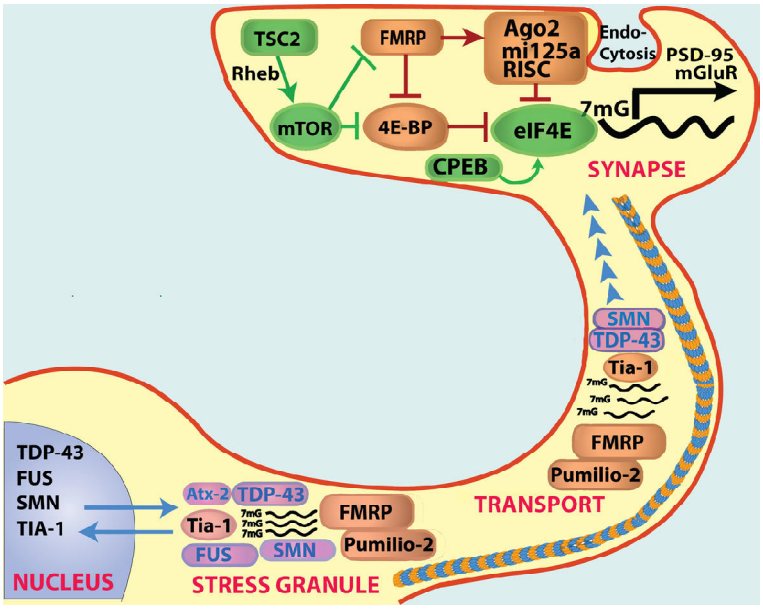

Fig. 2: Schematic representation of interaction of RBPs and mRNA in neurons. From Liu-Yesucevitz et al., 2011.

The two proteins contain four copies of the dsRBP domain, and were isolated in distinct ribonucleoprotein particles (RNPs) in somatodendritic compartment (Duchaine et al., 2002), displaying binding affinity for different mRNAs (Furic et al., 2008). Staufen is present in mRNA granules transported into dendrites, regulating the mRNA transport (Kanai et al., 2004). Moreover, Staufen has been isolated in large granules that contain polysomes (Krichevsky and Kosik, 2001), or from granules devoid by translation components and associated to kinesin motor proteins (Mallardo et al., 2003). Silencing of Staufen1 or 2 results in impaired LTP onset, reduced spine maturation and lower dendritic arborization in murine hippocampal pyramidal neurons (Goetze et al., 2006; Lebeau et al., 2008; Vessey et al., 2008). Staufen1 has been also reported to be involved in mRNA degradation by recruitment of Upf1 (Kim et al., 2005) or by its interaction with mammalian processing bodies (Zeitelhofer et al., 2008). Finally, Staufen1 is also recruited into stress granules

although is not necessary for their nucleation (Thomas et al., 2009; Thomas et al., 2005).

Fragile-X mental retardation proteins (FMRPs): FMRPs are RBP which mutation cause Fragile-X syndrome. CGG expansion in the 5'UTR of *Fmr1* gene, the most important member of FMRPs, inhibits its expression and cause abnormal development of spines and dysregulation of several signaling pathways (Bassell and Warren, 2008). Fmr1 contains two KH domains and one arginine-glycine-glycine (RGG box) to bind stem-G-quartet loop structures on RNA (Schaeffer et al., 2001). Fmr1 binds different neuronal mRNA, such as *Map1b, Arc, CaMKIIα* (Bassell and Warren, 2008) and *BDNF* (Vicario et al., 2015), and drives their dendritic localization through interaction with kinesin motors and microtubules (Antar et al., 2004; Davidovic et al., 2007). Fmr1 is a general repressor of translation of dendritic mRNA, and its absence is general associated with over-translation of its target mRNAs, such as *PSD95* mRNA in postsynaptic compartment. The mechanisms through which Fmr1 exerts this repression are still poor characterized however, micro RNAs (miRNA) seems to be involved. When phosphorylated, Fmr1 recruits RNA-induced silencing complex (RISC) (Jin et al., 2004). M*ir125a* through argonaute2 protein (Ago2) represses translation of *PSD95* mRNA. FMR1 dephosphorylation leads to the release of silencing complex and to induction of translation of target mRNA (Muddashetty et al., 2011). Therefore, Fmr1 mutation leads to aberrant spines formation and dysregulated synaptic signaling.

Cytoplasmic polyadenylation element binding proteins (CPEBS): CPEBs are a family of proteins involved in the regulation of localization and translation of mRNA. CPEBs contain two RRMs and two zinc-finger domains that mediates RNA binding, however CPEB1 preferentially binds to canonical CPE element (UUUUAU) while CPEB2-4 show affinity for different binding sites (Huang et al., 2006). CPEB1 is detected in soma and dendrites of neurons and induce the trafficking of different neuronal mRNA, such as *CaMKIIα* and *BDNF* (Huang et al., 2003; Oe and Yoneda, 2010), by binding to CPE elements in the 3'UTR. CPEB1 is a key regulator of translation of those mRNA harboring CPE elements on their 3'UTR. In resting condition *cis*-element recruits CPEB on it, together with and poly(A) polymerase (PAP) and poly(A) ribonuclease (PARN), that keeps poly(A) tails shortened (Kim and

Richter, 2006). Moreover, CPEB1 together with Maskin inhibits the eIF4E-eIF4G interaction, keeping mRNA translationally silenced (Mendez and Richter, 2001). Upon synaptic activity stimulation, Aurora kinase and CaMKII phosphorylation of CPEB induced the release of PARN and Maskin, allowing poly(A) tail elongation and binding of small ribosomal subunit for the initiation of protein synthesis (Atkins et al., 2004; Mendez and Richter, 2001).

Embryonic lethal abnormal vision (ELAV) like proteins: ELAVs were the first proteins discovered in regulation of *Drosophila* nervous system development (Koushika et al., 2000) controlling splicing and transcription of selected transcripts in neurons. Four homologues have been found in mammals: ELAVL1 (HuR) is widely expressed in all tissues, while ELAVL2 (HuB), ELAVL3 (HuC) and ELAVL4 (HuD) are expressed only in neuronal tissues (HuB also in gonads) (Good, 1995). ELAVLs share a common structure, with two RRMs very close to each other that mediates the recognition of AU-rich elements (AURE) in 3'UTRs (Levine et al., 1993; Liu et al., 1995) separated from a third RRM by an hinge region. In vertebrates, ELAVLs regulate nucleocytoplasmatic shuttling, stability and translation of target mRNA (Antic et al., 1999; Chen et al., 2002). In particular, HuD regulates degradation, activity dependent translation and dendritic targeting of *BDNF* mRNA (Allen et al., 2013; Vanevski and Xu, 2015; Vicario et al., 2015) by binding AURE in short and long 3'UTR.

Translin: Testis-Brain RBP, or Translin, is a protein mainly expressed in gonad and brain tissues that binds to ssDNA and RNA on specific sequences (Han et al., 1995). In testis, this protein regulates translation and localization of germ cells mRNA (Hecht, 1998; Morales et al., 1998). Translin can bind to the Y element, a sequence harbored in many localized mRNA, and promotes the formation of RNPs associated to microtubules (Kobayashi et al., 1998; Muramatsu et al., 1998; Wu et al., 1999). The binding of Translin promotes the dendritic localization of different neuronal mRNAs such as *CaMKIIα* and *BDNF* (Chiaruttini et al., 2009; Severt et al., 1999). Interestingly, a *BDNF* polymorphism associated to psychiatric disorders is localized in the binding sites of Translin and impairs the dendritic localization of this transcript (Chiaruttini et al., 2009).

Zipcode binding protein 1 (ZBP1): ZBP1 was identified during the study of *β-actin* mRNA trafficking in chicken embryonic fibroblast (Ross et al., 1997). Its structure is characterized by two RRMs and four hnRNPK domains for mRNA binding. ZBP1 regulates the localization of *β-actin* mRNA in axonal growth cones and dendritic spines, repressing its translation.(Bassell and Kelic, 2004; Eom et al., 2003; Perycz et al., 2011; Zhang et al., 2001). However, the phosphorylation of tyrosine 396 upon BDNF stimulation, induces RNP remodeling and allows the translation of *β-actin* mRNA (Huttelmaier et al., 2005).

Heterogeneous nuclear ribonucleoprotein A2/B1 (hnRNP A2/B1): hnRNP A2/B1 was one of the first RBPs to be involved in neural mRNA trafficking. It contains two RRM that mediate the binding to A2RE (Ainger et al., 1997), promoting the localization of several mRNA such *CaMKII* and *Arc* in dendrites (Gao et al., 2008). A glycine-rich domain allows interaction of hnRNP A2/B1 with other RBPs in RNP (Cartegni et al., 1996). Beside its role in trafficking hnRNPA A2/B1 splicing isoforms are differentially distributed in tissues and bind to nascent transcripts directly in nucleus, regulating all the aspect of mRNA splicing and translation (Han et al., 2010; He and Smith, 2009).

RBP are able to regulate any aspect of mRNA regulation, from splicing to nucleocytoplasmatic shuttling, stabilization, localization, translation and decay. The presence of multiple *cis*-elements in RNA sequences and complex interaction between the different RBPs through specific protein-protein domains suggest that multiple *trans*-acting factor may act in a synergic way to regulate mRNA homeostasis in multiple ways.

1.4 RNA granules in neurons: classification and function

In eukaryotic cells, self-assembled RNP in nuclear and/or cytoplasmatic structures not defined by membranes are called RNA granules (Erickson and Lykke-Andersen, 2011). These structures resulted highly heterogeneous for dimension, localization, function, mRNA and protein contents. However, they share one common feature: all mRNAs contained in RNA granules are translationally repressed but still able to enter in the translation process upon proper stimulation or signaling (Brengues et al., 2005; Huttelmaier et al., 2005; Teixeira et al., 2005). Beside this, different RNA granules

share RBP and RNA species that can be exchanged through dynamic interactions between them (Buchan and Parker, 2009; Kedersha et al., 2005). In soma and dendrites of neurons three major classes of granules were identified: transporting granules, stress granules and processing bodies.

Transporting granules: Transporting granules are specialized RNPs that regulate localization and translation of mRNA in different cell type (Kiebler and Bassell, 2006). Transporting particles were first identified in *Drosophila*, during the characterization of *MBP* localization in cultured oligodendrocytes (Ainger et al., 1993) and successively identified in neurons (Knowles et al., 1996). These granules are heterogeneous in dimension and shape and display rapid bidirectional movement (0.1-0.4 µm/s) along microtubules in dendrites of resting neurons (Knowles et al., 1996; Kohrmann et al., 1999). However, using MS2-GFP tagging system to characterize *CaMKIIα* RNP particles dynamics, it has been demonstrated that pools of transporting granules may switch to exclusive anterograde fast movement after synaptic activation (Rook et al., 2000).

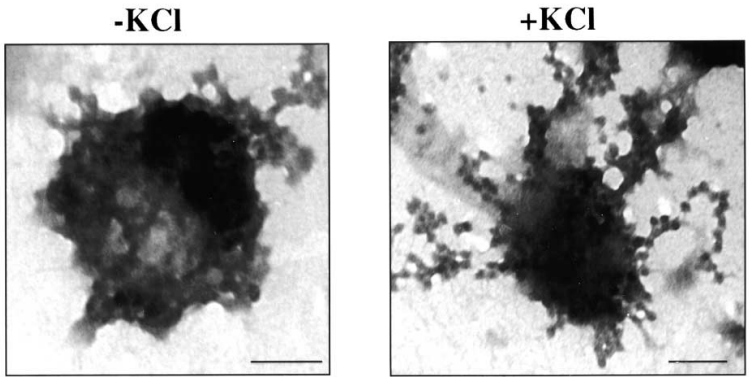

Fig. 3: Electron microscopy photos of RNA granule before and after depolarization stimulus. From Krichevsky and Kosik, 2001.

Different studies characterized RBPs in *β-actin* and *CaMKIIα* RNA granules . RBP content has been found enriched of Staufen1, hnRNP A2/B1, FMRP, Purα, PSF and DEAD box helicase proteins (Elvira et al., 2006; Kanai et al., 2004). Fractioning studies demonstrated that large transporting granules can be associated to ribosomes and endoplasmatic reticulum markers (Krichevsky and Kosik, 2001) while small size granules are devoid from translation machinery and are associated to kinesin protein (Mallardo et al., 2003). Despite the presence of components for active protein synthesis, mRNA in transporting particles is translationally repressed by

RBPs such as FMRP (Zalfa et al., 2006) or CPEBs (Huang et al., 2002). However, after synaptic activation dense structures of RNA granules are opened to make RNA content available for translation in polysomes (Krichevsky and Kosik, 2001). Assembly of transporting particles starts in the nuclear site of transcription of target mRNA (Doyle and Kiebler, 2011) and proceeds in cytoplasm, where self-interaction domains (Staufen1) or prion-like domains may drive packaging of transcripts and protein (Kim et al., 2013; Martel et al., 2010). How many RNA molecules and if different mRNA species are contained in the same particle is still debated. In neurons in fact, mRNAs sharing identical *cis*-elements have been found colocalized within the same granules (Gao et al., 2008; Tubing et al., 2010), but conversely, transporting particles harboring single RNA molecules have been detected in dendrites (Mikl et al., 2011; Park et al., 2014). Further assembly steps require association of granules to molecular motors, such as Dynein or Kinesin. Despite their role in the dynamics of transporting granules along dendrites has been assessed, little is known about the molecular aspects of their physical interaction (Kanai et al., 2004). Transporting granules localized to synapses may be anchored and kept translationally silenced until one specific stimulus relieves translational repression locally by post-translational modification of repressor RBPs (Huttelmaier et al., 2005; Zalfa et al., 2006). It was suggested (Doyle and Kiebler, 2011) that granules partially disassemble upon triggering of activity dependent translation by opening their dense structures allowing release of mRNA and ribosomes (Krichevsky and Kosik, 2001) or by the release of single RNP from granule (Mikl et al., 2011).

Stress granules: Stress granules (SGs) are large cytoplasmatic mRNPs involved in translation repression. Their main components belong to preinitiation and translation-related factors, mRNA and RBPs controlling RNA stability, translation repression and trafficking, and signaling proteins (Kedersha and Anderson, 2007). In normal conditions SG are not detected in the cell. However, they rapidly nucleate into large granules due to reduced translation in response to various forms of stress, such as oxidative stress, heat shock, UV damage and viral infection (Kedersha and Anderson, 2007). In general, the rate limiting step about SG formation is accumulation of non-translating mRNAs in the initial step of translation (Buchan and Parker, 2009), and drugs that stabilize polysomes inhibit their assembly (Kedersha et al., 2000). Assembly of SG is regulated by different factors including post-

transcriptional modification of SG components. Phosphorylation of eIF2α is essential for SG nucleation in response to different stresses (Buchan, 2014), while G3BP1 phosphorylation has an inhibitory effect (Tourriere et al., 2003). Interestingly RBPs that nucleates into SG share two features: first they repress translation of bound mRNA; second, they contain glycine-rich domains (i.e. FMRP), oligomerization domains (i.e. G3BP1) or prion-like domain (i.e. TIA-1/TIAR) that promote protein-protein interaction (Thomas et al., 2011). Finally, microtubules integrity and molecular motors (dynein and kinesin) are required for correct SG nucleation, although this type of granule displays no significant motility (Loschi et al., 2009).

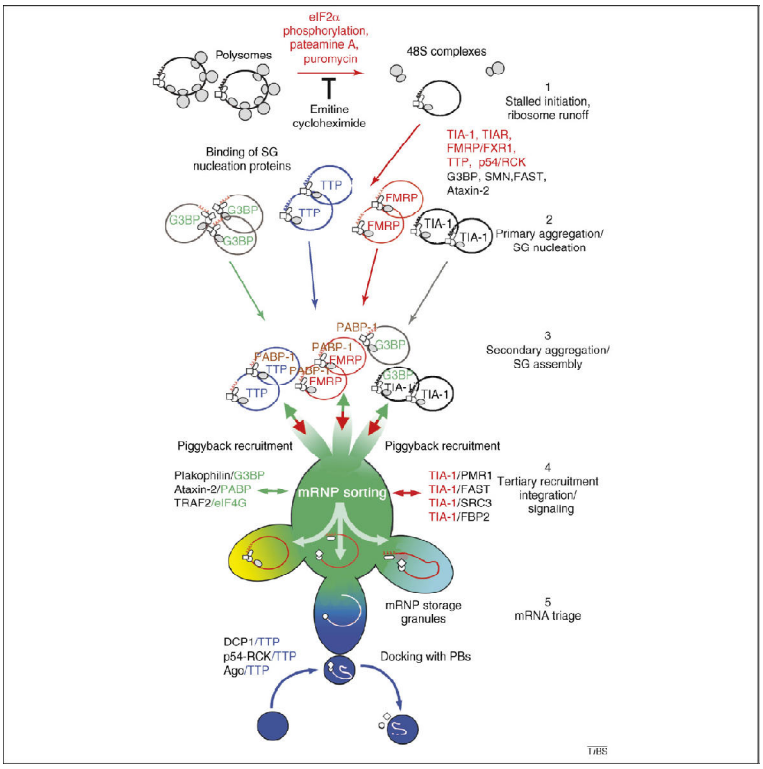

Fig. 4: Model of stress granule assembly. From Anderson and Kedersha, 2008.

T-cell internal antigen-1 (TIA-1) is one of the most important and representative component of SG. TIA-1 is an RBP with three RRM domains (Beck et al., 1996) that bind to U-rich 30-37 nts long bipartite element of 5' and 3' UTR, repressing translation of bound mRNA (Lopez de Silanes et al., 2005). Moreover, its prion-like domain is required for SG nucleation (Kedersha et al., 1999).

Once stress condition is passed and translation is relieved, SG are rapidly disassembled (Kedersha and Anderson, 2007), however mechanisms regulating

disruption of protein-protein interaction within granules are still poorly understood (Buchan, 2014). Despite dynamics and components of SG has been characterized in different organisms and cell types, their function remains still unclear and many hypothesis have been formulated. Accumulation of selected proteins and transcripts in SG may contribute to create a cytoplasmic gradient that may increase or decrease specific reactions or RNP association (Buchan and Parker, 2009). Despite stress granules formation *per se* does not impair general translation, selective mRNAs targeted by SG components may regulate their translation or stability status (Buchan, 2014). In contrast, with this hypothesis, fluorescence recovery after photobleaching (FRAP) studies have shown that SG components TIA-1 and PABP1 shuttle dynamically from SG to cytoplasm with an half-life of 2 and 8 seconds, respectively (Kedersha et al., 2000), suggesting that SG may act as sites of "RNA triage", a self-organized compartment in which mRNA is bound by RBPs that promote repression of translation or stabilization. The rapid dynamics of shuttling and the high variability of RNP allow a large number of RNA to exit from triage site and to be translated in polysomes (Anderson and Kedersha, 2008). Due to their interaction with other RNPs, such as processing bodies and transporting granules, SG may serve as docking station for RNP remodeling, exchanging RBP or RNA content from translationally stalled mRNA granules (Decker and Parker, 2012; Kedersha et al., 2005). However, a physical interaction between this RNPs is still uncertain (Souquere et al., 2009). Finally, different lines of studies are delineating a role for SG as "signaling hub". in which different molecules involved in several signaling pathways, such as mammalian target of rapamycin (mTORC1) (Takahara and Maeda, 2012), are recruited within SG (Kedersha et al., 2013). Despite its uncertain physiological function, a role of SG in disease is emerging. SG are hijacked during viral infection (Lloyd, 2013) and are involved in cancer cell survival mechanisms (Anderson et al., 2015). Remarkably, several RBPs that nucleate into SG are associated to neurodevelopmental and neurodegenerative disorders (Thomas et al., 2011) and cells harboring FMRP mutations displayed altered stress granule assembly (Didiot et al., 2009). Recently, it was suggested that SG aberrant formation driven by mutated RBPs and failure in its clearance due to impaired autophagy would be common mechanisms involved in neurodegenerative diseases as amyotrophic lateral sclerosis (ALS) (Buchan, 2014; Li et al., 2013b; Ramaswami et al., 2013). Indeed, 43 kDa TAR DNA binding protein (TDP-43) has been found in SG (Colombrita et al., 2009),

although it is not necessary for SG nucleation. However, the propensity for aggregation and the interaction of this protein with several factors implicated in SG homeostasis (Buratti and Baralle, 2012) suggest that precise mechanisms involving SG in neurodegenerative diseases have to be further investigated.

Processing bodies: Processing bodies (PB) are cytoplasmatic granules composed by translationally inactive RNPs assembled together with components of mRNA silencing and degradation (Erickson and Lykke-Andersen, 2011), including Dcp1-Dcp2 decapping enzymes complex, decapping activators, mRNA deadynales, exonucleases, miRNA silencing complex (Ago2, RISC, GW182), Nonsense-mediated decay factors and translation repressors (Cougot et al., 2004; Decker and Parker, 2012; Thomas et al., 2011). Similarly to SG, PB assembly is induced by accumulation of non-translating mRNA (Teixeira et al., 2005) and is driven by self-interaction domains found in their components (Erickson and Lykke-Andersen, 2011). However, PB are constitutively expressed in cells and translation initiation repression induced by certain stress may increase dimension and number of these granules (Kedersha and Anderson, 2007).

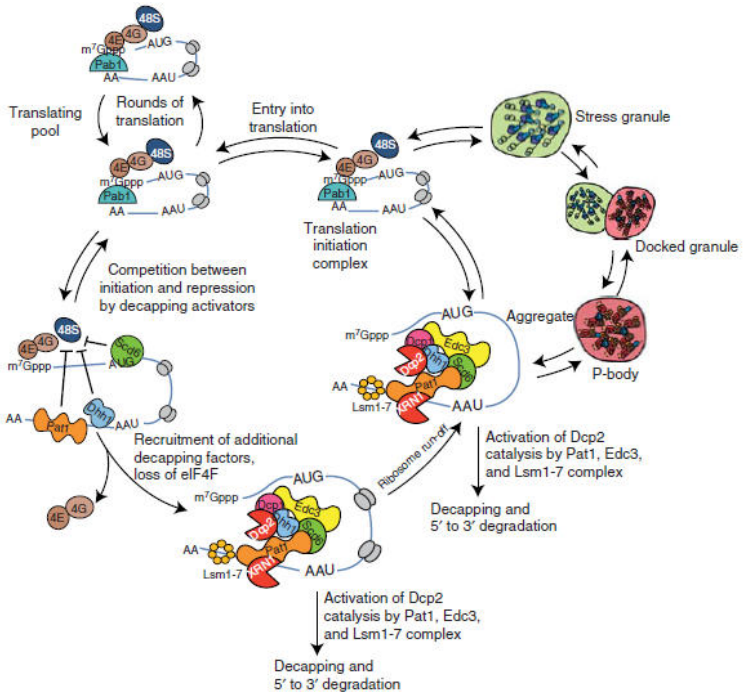

Fig. 5: mRNA cycling through polysomes, stress granules and processing bodies. From Decker and Parker, 2012

RNP sequestered into PB are only transiently associated, in fact FRAP studies highlighted a rapid cycle in and out PB of RNP, suggesting that once associated with PB, RNA contained in RNP could be degraded or re-enter into translation; supporting this last hypothesis, increased translation rate were known to induce PB disassembly. (Aizer et al., 2008; Erickson and Lykke-Andersen, 2011). Differently from SG, PB display high motility inside cells. Microtubule depolymerization leads to reduced motility and PB abnormal enlargement (Sweet et al., 2007), while in neurons association with kinesin motor protein is required for PB translocation in dendrites upon neuronal activation (Oh et al., 2013). Actually little is kwon about the effective role of this granules in cells. Despite the various mRNA degradation and silencing complexes, there are still no clear evidence that visible nucleation of this structure are required for silencing (Eulalio et al., 2007) or degradation of RNA (Stalder and Muhlemann, 2009). Their dynamic interaction with transporting particles and SG support again the hypothesis that PB are part of a complex mRNP remodeling and "RNA triage" platform (Anderson and Kedersha, 2008; Decker and Parker, 2012).

One intriguing role for PB in local protein synthesis at neuron synapses is emerging in the last years. PB has been isolated in dendrites of murine hippocampal cultured neurons (Zeitelhofer et al., 2008), where they are localized near postsynaptic density (Oh et al., 2013) and often docked to Staufen1 particles (Zeitelhofer et al., 2008). Moreover, PB respond differently to neuronal stimulation, disappearing or translocating into dendrites depending on type and extent of stimuli (Cougot et al., 2008; Huang et al., 2012; Oh et al., 2013; Zeitelhofer et al., 2008). Finally, BDNF treatment enhance Lin28 miRNA levels together with processing bodies, selectively regulating translation and dendritic arborization in hippocampal neurons (Huang et al., 2012).

In conclusion the different classes of mRNA granules and their RBP represent a highly conserved mechanisms in evolution, with similar dynamics during development or mature phases of different system . Despite uncertain functions and mechanisms that have to be still clarified, mRNP may represent a complex "hub" for regulation of mRNA homeostasis and signaling.

1.5 Local protein synthesis in dendrites

The reasons behind the multiple step process that localizes mRNA to synapses to be locally translated are many. First, the metabolic need for a sustained transport of proteins from somatic area to distal spines would be excessive for neuron. Secondly, a process based exclusively on protein delivery would not meet the fast response timing observed during neuronal response. Third, a selective transport of mRNA required for synaptic plasticity may represent a fine mechanisms of regulation to modulate neuronal activity. This hypothesis lead many authors to investigate if translation machinery was present in dendrites and spines. Electron microscopy studies confirmed the presence of polyribosomes at the base of dendritic spines (Spacek, 1985; Steward and Levy, 1982) and in proximity of postsynaptic density (Steward and Falk, 1986). Following studies isolated different components of translation initiation and elongation, endoplasmatic reticulum, tRNA and Golgi apparatus, confirming that a functional translational machinery is present in dendrites (Steward et al., 1996; Tiedge and Brosius, 1996; Torre and Steward, 1996). These evidences are in line with hypothesis that plasticity events in synapses could be regulated by local protein synthesis of localized transcripts (Steward and Schuman, 2001). Several lines of study corroborated this model: activity-dependent stimulation increases mRNA localization and protein synthesis in dendrites (Jiang and Schuman, 2002; Krichevsky and Kosik, 2001); protein synthesis of transcripts involved in synaptic plasticity occurs in dendrites severed from soma (Waung et al., 2008); finally, translation inhibitors impair both late phases long term depression (LTD) and potentiation (LTP) and synapse consolidation (Bramham and Wells, 2007; Liu-Yesucevitz et al., 2011). Several signaling pathways are involved in governing the translation of mRNA in dendrites. Phosphorylation of eukaryotic initiation factor (eIF4E) is the rate limiting step for translation initiation, and is exerted by extracellular signal-regulated kinase (ERK) after the release of eIF4E binding protein (eIF4EBP) induced by its phosphorylation by mTOR (Richter and Sonenberg, 2005). The latter may also activate p70S6K kinase and induce the translation of 5'terminal oligopyrimidine tract (5'TOP) mRNA (Hoeffer and Klann, 2010). This peculiar sequence is retained by mRNA encoding for protein of translation machinery, and their local translation during late phases of synaptic potentiation is necessary for the maintenance of sustained levels of translation. Elongation phase of translation is

regulated by the phosphorylation of eukaryotic elongation factor 2 (eEF2) that inhibits global peptides elongation but promote specifically the synthesis of neuronal mRNA such as *activity-regulated cytoskeleton protein* (*Arc*) and *CamKIIα* (Chotiner et al., 2003; Kanhema et al., 2006). These general mechanisms regulate positively or negatively local protein synthesis levels. Translation of specific transcripts is regulated by different *trans*-acting factors such as FMRP, CPEB and miRNA, which has been described in chapter 1.3.

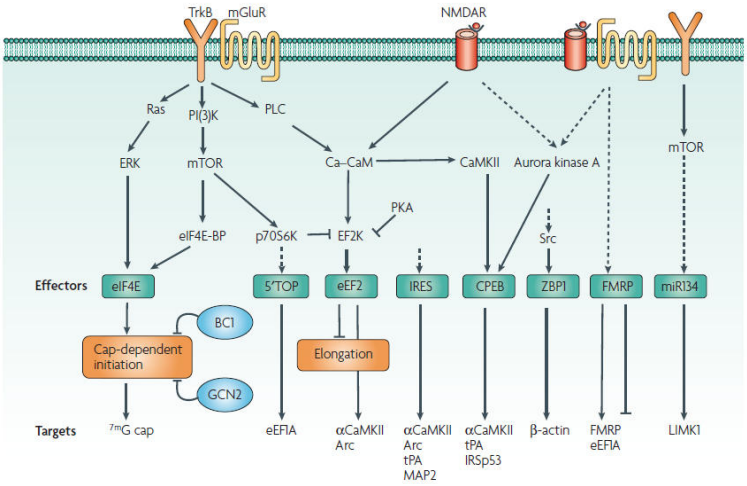

Fig. 6: Local translation control in dendrites, a schematic view. From Bramham and Wells, 2007

The importance of local protein synthesis at the synapse has been confirmed in the study of *Arc* mRNA during LTP in granule cells of dentate gyrus. Arc is an immediate-early gene which expression is induced upon synaptic activation (Plath et al., 2006). Its newly expressed mRNA is targeted to dendrites with a time course coincident with the need of protein synthesis during LTP and is specifically localized in proximity of postsynaptic density of excitatory synapses to be translated (Dynes and Steward, 2007). Supporting this hypothesis, the injection of *Arc* antisense oligonucleotides after 15 minutes of LTP induction resulted in a partial and reversible LTP inhibition, in accordance with the independence from transcription and translation of early LTP. However the injection of oligonucleotides between 2 and 4 hours after LTP induction resulted in decreased *Arc* mRNA and protein levels with consequent loss of nascent F-actin in stimulated synapse (Messaoudi et al., 2007). Finally, Arc knock-out mice displayed impaired LTP consolidation in dentate gyrus and CA1 (Plath et al., 2006).

Taken together these results strongly support that a sustained Arc protein synthesis of its dendritic mRNA is required for proper LTP consolidation.

Dysregulated control of local protein synthesis and consequent altered synaptic plasticity is one of the major hypothesis concerning Fragile-X syndrome pathogenesis. As discussed previously Fmr1 binds many dendritic targeted mRNA repressing their translation. Fmr1 KO mice display higher dendritic expression of CamKIIα, Arc and Map1b proteins. The mRNA of this proteins are bound specifically from Fmr1 and they are all involved in synaptic plasticity regulation (Bassell and Warren, 2008). mGluR-dependent LTD is enhanced in Fmr1 KO mice and occurs independently from synthesis. These evidences lead to the hypothesis of "mGluR theory", in which an excess of local protein synthesis given by the lack of Fmr1 leads to an excess of AMPAR internalization and exaggerated LTD (Bear et al., 2004). All these findings strongly support the hypothesis that a multistep process involving mRNA transcription, localization into dendrites and sustained local protein synthesis at synapses, is a key mechanisms for fine regulation of dendrites and synaptic plasticity.

2. Brain derived neurotrophic factor mRNA

2.1 BDNF functions and signaling

Neurotrophins (NTs) are a family of small secreted molecules that play a fundamental role in development and synaptic plasticity of mammals central nervous system (Chao et al., 2006). The first member, nerve growth factor (NGF), was discovered by Cohen and colleagues (Cohen et al., 1954), followed by the isolation of brain-derived neurotrophic factor (BDNF) by Barde and colleagues (Barde et al., 1982). In mammals other two neurotrophins, Neurotrophin 3 (NT-3) and 4 (NT-4) have been discovered in following studies. All neurotrophins are synthesized as pro-peptides that are proteolitically processed to their mature forms (Lessmann et al., 2003). Once secreted, NTs bind to tropomyosin-related tyrosine kinases receptors (Trk) with specific affinities: NGF binds to TrkA, BDNF to TrkB, NT-3 to TrkC and NT-4 to TrkB (Huang and Reichardt, 2003). Binding induces dimerization of receptors and their activation through trans-phosphorylation of tyrosine residues in the internal

cytoplasmatic domains, allowing the recruitment of signaling molecules. (Arevalo and Wu, 2006). Moreover, all pro-neurotrophins can bind to p75 neurotrophin receptor (p75NTR) with equal affinity, activating different signaling pathways respect to Trk receptors. BDNF is widely expressed in different species, resulting highly conserved in evolution. BDNF expression is prominent in central nervous system, particularly in

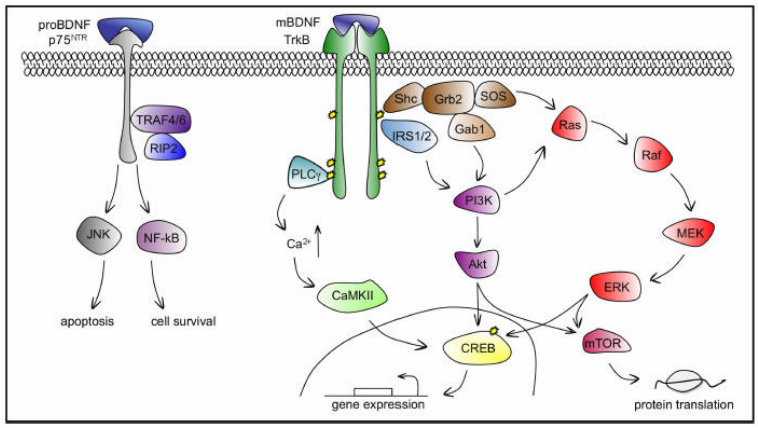

Fig. 7: BDNF-TrkB and BDNF-p75NTR pathways . From Cunha et al., 2010.

amygdala, cerebral cortex and hippocampus. Its expression increase during development, reaching maximum levels after birth and keeping constant during adult life (Friedman et al., 1991a; Friedman et al., 1991b; Katoh-Semba et al., 1998).

Signaling upon binding of BDNF to TrkB or p75NTR regulates different aspect of neuronal development, cell survival, axonal and dendritic outgrowth, spine development and synaptic plasticity (Cunha et al., 2010; Greenberg et al., 2009). After TrkB trans-phosphorylation three distinct signaling cascades are activated: MAP Kinase, PI3 Kinase and Phospholipase Cγ pathways (PLCγ). Shc and Frs2 adaptor proteins are recruited by phosphorylated tyrosine, inducing Ras activation. MAP kinase signaling cascade is therefore activated, resulting in the phosphorylation of eiF4E and inducing translation of target transcripts (Bramham and Wells, 2007). Moreover, BDNF potentiate glutamate release from presynaptic terminal through phosphorylation of synapsin (Kang and Schuman, 1995a; Kang and Schuman, 1995b). In postsynaptic terminals PI3K activates Akt kinase that phosphorylates mammalian target of rapamycin (mTOR), inducing cap-dependent translation local protein synthesis at synapses (Kang and Schuman, 1996) required for induction of

long term potentiation (LTP) from existing mRNA. PLCγ induces Ca_{2+} release in postsynaptic terminal, the activation of CaMKIIα and the phosphorylation of B2 subunit of NMDA receptor (Minichiello et al., 1999). In addition, intracellular release of Ca_{2+} activates CamKIV that phosphorylates cAMP responsive binding proteins (CREB) and induces expression of genes required for consolidation of L-LTP (Minichiello et al., 2002). Beside its role in synaptic plasticity, BDNF is also involved in the shaping of axonal and dendritic arborization, spinogenesis and spine maturation (Baj et al., 2011; McAllister et al., 1997; Tyler and Pozzo-Miller, 2003).

2.2 BDNF gene and RNA trafficking: a spatial code

BDNF gene is highly conserved among different species and displays a complex structure. In rodents, a common coding sequence (CDS) is spliced to eleven different 5'UTR exons splicing isoforms. Moreover, 3'UTR retains two different termination sites, raising the possible transcripts to a total of 22 (Aid et al., 2007). Such high complexity has been recently demonstrated to act as a spatial and quantitative code for BDNF mRNA trafficking and translation into dendrites (Baj et al., 2013; Chiaruttini et al., 2008; Tongiorgi, 2008; Vaghi et al., 2014; Vicario et al., 2015).

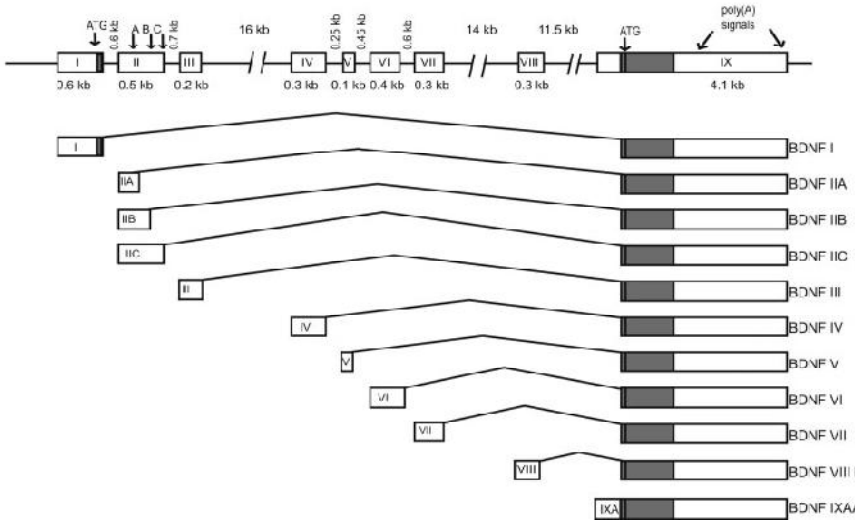

Fig. 8: Schematic representation of rat BDNF gene structure. From Aid et al., 2007.

BDNF mRNA is targeted *in vitro* into dendrites in a calcium-dependent mechanism upon depolarization or following exogenous BDNF administration (Righi et al., 2000; Tongiorgi et al., 1997). BDNF protein levels in dendrites increase after KCl

depolarization, and this increase persists after disruption of microtubules with Nocodazole treatment, excluding an anterograde trafficking of BDNF protein from soma (Tongiorgi et al., 1997). Moreover, the association of *BDNF* mRNA with polyribosomes after pilocarpine induced seizures *in vivo* demonstrated that mRNA localized into distal dendrites may be locally translated to regulate synaptic plasticity event and dendrites shaping (Tongiorgi et al., 2004). It was initially shown that BDNF CDS contains a signal that induce a constitutive targeting into dendrites mediated by Translin, an RBP involved also in the dendritic sorting of *CaMKIIα* mRNA (Chiaruttini et al., 2009). In addition, it was demonstrated that different *BDNF* mRNA splicing variants are differentially localized in neurons both *in vivo* and *in vitro* (Chiaruttini et al., 2008; Chiaruttini et al., 2009). In particular, the different 5'UTR splicing isoforms act as selectivity signals for this targeting, inducing retention in soma (exon1 and partially, exon 4) or permitting the dendritic targeting (exon2c and 6) (Chiaruttini et al., 2009). Exon6 variant results to be present and translated into dendrites severed from soma, confirming that *BDNF* mRNA is locally translated into dendrites (Baj et al., 2011). Strikingly, the overexpression of most proximal variants, exon1 and 4, induces proximal dendrites outgrowth, while overexpression of dendritically sorted exon2c and 6 variants promotes an increase in the arborization of distal dendrites. Silencing of the same variants results in opposite effects on dendrite shape (Baj et al., 2011).

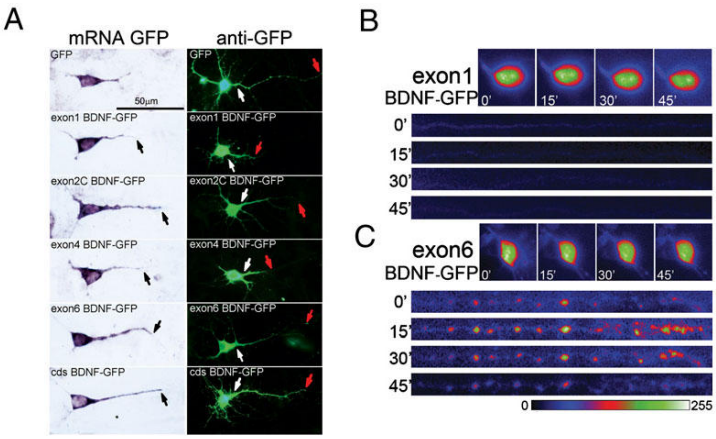

Fig. 9: A) *in situ* hybridization for GFP coding sequence of exon-BDNF-GFP transfected neurons and GFP expression (green). B-C) BDNF-GFP expression in severed dendrites of neurons transfected with exon1-BDNF-GFP (B) and exon6-BDNF-GFP (C) after KCl stimulation. Modified from Baj et al., 2011.

Interestingly, the different splicing variants exhibit also differential basal and stimulus-dependent translatability, measured by *in vitro* firefly luciferase assays. In particular, the “dendritic” exon2c and 6 resulted the only variants to be upregulated upon antidepressant treatment, known to raise BDNF levels in brain (Vaghi et al., 2014).

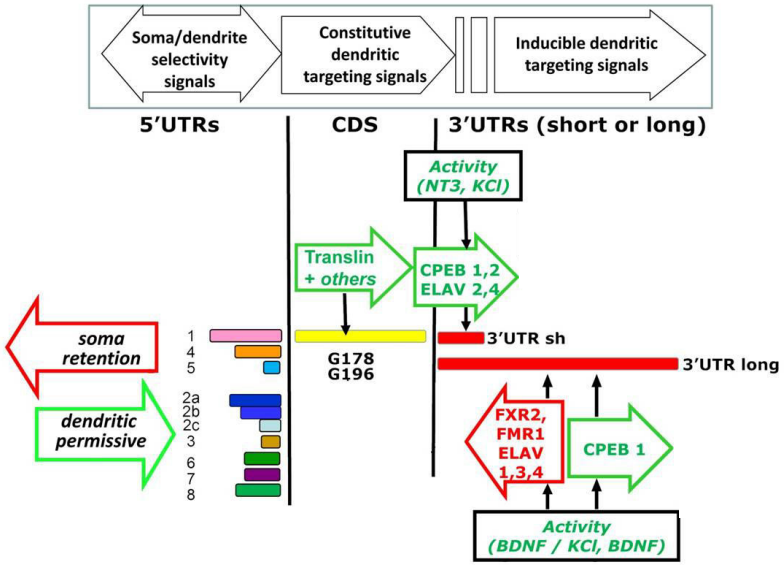

Fig. 10: Proposed model for combinatory mechanisms in *BDNF* mRNA trafficking. Modified from Chiaruttini et al., 2009.

Contrasting evidences regarding the role of 3'UTR in *BDNF* mRNA localization are present in literature. An and colleagues demonstrated that 3'UTR Long isoform is sufficient to induce dendritic targeting in resting neurons, while 3'UTR short transcripts are confined in soma. Moreover, transgenic mice lacking the long isoforms displays lower BDNF protein level in dendrites, spine abnormalities and LTP deficits in adult mice (An et al., 2008). In contrast, two independent studies demonstrated that the short 3'UTR is targeted to dendrites in an activity dependent manner, and CPEB1 is necessary for this trafficking (Baj et al., 2011; Oe and Yoneda, 2010). Finally, we recently demonstrated that short and long 3'UTR isoforms are targeted to dendrites in response to different neurotrophic stimuli and require distinct sets of RBPs (Vicario et al., 2015). In particular, 3'UTR short is targeted to dendrites after KCl in NT-3 stimulation and require CPEB1-2 and ELAVL2-4 proteins; conversely the 3'UTR long is selectively repressed in its dendritic sorting by FMRP and ELAVLs

protein, but the repressive signal is relieved upon BDNF stimulation, allowing dendritic trafficking of this transcript (Vicario et al., 2015).

BDNF involvement in LTP, synapse formation, remodeling and plasticity, and dendritic shaping strengthen BDNF position as a "neuronal shaper". Moreover, the refined mechanisms of localization and translation make BDNF an ideal candidate for pharmacological approaches for treatment of neuropathology in which neuronal atrophy occurs.

3. Rett syndrome

3.1 Clinical features and genetic causes

Rett syndrome (RTT) is a postnatal neurodevelopmental disorder with an occurrence of 1:10000 in girls and no ethnic or geographical restriction. Males are rarely affected by this syndrome and phenotypes observed are substantially different from those in female. RTT girls develop normally during the first 6-18 months of age, then a typical disease progression pattern is observed. The early onset stage is characterized by development arrest, microcephaly, weight loss and mental regression. This is followed by a general and rapid development regression with loss of acquired skills and appearance of autistic features, stereotyped hands movement, social withdrawal,

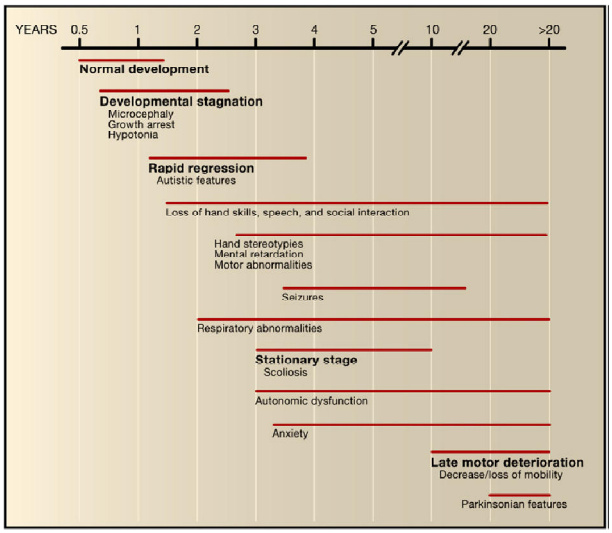

Fig. 11: Onset and progression of Rett syndrome. From Chahrour and Zoghbi, 2007

speech impairments, seizures, indifference for surrounding environment and unresponsiveness to social stimuli. The regression is followed by a stationary stage in which social skills and autistic-like behavior don not worsen. However, several autonomic dysfunctions occur, mainly resulting in respiratory abnormalities and heart failure. Moreover, patients suffer severe motor deterioration, with a significant and often complete loss of mobility and occasionally Parkinsonian features. Lifespan of RTT patients is lower respect healthy population and sudden death occurs in the 25% of cases (Chahrour and Zoghbi, 2007).

Identification of mutations responsible for RTT has been difficult due to the fact that 99% of cases are sporadic. Studies on familial cases and half-sisters affected by RTT confirmed that mutation occurs in the Xq28 region (Sirianni et al., 1998; Zoghbi, 1988). Finally, a systematic mutational analysis approach in this region identified mutations in *methyl-CpG-binding protein 2 (MeCP2)* gene as the cause of RTT (Amir et al., 1999). Up to now more than 300 mutations have been identified in *MeCP2* gene of RTT patients, including nonsense and missense mutations (~70% of the RTT cases) small C- terminal deletions (~10%) and complex rearrangements (~6%) (Williamson and Christodoulou, 2006). Severity of phenotypes are correlated with the type of mutation and the MeCP2 domain affected. Missense mutations or mutations in the C-terminal domain are correlated to milder phenotypes as compared to mutations causing early truncation of protein (Gonzales and LaSalle, 2010).

Different mouse models were created by reproducing the different mutation affecting human patients. All mouse models show most of the characteristics of RTT patients (neuronal atrophy, neurotransmitters alterations, cardio-respiratory deficits, motor impairments, altered social behavior), although the different strains display differences in the time-course of the onset and in the extent of the phenotypes (Katz et al., 2012). In this study, we used $Mecp2^{tm1.1Bird}$ (MeCP2B), a MeCP2-null strain that carries a deletion of exon3 and 4 in *MeCP2* gene (Guy et al., 2001) and earlier onset and severe phenotype with respect to other models. *MeCP2* gene has four different exons and several polyadenylation sites in the 3'UTR, resulting in four transcripts variants differentially expressed in tissues (Shahbazian et al., 2002). Alternative splicing of exon2 gives raise to two proteins that differ in the N-terminal: MeCP2 e1, generated by exon 1, 3 and 4, the most abundant isoform in brain, and

MeCP2 e2, generated by exon 2, 3 and 4 (Dragich et al., 2007). MeCP2 is a nuclear protein member of the family of methyl-CpG binding proteins (MBP) organized in three functional domains: methylated DNA binding domain (MDB), the transcription repressor domain (TRD) and the C-terminal domain (CTD) (Gadalla et al., 2011).

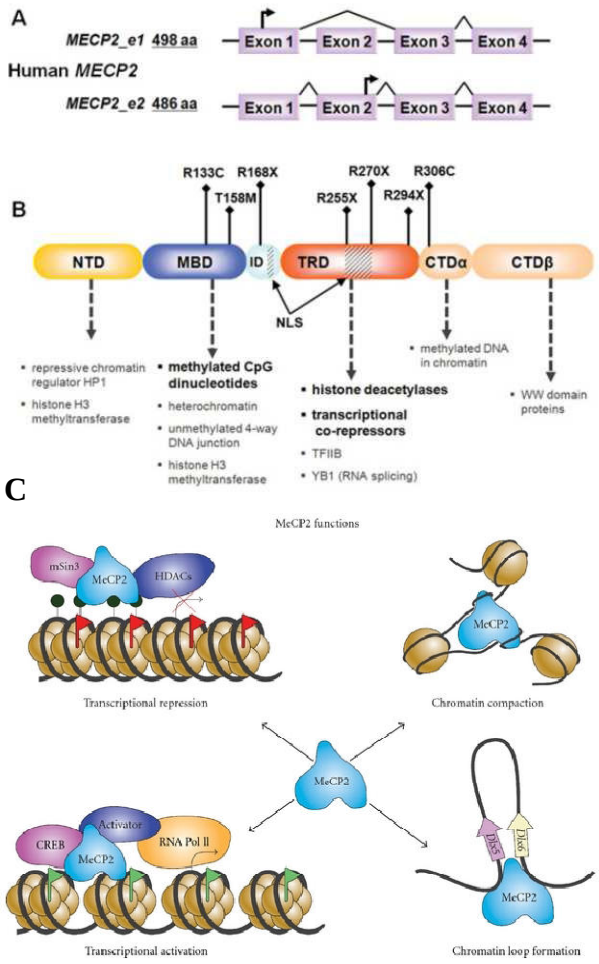

Fig. 12: Structure of human *MeCP2* gene (A) and protein (B). from Gadalla et al., 2011. Functions of MeCP2 protein (C), from Zachariah and Rastegar, 2012

MBD mediates binding of symmetrical methylated CpG, with particular affinity for those flanked by A/T-rich motifs. Moreover, this domain binds to four-way DNA junctions during chromatin remodeling (Zachariah and Rastegar, 2012). TRD domain associates with transcriptional co-repressors, such as Sin3a, for recruitment of histone deacetylases HDAC1 and 2. The C-terminal domain facilitates binding to DNA and increase the stability of MeCP2. Moreover, two nuclear localization signals (NLS) induce the nuclear import from the cytoplasm (Nan et al., 1996).

MeCP2 acts as general transcriptional repressor *in vitro*. This protein binds to methylated sequences in the promoter of target gene by MDB, than RTD recruits co-repressors (e.g. Sin3a, c-Ski and N-Cor) and the histone deacetylase enzymes, resulting in histones deacetylation, chromatin condensation and repression of target gene (Kokura et al., 2001; Nan et al., 1998). MeCP2 could also repress transcription in an HDAC-independent mechanism by directly binding of TRD to transcription factor IIB and impairing transcription initiation complex assembly. (Kaludov and Wolffe, 2000). MeCP2 is also considered a chromatin remodeling enzyme, being able to recruit different chromatin remodeling complex (Harikrishnan et al., 2005) or to directly shape chromatin structure through its CTD (Nikitina et al., 2007). Moreover, MeCP2 binds to Y box-binding protein (YB-1) involved in splicing (Young et al., 2005).

Despite the characterized role of MeCP2 as a transcriptional repressor, recent studies demonstrated that MeCP2 could associate to CREB1 transcription factor and other co-activators to positively regulate the expression of target genes. This evidence was corroborated by the fact that most of targeted gene were overexpressed in mice overexpressing MeCP2. Conversely, repression or knocking-out of MeCP2 mice have opposite effects on gene expression (Chahrour et al., 2008). Besides the extensive role of MeCP2 in repression/activation of transcription, transcriptional profile studies revealed only subtle differences in gene expression of MeCP2-null mice respect to wild type mice (Tudor et al., 2002). This finding suggested the hypothesis that MeCP2 is a transcriptional regulator of selected gene during specific phases of brain development instead than a general transcriptional regulator. In fact, MeCP2 alteration during cortical development in mouse brain does not affect the number and migration of neuronal precursor in prenatal brain. Moreover, strong MeCP2 nuclear staining from first postnatal days is observable in superficial cortex layers, hippocampus and other brain tissues, following the progression of neuronal maturation (Jung et al., 2003; Kishi and Macklis, 2004).

3.2 RTT brain dysregulation: neuronal atrophy, oxidative damage and protein synthesis

Neuronal atrophy: The spatio-temporal pattern of MeCP2 expression during postnatal brain development highlights the importance of a correct expression of this transcriptional regulator in neuronal maturation and synaptic plasticity. Its mutation leads to several abnormalities in the CNS, regarding In particular, decreased brain size and neuron complexity. First evidence of neuronal atrophy was revealed in magnetic resonance analysis of brain of RTT patients, in which a global hypoplasia of brain and a reduction of gray matter in anterior temporal regions were detected (Casanova et al., 1991; Reiss et al., 1993). Analysis of post-mortem brains revealed an higher dense packaging of neuron bodies, a reduction of neuron soma and dendrite size and a diffused atrophy of both gray and white matter associated to decrease brain weight (Subramaniam et al., 1997). Following studies using Golgi staining confirmed the previous neuronal atrophy features found, identifying In particular, layer II and III of frontal, motorial and inferior temporal cortex and layer II and IV of the subiculum in hippocampus as the most affected brain regions (Armstrong et al., 1995; Belichenko et al., 1997; Kaufmann and Moser, 2000). Moreover, decreased level of MAP2 and cycloxygenase2 (COX2) proteins, which are expressed during dendritic outgrowth and pruning, were decreased in frontal and temporal regions of RTT brain (Kaufmann et al., 1995; Kaufmann et al., 1997b). Furthermore spine numbers were found decreased in frontal cortex (Belichenko et al., 1997). Analysis of hippocampal CA1 region using fluorescent dye revelead also a decreased spine density in apical dendrites of hippocampal neurons (Chapleau et al., 2009).

MeCP2B mouse strain reflects neuronal atrophy features of human RTT brain. Cortical thickness, neuronal soma size, spine density and apical dendrite diameter are reduced in somatosensory cortex of adult MeCP2$^{-/y}$ brain (Fukuda et al., 2005; Kishi and Macklis, 2004). Reduced brain weight and reduced volume of cortex, hippocampus and cerebellum are significantly decreased in MeCP2B strain respect to wild type or other RTT models (Belichenko et al., 2009). Interestingly, neuronal atrophy caused by MeCP2 mutation is resembled also in *in vitro.* MeCP2 silencing reduces dendritic length in the first stages of rat hippocampal cultured neurons, while

overexpression of MeCP2 has the opposite effect (Larimore et al., 2009). Baj and colleagues demonstrated using a staging system of *in vitro* neuronal development that MeCP2$^{-/y}$ neurons display a delayed dendritic arborization outgrowth and spine maturation. Moreover, an increased excitatory and inhibitory synapse elimination are observed after a normal initial phase of development. This finding suggested that *in vitro* models could be a useful tool for elucidating the mechanisms underlying neuronal atrophy in RTT (Baj et al., 2014). Different neurotransmitters pathways result altered in RTT patient and animal models. In particular, monoamines deregulation are detected in brain and cerebrospinal fluid of both RTT patients and mouse models. This deregulation is high in prefrontal and motor cortex in the first stage of RTT onset, while a major deficit in hippocampus and cerebellum is observed in the late phase (Santos et al., 2010).

Oxidative stress: In recent works, systemic oxidative damage has been observed in the plasma of RTT patient (De Felice et al., 2009; De Felice et al., 2012; Durand et al., 2013). Treatment of RTT patient with ω-3 polyunsaturated fatty acids (ω-3 PUFAs) significantly reduces oxidative stress and clinical severity (De Felice et al., 2013). Oxidative damage has been detected also in brain of two different mouse models of Rett syndrome, with higher levels in the early onset of pathology. Restoration of MeCP2 expression rescues the oxidative damage condition, suggesting that oxidative damage may be involved in pathogenic mechanisms of RTT (De Felice et al., 2014).

Protein synthesis deficits: Recent lines of research on autistic-related disorders (ARD) are currently converging on the hypothesis that a dysregulation of protein synthesis through the PI3K/mTOR pathway represent a common mechanisms behind spine dysgenesis in this pathologies (Phillips and Pozzo-Miller, 2015). In fact, mTOR signaling is one of the most important pathway involved in local protein synthesis during synaptic activation and consequent plasticity events; supporting this all the major ARD, from Fragile-X syndrome to RTT, present contemporary alteration of LTP/LTD and mTOR pathways (Costa-Mattioli and Monteggia, 2013; Phillips and Pozzo-Miller, 2015). According to this hypothesis the work of Ricciardi and colleagues clearly demonstrated severe defects in mTOR pathway of RTT mouse model brains. Male MeCP2$^{-/y}$ and female MeCP2$^{-/+}$ display a reduction in rpS6

phosphorylation in S1 cortex and hippocampus, with the extent of deficit worsening during ageing. Translation results generally impaired at the initiation level, with reduced polysomal incorporation for several neuronal mRNA as *CamKIIα, PSD95* and *hnRNP A2/B1.* Reduced phosphorylation of p-p70 S6K, mTOR and pAKT confirmed the severe impairment in protein translation (Ricciardi et al., 2011).

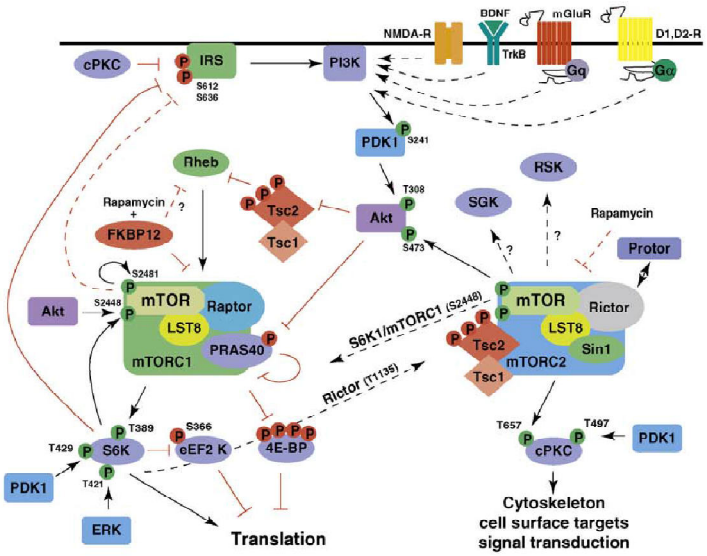

Fig. 13: mTOR signaling pathways. From Hoeffer and Klann, 2010.

Similar results were obtained in a study that employed neurons differentiated from human embryonic stem cells with a deletion of exon3 in MeCP2 gene. In this system, phosphorylation of S6 and AKt is significantly reduced and accompanied by reduced protein synthesis. Normal levels are restored by suppression of PTEN or exogenous treatment with BDNF, both known to positively regulate mTOR signaling pathway (Li et al., 2013a). Taken together, this evidence suggests that altered local protein synthesis mediated by mTOR may be involved in neuronal atrophy affecting RTT.

3.3 MeCP2 targets: BDNF and Rett syndrome

In rodents, BDNF expression is low in prenatal brain and raises dramatically during postnatal development phases, remaining stably high in the adulthood (Kolbeck et al., 1999; Maisonpierre et al., 1990). MeCP2 resemble a similar expression pattern during brain development (Kishi and Macklis, 2004). Moreover, MeCP2 protein binds

directly to *BDNF* promoter, regulating its expression (Klose et al., 2005). This evidence suggested that BDNF could be dysregulated in RTT.

Evidence of BDNF levels alteration in RTT human patient are controversial due to technical limitations in measurements. BDNF protein levels have been found unaffected in blood serum and cerebrospinal fluid of RTT patients (Riikonen, 2003). Conversely, lower *BDNF* mRNA levels have been detected in *post-mortem* brain samples of RTT patients (Abuhatzira et al., 2007; Deng et al., 2007). However, different RTT mouse models displays alterations in BDNF expression. Protein levels are mostly unaffected in the first 3-4 postnatal weeks compared to wild type mice (Chang et al., 2006; Wang et al., 2006). During the earlier phases of RTT onset, BDNF levels decrease in caudal region of brain, such as brainstem and cerebellum (Kline et al., 2010; Ogier et al., 2007; Wang et al., 2006), while after 7 weeks a general reduction of BDNF levels is detectable in entire brain of MeCP2 KO male mice (Chang et al., 2006; Li et al., 2012; Lonetti et al., 2010). Symptomatic heterozygous female displays lower BDNF levels in the entire brain with a later onset (Schmid et al., 2012).

Two major models regarding the mechanism of transcriptional regulation of *BDNF* gene by MeCP2 emerged: a repression model and an activation model. The first is supported by the evidence that MeCP2 binds to exon IV *BDNF* promoter in resting primary neurons, preventing its transcription. After KCl stimulation, MeCP2 dissociates from exon IV promoter allowing *BDNF* transcription (Chen et al., 2003; Zhou et al., 2006). MeCP2 phosporylation on Ser^{421} is critical for the release of this transcription regulator from *BDNF* promoter (Chen et al., 2003). Additionally, methylation of CpG sites in *BDNF* IV promoter is decreased after neuronal depolarization (Martinowich et al., 2003). Although this model resembles the classical mechanism of MeCP2 action, it failed to explain the lower levels of BDNF protein in MeCP2 KO brains. On the other side, several lines of evidence support an activation model for *BDNF* and MeCP2. In primary neurons, MeCP2 overexpression causes a rise in *BDNF* mRNA levels, while knocking-out *MeCP2* results in decreased exon IV transcripts level (Klein et al., 2007). This was confirmed also in hypothalamus, where BDNF and MeCP2 levels are strictly correlated (Chahrour et al., 2008). Moreover, a double point mutation in two serines induces MeCP2 association to exon IV promoter

and increased *BDNF* IV variant expression (Li et al., 2011). Colocalization between MeCP2 and the transcriptional activator CREB1 suggests that direct interaction of MeCP2 with a *BDNF* promoter is required for activation of its transcription (Chahrour et al., 2008). Recently, an indirect role for miRNA in the regulation of MeCP2 (miR212) (Klein et al., 2007) and BDNF (Wu et al., 2010) expression is emerging. Both models however fail into explaining why BDNF levels in the brain are unaltered in the first stages of RTT and then decrease at later stages (Li and Pozzo-Miller, 2014). Moreover, in MeCP2 KO neurons different splicing variants of BDNF, as I and IV, results upregulated while other downregulated (Abuhatzira et al., 2007; Ogier et al., 2007). Recently a "dual operation model" has been proposed on the basis of MeCP2 regulation of *early growth response factor-2 (EGR2)* (Gonzales et al., 2012). In this model, MeCP2 remains bound to target genes and recruits different activator or repressor transcriptional factor depending on phosphorylation status of Ser^{80} and Ser^{229} (Gonzales et al., 2012). However, the mechanisms and the role of MeCP2 in *BDNF* regulation require further research.

3.4 Pharmacological therapies for the rescue of rett syndrome

Efficient treatments for the cure of RTT are still lacking. Several lines of studies demonstrated that RTT phenotype can be reverted by the reactivation of normal level of MeCP2 expression (Gadalla et al., 2011). In particular, MeCP2 KO mice in which transgenic expression of MeCP2 under the control of *Tau* promoter is restored, display increased life span, brain weight and physical development (Luikenhuis et al., 2004). Other transgenic approach, using Cre recombinase and tamoxifene induced expression of MeCP2, confirmed the reversion of RTT phenotype (Giacometti et al., 2007; Guy et al., 2007). The reintroduction of normal levels of *MeCP2* expression is able to revert atrophic phenotype of MeCP2 KO neurons also *in vitro* (Larimore et al., 2009), supporting the previous evidence. Interestingly, conditional increased expression of *BDNF* in postnatal forebrain of MeCP2 KO brain results in reversion of neuronal atrophy (Chang et al., 2006). The ability of BDNF to rescue RTT neuronal atrophy has been also confirmed *in vitro* through BDNF overexpression (Larimore et al., 2009), exogenous administration or miR-15a downregulation (Gao et al., 2015). In conclusion, MeCP2 restoration and BDNF expression represent two possible candidates for RTT treatment. However, the gene therapy approach (Gadalla et al., 2011) or BDNF exogenous administration are actually not suitable for a therapy in

RTT due to dosage, correct expression and delivery issues that have still to be resolved.

Recently, pharmacological treatment for the regulation of expression or downstream effectors of BDNF in RTT models have been employed. AMPAkine CX546 compound induces desensitization to AMPA-type glutamate receptor, increasing BDNF levels and ameliorating respiratory frequencies and rescuing brain volume in MeCP2 KO mice (Ogier et al., 2007). Two different TrkB activator improve lifespan and cardio-respiratory functions in RTT mice (Johnson et al., 2012; Schmid et al., 2012). A clinical trial with insuline-growth factor-1 (IGF-1) therapy, that was demonstrated to raise BDNF level and improve RTT mice lifespan and cardio-respiratory phenotype, is currently underway (Tropea et al., 2009).

A different approach using antidepressants (ADs) for the cure of RTT have emerged in last years. Alterations in monoamine levels, as norepinephrine (NE), serotonin (5HT) and dopamine (DA), have been reported in brain and cerebrospinal fluid of both RTT patients and mouse models (Santos et al., 2010). BDNF and monoamine deficits were reported also in major depressed patients. AD treatment is known to increase BDNF levels and its downstream signaling in hippocampus and prefrontal cortex (Castren et al., 2007). Moreover, ADs that enhance serotoninergic and noradrenergic pathway induced an increased expression of *BDNF* mRNA in rat brain (Coppell et al., 2003; Dias et al., 2003; Jacobsen and Mork, 2004). Desipramine, a selective inhibitor of NE reuptake, has been used to treat MeCP2 KO mice. Despite the amelioration of respiratory deficits and lifespan, (Roux et al., 2007), Desipramine induced heart failure during clinical trials. Recently, a novel promising approach using Mirtazapine (1,2,3,4,10,14b-hexa-hydro-2-methylpyrazinol [2,1-alpyridol[2,3-c][2]benzazapine) for the cure of RTT has been reported. Mirtazapine enhances serotoninergic and noradrenergic pathways via an antagonistic action on α2-adrenergic autoreceptors and heteroreceptors and the blockade of 5-HT2 and 5-HT3 receptors (Holm and Markham, 1999) and has been demonstrated to be devoid of cardio-respiratory side-effects (Burrows and Kremer, 1997; Hartmann, 1999). Chronic treatment of rats with Mirtazapine increases the expression of *BDNF* mRNA in hippocampus and cerebral cortex (Rogoz et al., 2005). Treatment of MeCP2$^{-/y}$ mice for 2 weeks rescues cortical thickness and brain weight and results in full recovery of

neuronal atrophy of pyramidal neurons of somatosensory cortex. Hearth rate, breath rate and anxiety levels resulted normalized after treatment. Finally, GABAergic and glutamatergic receptor activity are restored (Bittolo et al., 2016).

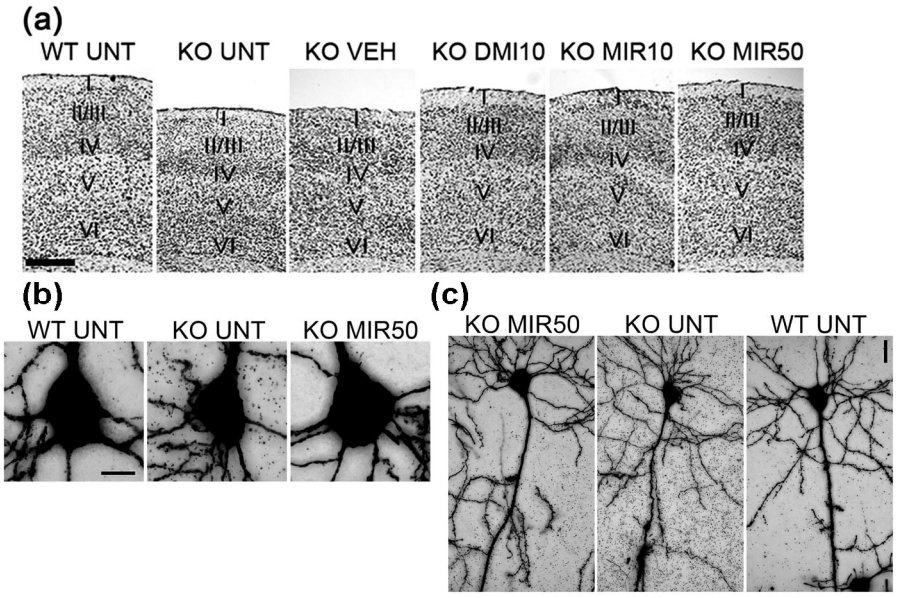

Fig. 14: Rescue of neuronal atrophy after Mirtazapine treatment in RTT. (a) Nissl staining of somatosensory cortex in wild type and MeCP2 KO neurons untreated or treated with mirtazapine. (b-c) Golgi staining of pyramidal cortical neurons of wild type and MeCP2 KO neurons. (from Bittolo et al., 2016)

These findings suggest that enhancement of BDNF expression through selective modulation of monoaminergic pathway could represent a promising way for the treatment of RTT. However the molecular mechanisms underlying neuronal atrophy and its rescue in RTT have to be further investigated.

AIMS

Dendritic trafficking and local synthesis of *brain-derived neurotrophic factor* (*BDNF)* mRNA is a mechanism involved in correct neuronal development, spinogenesis and synaptic plasticity. The mechanisms of BDNF mRNA localization in neurons has been deeply investigated in various studies. It is now clear that the different *BDNF* transcript variants act collectively as a spatial code for dendritic localization. BDNF coding sequence is bound by Translin which provide a constitutively active signal for dendritic targeting of this mRNA. In contrast, 5'UTR splicing variants act as selectivity signals for this targeting, inducing retention in proximal segments (exon1 and 4) or the localization in distal dendrites (exon 2 and 6). Finally, 3'UTRs sequences regulate activity dependent trafficking, responding selectively to neurotrophic (BDNF and NT-3) stimuli and requiring different subset of RNA binding proteins (RBPs): the cytoplasmic polyadenylation element binding proteins (CPEBs), the Embryonic Lethal Abnormal Vision-like proteins (ELAVLs) and the Fragile-X Mental Retardation Protein (FMRP). However, two aspects of this complex mechanism were not clarified and were investigated in this work:

- If the 5'UTR variants alone, without CDS, encode signals that regulate dendritic trafficking or soma retention;
- If ELAVs and FMRP physically bind to *BDNF* mRNA and what is the grade of association of the different RBPs family members with this transcript

In this study we also focused our attention on Rett Syndrome, an X-linked neurodevelopmental disorder affecting 1:10.000 females. RTT is characterized by altered levels of BDNF and a general neuronal atrophy reported both *in vivo* and *in vitro*. Moreover a systemic condition of oxidative stress was reported. Furthermore, general translation levels and mammalian target of rapamycin (mTOR) signaling pathway are known to be severely impaired. Despite this evidence, little is known about specific deficits in BDNF mRNA trafficking and RBP machinery in dendrites. In fact, trafficking and local protein synthesis of BDNF is crucial for LTP onset and consolidation, spine maturation and neurites outgrowth. Additionally, mTOR signaling is the most important pathway involved in local protein synthesis induced by BDNF in spines. Mutations in RBP, such as Fmr1, are known to alter *BDNF* localization and to alter synaptic plasticity. Finally, RBPs were also involved in the response to oxidative

stress through the nucleation of stress granules. For this reason, we used MeCP2$^{-/y}$ hippocampal neurons of a well characterized RTT mouse model to evaluate:

- If *BDNF* mRNA localization into dendrites is altered
- If most representative classes of mRNA granules (transporting granules, stress granules and processing bodies) in dendrites displayed the same features in terms of numbers, dimensions and density
- If mRNA trafficking machinery respond correctly to neurotrophic stimuli and to oxidative damage

In parallel, we used the same mouse model to perform a morphological rescue of neuronal atrophy in RTT syndrome. Mirtazapine is a selective antagonist of α2-adrenergic autoreceptors and heteroreceptors and a blocker of 5-HT2 and 5-HT3 receptors, and it's known to raise BDNF levels in rat brain after chronic administration. A recent work by Bittolo and colleagues demonstrated that chronic administration of Mirtazapine rescues neuronal atrophy deficits in the brain of RTT mouse. Using a well characterized *in vitro* staging system for the study of neuronal atrophy we treated MeCP2$^{-/y}$ cultured neurons with Mirtazapine to evaluate:

- If a chronic (9 days) treatment with Mirtazapine induce a rescue of neuronal atrophy also *in vitro*
- If an acute (3 days) treatment with Mirtazapine induce a rescue of neuronal atrophy also *in vitro*

The possibility to reproduce in vitro the same effects of Mirtazapine observed in vivo will validate the use of MeCP2$^{-/y}$ cultured hippocampal neuron for screening of further drugs for the rescue of neuronal atrophy and oxidative stress in RTT.

MATHERIALS AND METHODS

1. Animal treatment

Animals were treated according to the institutional guidelines in compliance with national laws (Decreto Legge N116, Gazzetta Ufficiale, suppl 40, 18-2-1992), the European Council Directive 86/609 and NIH Guide for the Care and Use of Laboratory Animals. Animals were housed in groups under standard animal room conditions (12:12 h light/dark cycle, ambient temperature 23°C, ad libitum access to food and water).

C57/BL6 were purchased from Charles River laboratories (Calco, LC, Italy). Female MeCP2 heterozygous (Guy et al., 2001) (B6-129P"(C)-Mecp2tm1.1Bird/J strain, stock number: 003890) were purchased from Jackson Laboratories and bred with wild type C57/BL6 male to obtain wild type and hemizygous male littermates.

2. Primary hippocampal neuronal cultures

Primary rat hippocampal neuronal cultures were prepared from p0-p2 Wistar pups as previously describe (Tongiorgi et al., 1997) with slight modifications. The hippocampi were dissected and collected into tube with ice-cold Hanks balanced solution (HBSS; 4.2 mM $NaHCO_3$, 12 mM Hepes, 33 mM D-glucose, 2 mM Kinurenic acid and 0.95% Hank's salt powder, all purchased from Sigma). Tissue was digested for 8 minutes with trypsine 0.25% (Euroclone) in HBSS solution, then an equal volume of DMEM (Euroclone) supplemented with penicillin/streptomycin (Eurocolone) and 10% fetal bovine serum (FBS, Euroclone) was added to stop enzymatic digestion. Digested tissue was centrifuged at room temperature for 5 minutes at 800 rpm, supernatant was removed and replaced with pre-warmed DMEM + 10% FBS. Tissue was homogenized by pipetting, the homogenate was filtered through a 40 µm cell strainer (Falcon DB). Cells was plated at a density of 1 x 10^5 cells in a 24 multi-well plate (Sarstedt) on 12 mm cover glasses (Sacco) pre-treated with 0.1% poly-ornithine (Sigma) and coated with 2% Matrigel (BD science). After one hour, medium was replaced with fresh pre-warmed Neurobasal (Invitrogen) supplemented with B-27 (Invitrogen) and penicillin-streptomycin. Medium supplemented with 0.5 µM Cytosine β-D-arabinofuranoside (Sigma) was replaced at days *in vitro* (DIV) 2 to stop non neuronal cell proliferations. Half medium was changed twice a week.

Primary hippocampal cultured neurons from Mecp2 null mice (Mecp2$^{tm1.1Bird}$ C57BL/6) were prepared as described above with slight modifications. Separated Petri dishes and tubes were used for each animal in order to obtain pure cultures from single animal brain. After sacrifice, approximately 1 mm of tail was collected to perform the genotyping. Cell homogenate from two hippocampi of a single mouse was plated on 4 wells (approximately 0.8x10^5 cells/well) of 24-well plate.

3. Genotyping

Tails were collected in a 1.5 ml vial and incubated at 55°C in digestion buffer composed by 100 mM Tris-HCl pH 8.0 (Sigma), 200 mM NaCl (sigma), 5 mM EDTA (Sigma), 0.2% sodium dodecyl sulfate (Sigma) and 0.1 mg/ml proteinase K (Roche). Samples were spinned to pull down undigested tissue debris, than supernatants were collected and an equal volume of 2-Propanol (Sigma) was added to precipitate DNA. Sample were centrifuged at 4°C for 20 minutes at 13000 rpm, supernatant was removed and DNA pellet was washed with 30% water/70% ethanol (Sigma) solution. Dried pellet was dissolved in deionized water.
PCR reaction to determine animal genotype was carried out using GoTaq G2 flexi polymerase (Promega) following manufacturer instructions. Primer used were purchased by Jackson Laboratory with the following sequences: 5'-AAATTGGGTTACACCGCTGA-3' (Common Forward 9875, Jackson Laboratory), 5'-CTGTATCCTTGGGTCAAGCTG-3' (Wild Type Reverse oIMR7172, Jackson Laboratory), 5'- CCACCTAGCCTGCCTGTACT-3' (Mutant Reverse 9877, Jackson Laboratory). PCR parameters were set as followed: Denaturation 94°C for 3 minutes, Denaturation 94°C for 30 seconds, Annealing 58°C for 35 seconds, Elongation 72°C for 35 seconds (30 cycles), Final elongation 72°C for 2 minutes. PCR products were separated on a 1.5 % agarose gel with Gel Red 0,0001% (Biotium). PCR products from wild type mice displayed a single band of 465 base pairs, while those of mutant mice displayed a single band of 240 base pairs.

4. Cell line cultures

Hek293T cell line were cultured in DMEM supplemented with 10% FBS in an 5% CO_2 humidified incubator. In order to perform immunofluorescence, cells were plated on 12 mm cover glasses at approximately 3x10^4 cell per well in a 24 multi-well plate.

After 24 hour from plating cells were treated with 0.5 mM sodium arsenite (Sigma) alone or in the presence of 20 µg/ml cycloheximide (Sigma) for 1 hours. After treatment cells were fixed in 4% paraformaldehyde in PBS at room temperature for 15 minutes.

5. Primary hippocampal neurons transfection

Rat hippocampal cultured neurons were transfected at DIV6 with different constructs using Lipofectamine 2000 (Invitrogen) following manufacturer instructions. 2 µl of Lipofectamine 2000 and 1 µg of plasmid DNA (exon 1, 2a, 2b, 2c, 3, 4, 5, 6, 7, or 8 - GFP chimaeric constructs) were used for each well. After one hour, medium with transfectant reagent was removed and replaced with fresh medium. After 24 hours from transfection, cells were depolarized in a solution of 10 mM KCl, 1.8 mM $CaCl_2$, 1.6 mM $MgSO_4$, 100 mM NaCl, 26 mM $NaHCO_3$, 1mM NaH_2PO_4, 30 mM HEPES and 0.7% D-Glucose. All reagents were purchased from Sigma. After 3 hours of depolarization, treated and untreated cells were fixed in a 4% paraformaldehyde in PBS at room temperature for 15 minutes to perform *in situ* hybridization.
Mouse hippocampal cultured neurons from wild type or from $MeCP2^{-/y}$ were transfected at DIV9 as described above with slight modification. 1 µg of pEGFP-N1 (Clonetech) DNA were used for each well. After one hour, medium with transfectant was replaced with fresh medium supplemented with the different pharmacological treatments (see below). Cells were fixed at DIV12 in a 4% paraformaldehyde (PFA) in PBS at room temperature for 15 minutes.

6. Immunofluorescence protocol

For immunofluorescence assays, cells were fixed for 15 minutes at room temperature in 4% PFA in PBS. Permeabilization of cellular membranes was performed using PBS 0.1% Triton X-100 (PBSxT) for 15 minutes at room temperature. Blocking of unspecific sites was obtained by incubating coverslips with PBSxT and 2.5% bovine serum albumin (BSA; Sigma). Blocking solution was removed and incubation in primary antibody was performed, with antibodies diluted in blocking solution as following: anti-TIA-1 (Santacruz) 1:100, anti-DCP1a (Abnova) 1:100, anti Staufen1 (Abcam) 1:100, anti Map2 (Sigma) 1:200, anti-Map2 (Santacruz) 1:200. Primary antibodies were incubated for 2 hours at room temperature. Excess of primary

antibody was washed with PBS, then coverslips were incubated for 1 hour at room temperature with the following secondary antibodies all diluted 1:200 in blocking solution: anti-rabbit alexa fluor 488/568/647 (Invitrogen), anti-mouse alexa fluor 488/568 (Invitrogen) and anti-goat 488/647 (Invitrogen). After washing, the excess of secondary antibody was washed away with PBS, nuclei were stained with Hoechst 33342. Finally, coverslips were mounted with Mowiol (Sigma).

7. *In situ* hybridization and Fluorescent *in situ* hybridization (F.I.S.H.)

In situ hybridization was performed as previously described (Tongiorgi et al., 1997) with slight modifications. Cells were fixed for 15 min at RT in 4% PFA in PBS, washed in PBS 0.1% Tween20 (Sigma) (PBST), and permeabilized in absolute ethanol for 15 min at -20°C. After rehydration with increasing concentration of PBST (50% ethanol/50% PBST, 30% ethanol/70% PBST and finally PBST), cells were hybridized with approximately 50-100 ng/coversplip of antisense or sense probes for *GFP* or *BDNF* coding sequence. Before probe hybridization, coversplips were equilibrated at 55°C in hybridization buffer containing 20 mM Tris-HCl pH 7.5 (Sigma), 300 mM NaCl (Sigma), 1mM EDTA (Sigma), 0.5 mg/ml polyadenylic acid (Sigma), 0.5 mg/ml salmon sperm (Labtek Eurobio), 1X Denhardt's solution, 100 mM Dithiothreitol (DTT, Sigma) and 50% deionised formamide (Sigma). After 1 hour, hybridization buffer was removed and replaced with the hybridization mix (hybridization buffer + 10% dextran sulfate, Sigma) containing probes. Coverslips were incubated over night at 55°C. After that, hybridization mix was removed, coverslips were washed with 2X Sodium Saline Citrate (Sigma) buffer (150 mM NaCl, 15mM $C_6H_5Na_3O_7$) containing 0.1% Tween20 (SSCT 2X) and 50% formamide at 55°C twice, then with SSCT 2X at 55°C once and finally in SSCT 0.1X at 60°C twice. Coverslips were incubated with PBST 5% fetal bovine serum (FBS; Euroclone) for 1 hour at room temperature to block unspecific binding of primary antibodies, then incubated with anti-digoxigenin alkaline phosphatase conjugated antibody (Roche) in PBST 5% FBS for 2 hours at room temperature. After washing with PBST to remove the excess of unbound antibody, hybridized probes were detected by developing *in situ* signal with 70 mg/ml 4-nitroblue tetrazolium (NBT, Labtek Eurobio) and 50 mg/ml 5-bromo-4-chloro-3-indolyl-phosphate(BCIP, Sigma) in a buffer solution containing 100 mM Tris-HCL pH 9.5, 50 mM $MgCl_2$, 100 mM NaCl and 1 mM Levamisol (Sigma). Developing was carried out in the dark and time of incubation was

determined empirically. Reaction was stopped by removing developing buffer and replacing it with a stop solution containing 10 mM Tris-HCl pH 8.0 and 1 mM EDTA pH 8.0. Coverlips were washed with PBS and deionised water and then mounted with Mowiol (Sigma).

For fluorescent *in situ* hybridization, after PFA fixation cells were incubated with 0,3% H_2O_2 in PBS for endogenous peroxydase quenching. After probe hybridization and stringency washes, coversplis were incubated first with a blocking solution (TNB, Perkin Elmer) for 1 hour, then with anti-digoxigenin horse-radish peroxidise conjugated (Roche) diluted 1:300 in TNB at room temperature for 1h. HRP detection was performed using Tyramide System Amplification kit – Cyanine 3 coupled or Tyramide Plus System Amplification kit – Cyanine 3 (Perkin Elmer) following manufacturer instructions. After three washes in Tris NaCl Tween buffer (TNT; 100mM Tris-HCl pH 7.5 buffer, 150 mM NaCL, 0.05 % Tween 20), cells were incubated with the primary antibodies against different RNA binding proteins diluted in PBST/FBS 5% as following: anti-CPEB2 (Life Span) 1:50, anti-CPEB3 (Abcam) 1:50, anti-CPEB4 (Abcam) 1:50, anti-Elav1 (Abcam) 1:50, anti-Elav2 (Abcam) 1:200, anti Elav3 (Santacruz) 1:50, anti-Fmrp (Abcam) 1:100, anti-Fxr2 (Abcam) 1:100, anti-Translin (kind gift of prof. Baraban) 1:200, anti-TIA-1 (Santacruz) 1:50, anti-DCP1a (Abnova) 1:100, anti Staufen (Abcam) 1:50, anti Map2 (Sigma) 1:200, anti-Map2 (Santacruz) 1:200. The following secondary antibodies were diluted in blocking solution 1:200 and incubated for 1 hour at room temperature: anti-rabbit alexa fluor 488/647 (Invitrogen), anti-mouse alexa fluor 488/647 (Invitrogen) and anti-goat 488/647 (Invitrogen). Nuclei were stained with Hoechst 33342 and coverslips were mounted with Mowiol (Sigma).

8. Digoxigenin-labeled probes synthesis

Probe synthesis was performed as previously described (Chiaruttini et al., 2009). The open reading frame of GFP or BDNF CDS were subcloned into pBluescript or pGEM vectors respectively and DIG-labeled probes were synthesized with DIG-RNA labelling kit (Roche Diagnostics) using linearized plasmids as templates, according to the manufacturer's instructions. GFP sense and antisense probe were fragmented through alkaline hydrolysis in a carbonate buffer (40 mM $NaHCO_3$, 60 mM Na_2CO_3, pH 10.2) in order to increase probe penetration into cells.

9. Cloning and generation of *BDNF* 5'UTRs exons-pEGFP-N1 constructs

All the different 5'UTR isoforms (exon 1, 2a, 2b, 2c, 3, 4, 5, 6, 7, 8) of rat *BDNF* gene were cloned into a pEGFP-N1 vector (Clonetech) to obtain the expression of the chimaeric transcript 5'UTR *BDNF* exon - GFP coding sequence. Total RNA was extracted from adult rat brain using TRIzol (Thermofisher) and retro-transcribed to cDNA using Superscript-II transcriptase (Promega). Forward primers for 5'UTR exons cloning introduced a XhoI restriction site into the amplicon, while reverse primers introduced an AgeI restriction site. Amplification of the specific exon sequences were obtained using Phusion high-fidelity DNA polymerase (Finnzymes). Primers and condition used for the cloning of the specific 5'UTR sequences were reported in table 1. Amplified sequence were isolated on agarose gel using GenElute Gel extraction kit (Sigma) and then cloned into pEGFP-N1 vector digested with XhoI and AgeI restriction enzymes. Ligase reaction was performed using T4-DNA ligase. All restriction and ligase enzymes were purchase from New England Biolabs.

10. Densitometric analysis on non-radioactive *in situ* hybridization

Non-radioactive *in situ* hybridization for GFP coding sequence was analyzed by viewing stained cultures under bright-field illumination as previously describe (Chiaruttini et al., 2009; Tongiorgi et al., 1997) with slight modifications. The positive transfected neurons were acquired by a Nikon AXM1200 digital camera on a Nikon E800 Microscope with interference contrast-equipped lens (60x magnification) and then analyzed with the image analysis program ImageJ (NIH), using the “Straighten” plugin, on apical dendrites of bona-fide pyramidal neurons identified by morphological criteria. Dendrites were traced in a conservative manner, starting from the base of dendrite after soma and up to the point in which *in situ* labeling was clearly distinguishable. Background level for each image was determined by evaluation of the mean gray value in the distal portion of apical dendrites of transfected neurons in which *in situ* labeling was not present.

At least 50 neurons from 3 or 4 independent cultures were analyzed for GFP, exon 1, 2a, 2b, 2c, 4 and 6 densitometric analysis, while at least 30 neurons from 2 - 4 independent cultures were analyzed for exon 3, 5, 7 and 8.

Densitometric analysis on fluorescent *in situ* hybridization for *BDNF* coding sequence was performed on confocal images acquired as described in the next part of this

chapter. 3D multi-stacks images of MAP2 and BDNF channels were projected in a 2D image using Z-project function of ImageJ. Resulting images were maximum projection of the signal in all stacks. MAP2 staining was used to trace the linear ROI (width 2 µm) following the apical dendrite until clearly distinguishable. The ROI obtained from this tracing was applied to FISH channel and mean gray value along the ROI was measured. At least 20 neurons from two different cultures were analyzed for each condition.

	Primer Forward	**Primer Reverse**	**PCR CONDITIONS**			
Exon I	AATTCTCGAGTAAAGCGGTAGCCGGCTGGTGCAGG	GTCTACCGGTTTTGCTGTCCTGGAGACTCAGTGTC	Denaturation	98°C	10 sec	31 cycles
			Annealing	57°C	20 sec	
			Extension	72°C	40 sec	
Exon IIa	GATCCTCGAGGCTTTGGCAAAGCCATCCGCACGTGAC	GCCACCGGTCTGGATGAAGTACTACCACCTCGGAC	Denaturation	98°C	10 sec	31 cycles
			Annealing	58°C	20 sec	
			Extension	72°C	35 sec	
Exon IIb	GATCCTCGAGGCTTTGGCAAAGCCATCCGCACGTGAC	GTTACCGGTGGAGCTTGCCAAGAGTCTATTCCAG	Denaturation	98°C	10 sec	31 cycles
			Annealing	58°C	20 sec	
			Extension	72°C	35 sec	
Exon IIc	GATCCTCGAGGCTTTGGCAAAGCCATCCGCACGTGAC	GAAACCGGTCTTCTTTGCGGCTTACACCACCCCGGTGGCTAG	Denaturation	98°C	10 sec	31 cycles
			Annealing	58°C	20 sec	
			Extension	72°C	35 sec	
Exon III*	AGGCTCGAGGCCCTCACGATTCTCGCTGGATAG	GCTAACCGGTCTGGGCTCAATGAAGCATCCAGCCC	Denaturation	94°C	15 sec	31 cycles
			Annealing	55°C	15 sec	
			Extension	68°C	20 sec	
Exon IV	AATTCTCGAGACCCACTTTCCCATTCACCGAGG	GACTACCGGTCAGTCACTACTTGTCAAAGTAAACATCAAGGC	Denaturation	98°C	10 sec	31 cycles
			Annealing	58°C	20 sec	
			Extension	72°C	20 sec	
Exon V	GACTCTCGAGAAACCATAACCCCGCACACTCTGTGTAGTTTCATTGTGTGTTCG	GACTACCGGTCTTCCCGCACCTTCCCGCACCACAGAGCTAGAAAAAGCGAACACAC	Denaturation	98°C	10 sec	31 cycles
			Annealing	58°C	20 sec	
			Extension	72°C	15 sec	
Exon VI**	GACTCTCGAGCCAATCGAAGCTCAACCGAAGAGC	GATCACCGGTCTCAGGGTCCACACAAAGCTCTCGG	Denaturation	98°C	10 sec	31 cycles
			Annealing	57,5°C	20 sec	
			Extension	72°C	15 sec	
Exon VII	GACTCTCGAGCACTGTCACCTGCTTTCTAGGGAGTATTACC	GTACACCGGTCTCCCGGATGAAAGTCAAAACTTTCACTTCCTCTGGAGG	Denaturation	98°C	10 sec	31 cycles
			Annealing	58°C	20 sec	
			Extension	72°C	20 sec	
Exon VIII	GTCACTCGAGGTTATAGAGTTGGATGCAAGCGTAACCCG	GCATACCGGTGACACCATTTTCAGCAATCGTTTGTTCAGCTCC	Denaturation	98°C	10 sec	31 cycles
			Annealing	58°C	20 sec	
			Extension	72°C	35 sec	

Table 1: Primers and PCR conditions for *BDNF* 5'UTR cloning

11. Protocol for CLIP

The CLIP (Cross-Linking and Immunoprecipitation) assay for ELAV was performed as previously described by Ratti and colleagues (Ratti et al., 2006) and for FMRP

was carried out using brains lysates from WT and *Fmr1*-KO mice as described by Davidovic and colleagues in 2011(Davidovic et al., 2011). Radiolabeled riboprobes for BDNF 3'UTR sequences were obtained by transcribing pBluescript KS containing BDNF 3'UTR short, 3'UTR mid and 3'UTR end sequences. Oligos and conditions used for *BDNF* coding sequence RT-PCR on CLIP were the following: forward primer 5'- GAAGTAAACGTCCACGGACAA -3', reverse primer 5'- GATGTCGTCGTCAGACCTCTC -3', denaturation 95°C 30'', annealing 56°C 10'', elongation 72°C 30'' for 40 cycles. PCR oligos and conditions used for Pgk1 and Map1b were previously described by Edbauer and colleagues in 2010 (Edbauer et al., 2010).

12. Bioinformatic Analysis

Analysis of evolutionary conserved regions in *BDNF* CDS and 3'UTRs was performed using phastCons alignment software (Siepel et al., 2005).

The research of putative *cis*-elements for RNA Binding Proteins on rat BDNF 5'UTR sequence was performed using RBPDB database (http://rbpdb.ccbr.utoronto.ca). A threshold of 0.8 was set, then FASTA sequence were scanned by algorithm.

The research of putative cis-elements for RNA Binding Proteins on rat BDNF 3'UTR sequence was performed using Bioedit software (http://www.mbio.ncsu.edu/BioEdit/bioedit.html) and RBPDB database (http://rbpdb.ccbr.utoronto.ca). The RNA motifs reported in literature for the cited RBPs were pairwise aligned on the target sequence and at least 80% homology was set as threshold to define a putative cis-element.

13. Confocal microscopy

Confocal images were acquired by Nikon Eclipse C1 confocal microscope system on a Nikon TE-2000U inverted microscope with a Plan-Apochromat 60x/1.4 oil-immersion objective lens. Sequential scanning laser was used to avoid cross talk between different fluorochromes. Only pyramidal neurons with clear dendrites were acquired. Voxel dimensions were 80 nm for XY and 200-250 nm for Z.

14. Colocalization analysis

Rat hippocampal neurons were cultured, fixed at DIV7 and processed for F.I.S.H. coupled to immunofluorescence as described above. Regions of interest (ROI) had a 10 x 5 x 2.4 µm size located in the proximal (10 µm far from soma) and distal (at least 60 µm far from soma) compartments of apical dendrites. After ROI selection, images were cropped, then background was automatically subtracted using Imaris software (Bitplane) background subtraction module with filter width of 1 µm. Images were then deconvolved using Huygens software with classical CMLE algorithm using a signal to noise ratio (SNR) of 20. "Coloc" function of Imaris was used to perform colocalization analysis. Automatic threshold was applied to each image before Mander's coefficients calculation for colocalization analysis with CPEBs, ELAVs and FXRPs proteins.

Colocalization analysis of *BDNF* mRNA with TIA-1 and Dcp1a was performed as described above with slight modifications. SNR value of 10 was applied for TIA-1 and Dcp1a signal. Threshold for colocalization analysis was evaluated following guidelines reported in this chapter, paragraph 16.

At least 20 neurons from 3 independent cultures were measured for colocalization analysis with CPEBs, ELAVs and FXRPs, while at least 10 neurons from 2 different cultures were analyzed for TIA1 and DCP1a colocalization profile.

15. Western Blot

Primary hippocampal neurons from wild type or MeCP2 null mice were treated at DIV12 with 0.5 mM arsenite or 1% PBS for 1 hour. After a quick wash in ice cold PBS, cells were lysated using cold extraction buffer (150 mM NaCl, 1.0 % Triton X-100, 0.5% sodium deoxycholate, 0.1% SDS, 50 mM Tris pH 8.0, 1mM EDTA pH 8.0, protease inhibitors cocktail). Lysates were collected in pre-cooled microcentrifuge tubes, passed through insulin syringe to disaggregate genomic DNA and stored at -80°C until use.

Protein concentration of samples was determined by Bradford protein assay (Sigma). 30 µg of total protein were boiled in Laemmli buffer (2% SDS, 10% Glycerol, 60 mM Tris-HCl pH 6.8, 100 mM DTT), separated by SDS-PAGE on 12% polyacrylamide gel and blotted electrically on nitrocellulose membrane. Blotted membrane was first

blocked for 1 hour at room temperature with PBST and 5% non fat milk and then incubated over night at 4°C in the same solution with different primary antibodies diluted as following: anti Staufen1 (Abcam) 1:1000; anti TIA-1 (Santacruz) 1:500; anti Dcp1a (Abnova) 1:1000; anti-Actin (Sigma) 1:2000; anti MeCP2 (sigma) 1:10000. Membrane was washed three times in PBST and incubated 1 hour at room temperature with the following secondary antibodies diluted in blocking solution: anti mouse-HRP conjugated (Sigma) 1:10000; anti rabbit-HRP conjugated (Sigma) 1:10000; anti goat-HRP conjugated (Dako) 1:2000. Membrane was washed three times in PBST and HRP detection was performed using chemiluminescent substrate ECL plus (GE Healthcare) and X-ray films (Aurogene). Membrane was eventually stripped from antibodies by incubating it at 50°C in a stripping solution (2% SDS, 62.5 Tris HCl pH 6.8, 0.8 % β-mercaptoethanol; all purchased by Sigma) for 30 minutes, rinsed in water, washed in PBST and blocked again with PBST and 5% non fat milk.

Western blot quantification was carried out using Quantity One Analysis software (Bio-Rad). Two independent western blot analysis on lysates from two different cultures were analyzed.

16. Transporting granules, Stress granules and Processing bodies analysis

Primary hippocampal neurons from wild type or MeCP2$^{-/y}$ mice were treated at DIV12 with 1% PBS, 0.5 mM sodium arsenite, 50 ng/ml BDNF (Alomone) and NT-3 (Alomone) for 1 hour. After treatment coversplis were fixed and processed for immunofluorescence or fluorescent *in situ* hybridization.

Images were acquired at confocal microscope, then background was subtracted using Imaris software (Bitplane) background subtraction module with filter width of 1 µm. Images were deconvolved using Huygens software with classical CMLE algorithm using a signal to noise ratio (SNR) of 10. Stacks were realigned to correct possible misalignment and compressed to a unique stack using z-stack project function of ImageJ (NIH). Maximum projection option was selected in order to keep signals comparable between different images.

Each image were binarized by applying a threshold, in order to create the masks for the analysis of individual ribonucleoprotein particles (RNP). For this purpose five *bona fide* RNP were detected into the soma and apical dendrite, then they were

selected using a circle ROI with fixed diameter of 0.56 µm for all RNP and 0.96 µm for arsenite induced stress granules. Threshold were calculated for each ROI selected, then the average of the five threshold was applied to the whole neuron. Watershed filter (ImageJ) was applied to thresholded image to separate adjacent spots.

Particle analysis was performed on binarized images to highlight RNP masks using analyze particle tool of ImageJ. Only particles that had at least a 4 pixels aggregate dimension (approximately 160 nm of diameter) and a circularity of 0.2 were considered. ROIs obtained from particle analysis were used on 2D maximum projected images to analyze the size (RNP area expressed in μm^2), the intensity (the average gray level of the RNP expressed in arbitrary units) and the number (n° of RNP/µm) of the RNPs. Measurements were carried out on the first 100 µm of apical dendrite.

Masks obtained from thresholded images of TIA-1 and DCP1a or Staufen1 channels were overlaid in order to evaluate the percentage of TIA-1 positive granules that retained docking RNP on their surface. In order to be considered positively docked the granules had to fulfill the same conditions of the particle analysis (dimension and circularity) and had to display an overlap between the two masks. The percentage of TIA-1 granules with RNP docked on their surface (dTIA1) is given by the formula 100 * dTIA1/total TIA1 granules.

At least 10 neurons from 2 independent cultures were analyzed for each condition.

17. Pharmacological treatment of MeCP2$^{-/y}$ neurons

Wild type and MeCP2$^{-/y}$ primary neuronal cultures were obtained as described above. At DIV3 the following compounds were added to culturing media: 50 µM Serotonin hydrochloride (5-HT, Sigma) and 50 µM (-)-Norepinephrine (NE, Sigma), 10 µM Mirtazapine (Abcam) and ≤1% of PBS/DMSO (Sigma) as vehicle treatment. Media supplemented with these compounds were replaced at DIV6 and DIV9, after transfection of pEGFP-N1 with Lipofectamine 2000. Alternatively, treatments started at DIV9, after media replacement following transfection. In both cases (chronic treatment, 9 days; acute treatment, 3 days) coverslips were fixed at DIV12, stained for MAP2 protein and nuclei and mounted with mowiol (sigma).

18. Morphological analysis of GFP positive neurons

Images of neurons transfected with pEGFP-N1 plasmid were acquired on a Nikon Eclipse E800 epifluorescence microscope with a 20X objective and a Nikon DXM1200 camera. The same acquisition parameters were maintained between different treatment within the same experiment in order to have comparable morphological measurements.

Morphological parameters measured were: total dendritic length (the length of the whole dendritic arborization of a single transfected neuron), number of primary dendrites (the number of dendrites originated directly from soma) and number of secondary dendrites (the number of dendrites originated from primary dendrites and other secondary dendrites; higher orders beyond secondary dendrites were considered as the same).

Analysis was carried out as previously described (Baj et al., 2014) using ImageJ plugin NeuronJ on 8-bit gray scale images adjusted for brightness and contrast in order to improve dendrites tracking efficiency by the algorithm. Dendritic trees were analyzed separately starting from apical dendrite.

Neurons with less than three primary dendrites were excluded from the analysis.

At least 30 neurons from 2-3 independent cultures were analyzed for chronic or acute treatments measurements.

19. Statistical analysis

Statistical data analysis and graph generation were carried out using Sigma Plot 11 software (Systat Software Inc.). Student's t-test and Mann-Whitney Rank Sum test were used for the comparison of two groups. One-way Anova and Kruskal-Wallis Anova on ranks were used to compare multiple groups. Comparison against a control group or multiple comparison were carried out using Dunn's method. The following tests were used in the different experiments:

- 5'UTR-GFP densitometries: Kruskal-Wallis Anova on ranks for exon-GFP untreated or depolarized vs GFP control or depolarized condition in all exon-GFP experiments; ***, p≥0.001, **, p≥0.01, *, p≥0.05, exon-GFP ctrl vs GFP ctrl and exon-GFP KCl vs GFP KCl; ###, p≥0.001,##, p≥0.01, #, p≥0.05 exon-GFP ctrl vs exon-GFP KCl.

- Colocalization analysis with CPEBs, ELAVLs and FMRPs: Student's t-test and Mann-Whitney Rank Sum test for proximal vs distal compartment comparison in colocalization experiments of *BDNF* mRNA with CPEBs, ELAVs and FXRPs proteins; ***, p≥0.001, **, p≥0.01, *, p≥0.05, proximal vs distal compartment.
- *BDNF* F.I.S.H. densitometric analysis, RNPs analysis, Colocalization analysis with TIA-1 and Dcp1a: Kruskal-Wallis Anova on ranks to compare BDNF, NT-3 and Arsenite treatments to their respective vehicle condition for wild type and MeCP2 knock-out neurons; ***, p≥0.001, **, p≥0.01, *, p≥0.05 NT-3, BDNF or Arsenite treated conditions vs their respective vehicle. Student's t-test and Mann-Whitney Rank Sum test to compare wild type vs MeCP2 KO with same treatment, ###, p≥0.001,##, p≥0.01, #, p≥0.05 WT vs KO, same condition (vehicle, NT3, BDNF or arsenite).
- Pharmacological rescue: Kruskal-Wallis Anova on ranks to compare Serotonin + Norepinephrine or Mirtazapine treatments to their respective vehicle condition for wild type and MeCP2 knock-out neurons in pharmacological rescue analysis, ***, p≥0.001, **, p≥0.01, *, p≥0.05 Serotonin + Norepinephrine or Mirtazapine treated condition vs its respective vehicle. Student's t-test and Mann-Whitney Rank Sum test to compare wild type vs MeCP2 KO with same treatment, ###, p≥0.001,##, p≥0.01, #, p≥0.05 WT vs KO, same condition (vehicle, Serotonin + Norepinephrine or Mirtazapine).

RESULTS

1. Analysis of 5'UTR regions of *BDNF* to mRNA trafficking

Previous *in vivo* and *in vitro* studies demonstrated that *BDNF* transcripts are differentially distributed in the proximal or distal region of dendrites, depending on the exon composition. In particular, it was shown that the alternatively spliced 5'UTR exons act as selectivity signals able to modify the constitutive dendritic targeting mediated by the coding sequence (CDS) of *BDNF*, with exon 1 and exon 4 retaining the transcript in the first 30% of dendrite, and exons 2b, 2c and 6 allowing the transport to distal dendritic compartment (Baj et al., 2011; Chiaruttini et al., 2009). However, the individual contribution of the eleven 5'UTR regions in BDNF mRNA trafficking was not investigated. Accordingly, we decided to investigate if constitutive or activity-dependent targeting signals were encoded in the eleven 5'UTR splicing isoforms of *BDNF* rat gene that were cloned upstream to the GFP reporter gene. First, we cloned the different exons in a pEGFP-N1 vector (for details see materials and methods) and then, we transfected the chimaeric constructs in DIV6 hippocampal cultured neurons. After 24 hours from transfection, we fixed the cells and performed non-radioactive *in situ* hybridization against *GFP* coding sequence, used as reporter transcript, in order to evaluate the contribution to dendritic trafficking of the different isoforms.

Figure 1A shows a representative *in situ* hybridization staining obtained using antisense probe against *GFP* coding sequence in a neuron transfected with one chimaeric construct. Strong signal was detected in soma area of transfected neuron, and in situ labeling within the apical dendrite was clearly distinguishable from background. The central panel of figure 1A shows the process of straightening used to prepare the image for densitometric analysis performed with ImageJ. The red line represents the region of interest in which the mean gray value was measured to evaluate the mRNA levels in the different compartments. Specificity of *in situ* labeling was determined by using sense probe for *GFP* coding sequence on transfected neurons or *GFP* antisense probe in non-transfected neurons. In both cases, the *in situ* signal obtained is indistinguishable from background (fig. 1A, bottom panels).

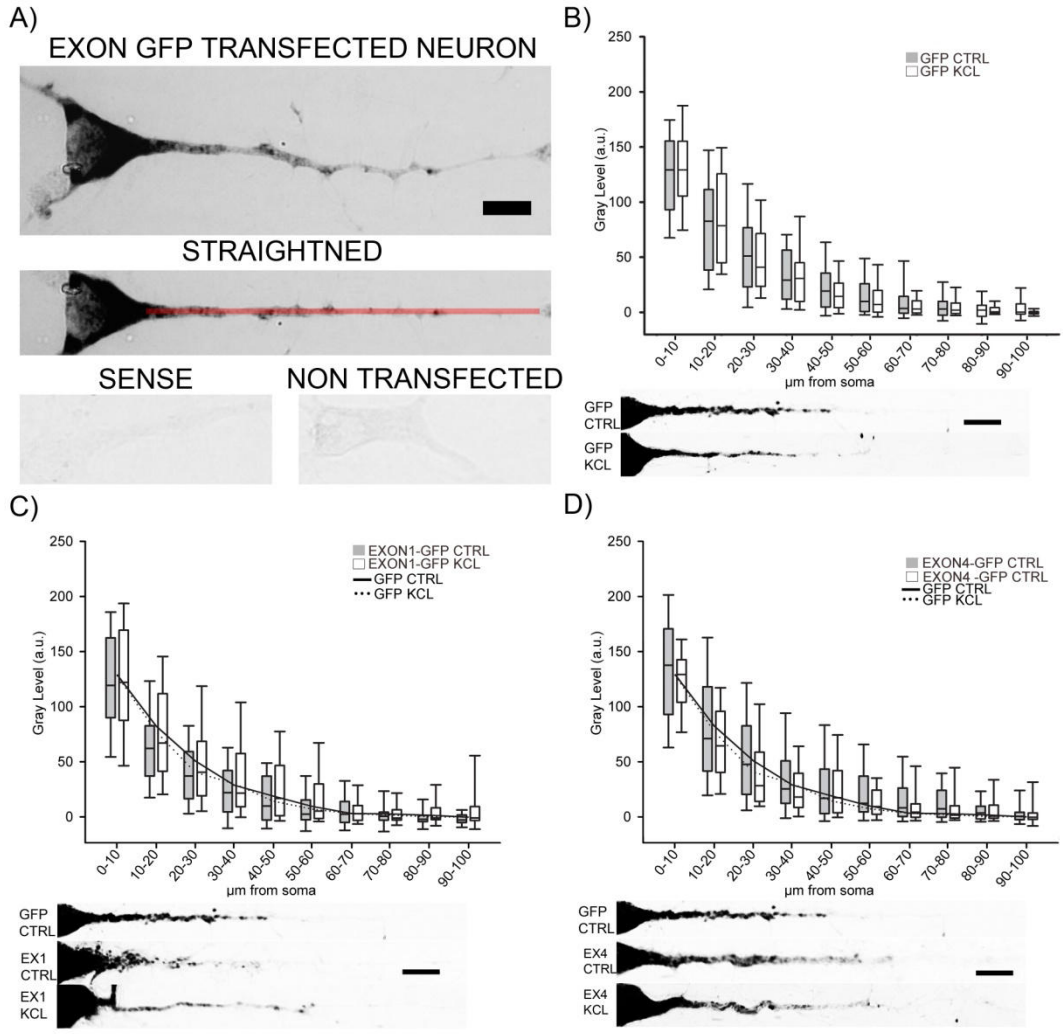

Figure 1. Trafficking of GFP, exon 1-GFP and exon 4-GFP transcripts in hippocampal neurons. A) Representative image of *in situ hybridization* against GFP coding sequence on hippocampal neuron transfected with pEGFP-N1 plasmid before (upper panel) and after straightening (central panel). Bottom panels represent two control *in situ* hybridization on pEGFP-N1 transfected neurons using GFP coding sequence sense probe (left) and on non-transfected neurons using antisense probe. Scale bar: 10 µm. B-D) Densitometric analysis on *in situ hybridization* of apical dendrites of neurons transfected with GFP (panel C), exon 1- GFP (panel C) and exon 4-GFP (panel D) untreated (gray boxes) or treated with 10 mM KCl for 3 hours (white boxes). Below each graph a representative straightened *in situ* hybridization is reported. Lines in graph C and D represent the plot of median gray value of GFP densitometric analysis untreated (solid line) and after KCl stimulation (dashed line). Scale bar: 10 µm.

We next evaluated if the mRNA of the *GFP* coding sequence alone was transported into dendrites. According to our own previous evidence (Baj et al., 2011; Chiaruttini et al., 2009) in situ labeling for *GFP* mRNA is present only in the proximal dendrites of transfected neurons (fig. 1B, bottom panel with representative dendrite stretches of

untreated GFP transfected neurons; GFP CTRL scale bar: 10 µm), as confirmed by densitometric analysis (fig.1B, gray bars). Gray bars represent the plot of the mean gray value of control neurons analyzed, binned in 10 µm compartment starting from soma up to the first 100 µm of apical dendrite.

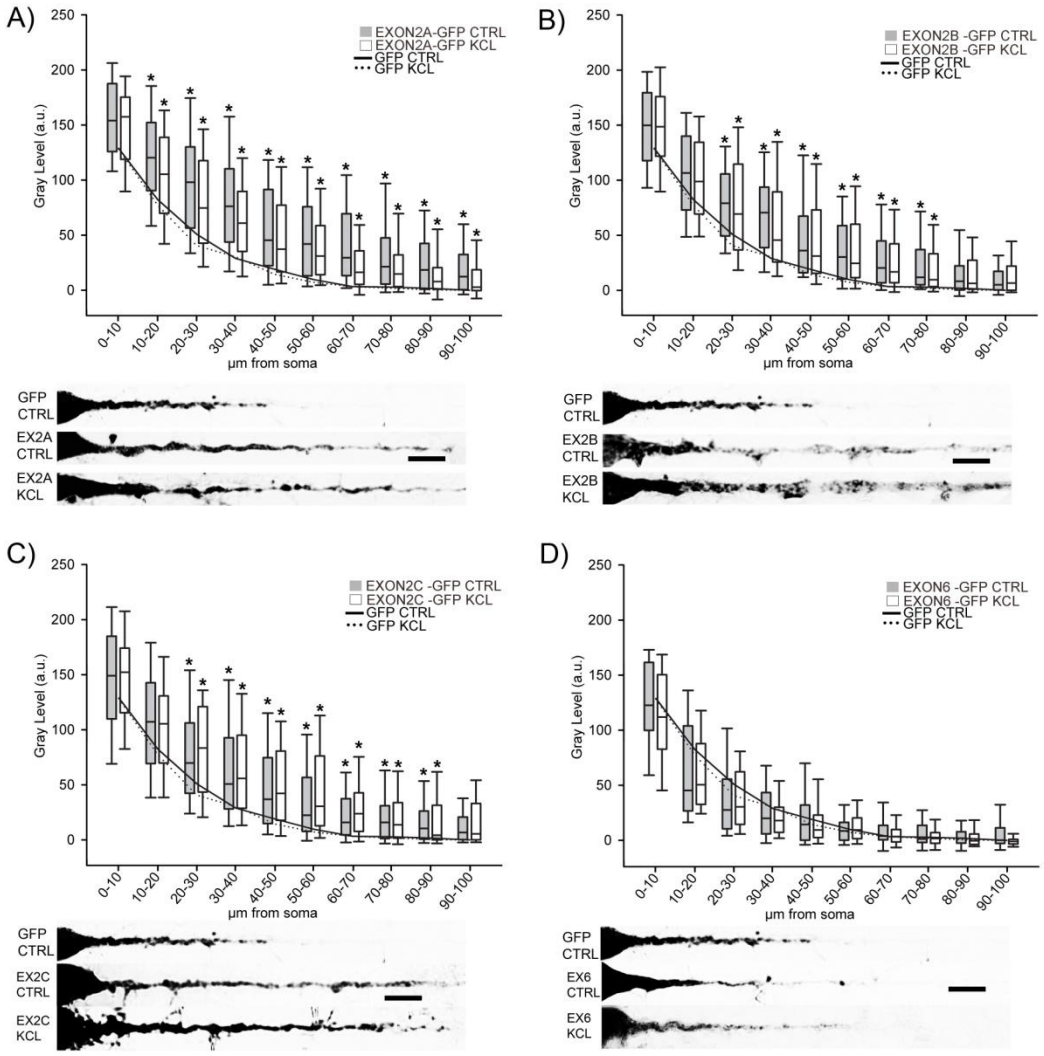

Figure 2. Trafficking of exon 2a-GFP, exon 2b-GFP, exon 2c-GFP and exon 6-GFP transcripts in hippocampal neurons. A-D) Densitometric analysis on *in situ hybridization* of apical dendrites of neurons transfected with exon 2a-GFP (panel A), exon 2b-GFP (panel B), exon 2c-GFP (panel C) and exon 6-GFP untreated (gray boxes) or treated with 10 mM KCl for 3 hours (white boxes). Below each graph a representative straightened *in situ* hybridization is reported. Lines in graphs represent the plot of median gray value of GFP densitometric analysis untreated (solid line) and after KCl stimulation (dashed line). Scale bars: 10 µm. *, $p \leq 0.05$ exon-GFP ctrl respect to GFP control and exon-GFP KCl vs GFP KCl

In parallel cultures, transfected neurons were treated for 3 hours with 10 mM KCl solution (see materials and methods for details) to asses if *GFP* mRNA is targeted to dendrites in response to activity dependent stimulus. Densitometric analysis on KCl-

treated transfected neurons (fig 1B, white bars; GFP KCL) confirmed that GFP mRNA distribution is unaffected by depolarization.

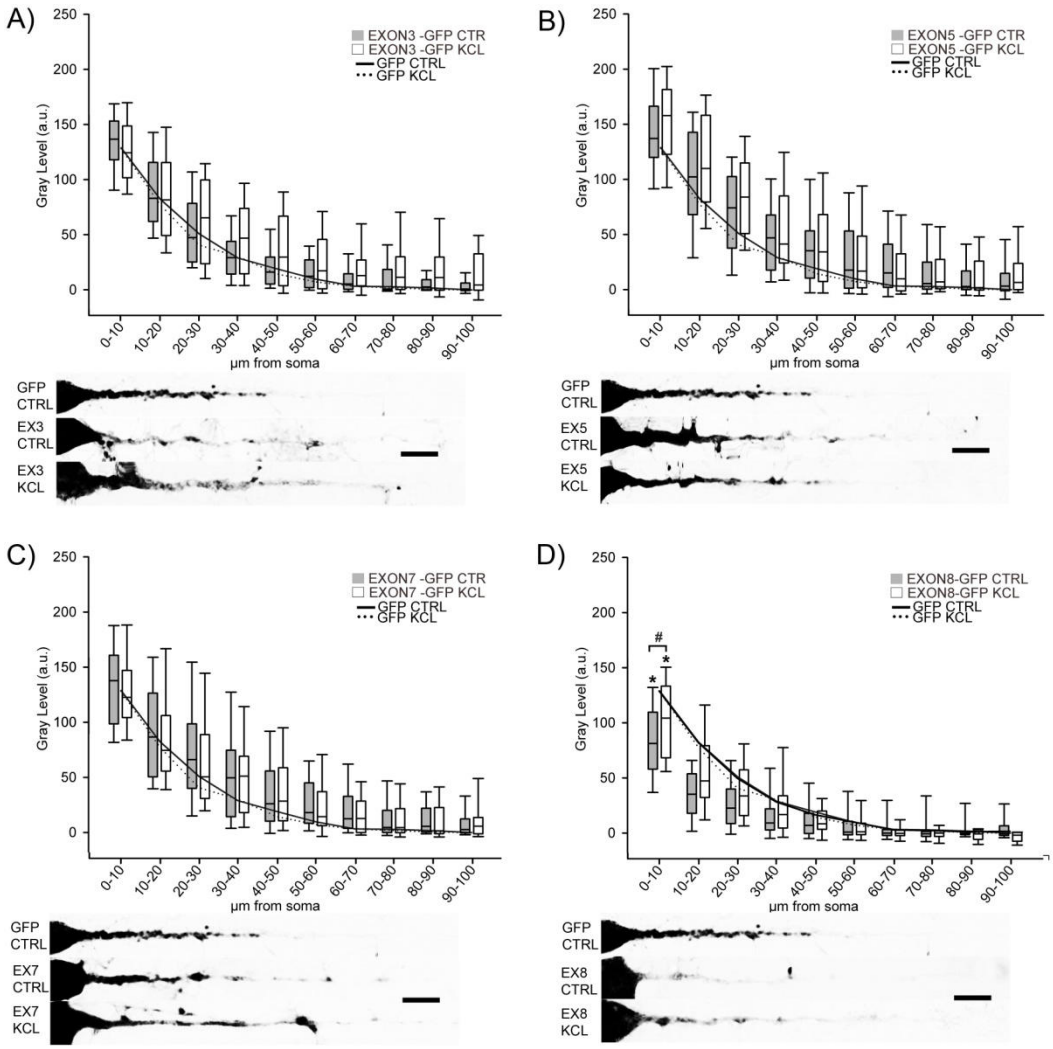

Figure 3. Trafficking of exon 3-GFP, exon 5-GFP, exon 7-GFP and exon 8-GFP transcripts in hippocampal neurons. A-D) Densitometric analysis on *in situ hybridization* of apical dendrites of neurons transfected with exon 3-GFP (panel A), exon 5-GFP (panel B), exon 7-GFP (panel C) and exon 8-GFP untreated (gray boxes) or treated with 10 mM KCl for 3 hours (white boxes). Below each graph a representative straightened *in situ* hybridization is reported. Lines in graphs represent the plot of median gray value of GFP densitometric analysis untreated (solid line) and after KCl stimulation (dashed line). Scale bars: 10 µm. *, p≤0.05 exon-GFP ctrl respect to GFP control and exon-GFP KCl vs GFP KCl. #, p≤0.05 exon-GFP ctrl vs exon-GFP KCl.

Using the same approach, we evaluated the distribution of chimaeric BDNF exons-GFP transcripts in untreated or depolarized neurons transfected with the different constructs. Exon 1 and exon 4, which were previously shown to inhibit constitutive dendritic targeting of *BDNF* CDS, were not able to alter the distribution of the GFP reporter mRNA, displaying a distribution similar to *GFP* mRNA alone (fig. 1C and fig.

1D). A slight but not significant decrease of exon 1-GFP transcripts was visible into the proximal domain of the apical dendrites.

Exon 2 and exon 6 splicing variants were previously demonstrated to be permissive for dendritic targeting mediated by *BDNF* CDS (Baj et al., 2011; Chiaruttini et al., 2009). When exon 2 variants were cloned upstream of *GFP* coding sequence (fig 2A, B and C, exon 2a, 2b and 2c-GFP, respectively), they resulted to be able to induce a significant constitutive dendritic targeting of the reporter transcripts, as shown in representative dendritic stretches in which *in situ* staining is clearly visible in the distal compartments of apical dendrites. Densitometric analysis of unstimulated transfected neurons confirmed the positive trafficking (fig 2A, B and C, gray bars, exon 2a, 2b and 2c -GFP CTRL respectively; *, $p<0.05$). Depolarization following KCl treatment did not affect this constitutive dendritic targeting sorting respect to untreated condition, with exon 2a, b and c chimaeric transcripts still targeted into distal compartments of dendrites respect of those of *GFP* alone after depolarization (fig 2A, B and C, white bars, exon 2a, 2b and 2c -GFP KCl respectively; *, $p<0.05$). Exon 6-GFP chimaeric transcript instead did not display any regulation for the trafficking of reporter transcripts into dendrites, both in unstimulated and depolarized condition (fig 2D).

Finally, we evaluated trafficking of the remaining *BDNF* 5'UTR splicing variants, less characterized *in vitro* for their contribution to mRNA sorting. Exon 3-GFP chimaeric mRNA distribution in unstimulated condition was not significantly different respect to those of *GFP* alone (fig. 3A, gray bars) but weakly induced transport into dendrites after depolarization stimulation (fig. 3A, white bars), although not statistically significant. Exon 5 and exon 7-GFP (fig. 3B and C respectively) displayed a similar and not significantly different distribution respect to reporter transcript alone in both condition analyzed. Exon 8-GFP (fig. 3D) resulted to be less abundant in dendrites of untreated neurons respect to *GFP* transcript (fig. 3D, gray bars, exon 8-GFP CTRL; *$p<0.05$), especially in the first 40 µm. KCl depolarization weakly increase the trafficking of this transcripts (fig. 3D, white bars, exon 8-GFP KCl; #,$p<0.05$) but not in a significant manner respect to reporter transcript alone.

Given these results, we decided to investigate if any *cis*-element for the binding of RNA binding proteins (RBP) involved in mRNA trafficking were present in the 5'UTR

sequences. We performed a bioinformatic analysis using the RBPDB database (http://rbpdb.ccbr.utoronto.ca) containing 757 different RNA recognition motifs, to identify putative RBP binding sites present in each BDNF 5' splicing isoform sequences used to generate the chimaeric constructs. A threshold of 0.8 was set, then FASTA sequence were scanned by algorithm. Exon 3 showed 3 AU rich sequences, one at the 5' end recognized by ELAV2 and two ELAV1-binding sites in the 3' end, involved mostly in splicing, mRNA stability and translation initiation. Exon 7 showed a recognition site for hnRNPA1 involved in nucleo-cytoplasm shuttling. Exon 2c, the longest of the three exon2 splicing isoforms that showed constitutively-active dendritic transport, presented five AUUU motif targetable by ELAV1 protein, a protein well known for its role in mRNA stability and transport (Chen et al., 2002), seven GGUG motif targetable by FUS, an heterogenous ribonuclear protein involved in mRNA transcription, nuclear export and dendritic trafficking (Sama et al., 2014), and two Pumilio2 binding sites, one of better characterized RNA binding proteins acting as translational repressor (Wickens et al., 2002). Exons 1, 4, 5, 6 and 8 did not show significant homology to any of the RNA recognition motifs present in the RBPDB database associated to mRNA trafficking that differed from those described in exon 2 analysis. As the role of these RBPs in mRNA trafficking and their capability to bind 5'UTR regions are still poorly characterized, further investigations to clarify the mechanisms underlying dendritic trafficking of *BDNF* 5'UTR exon 2 isoforms are required.

2. Association of multiple RNA binding protein families to *BDNF* mRNA

Despite the selectivity signals retained in the 5'UTR region of *BDNF*, the active targeting signals responsible for dendritic trafficking of this transcripts were mainly found to be localized in the CDS and the two different 3'UTR isoforms, the short and the long. In fact constitutive dendritic targeting signals were demonstrated to be retained in the CDS and mediated by Translin RNA binding protein (Chiaruttini et al., 2009) while activity dependent targeting was mediated by the 3'UTRs (Baj et al., 2011). Moreover the association of different RNA binding protein, such as FMR1 and CPEB1, is necessary for the correct localization of *BDNF* mRNA (Louhivuori et al., 2011; Oe and Yoneda, 2010). This evidence suggested that binding of other RBPs could be involved in the complex mechanisms underlying dendritic trafficking of *BDNF* transcripts. In order to identify RBPs families interacting with 3'UTRs short and

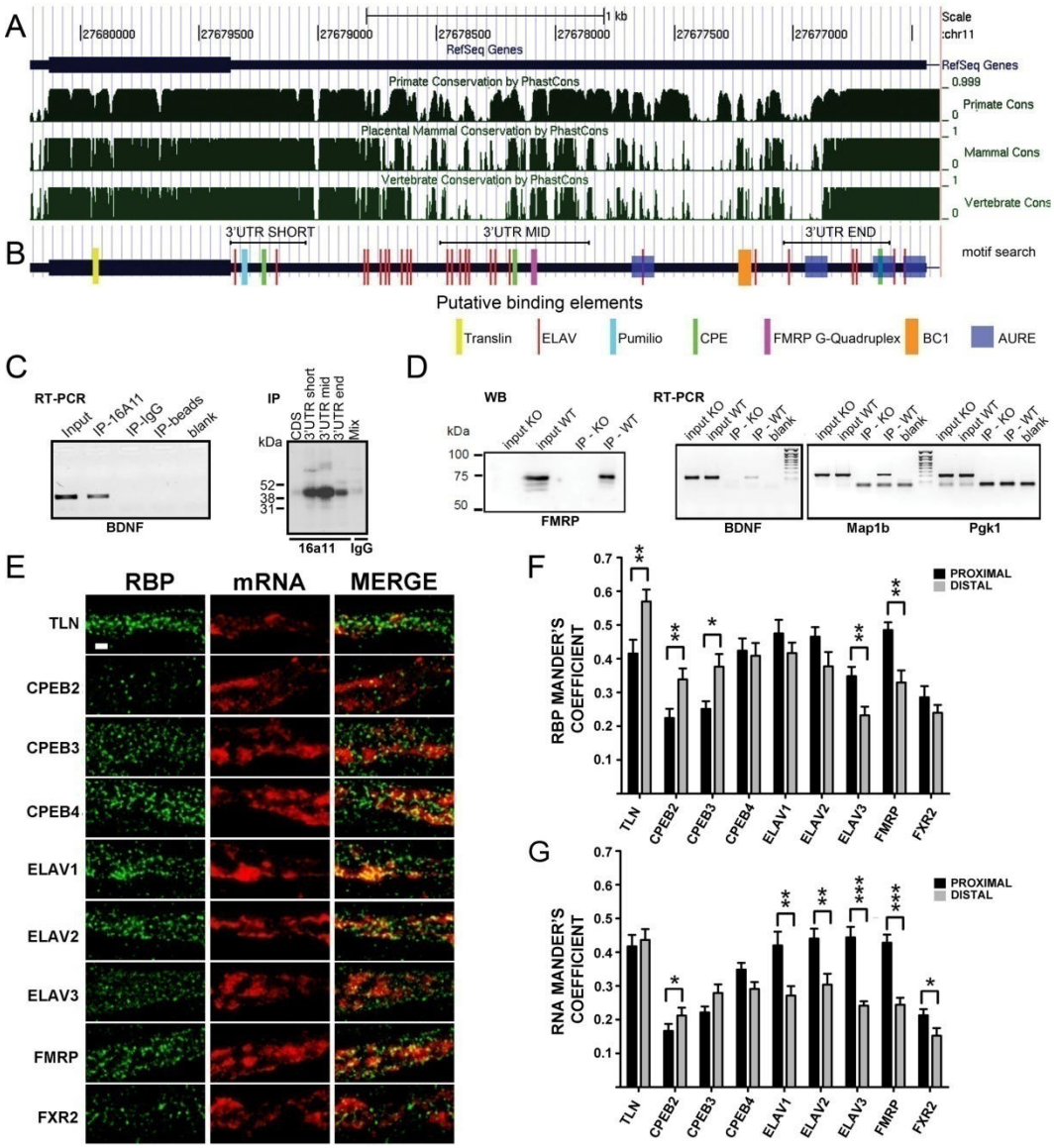

Figure 4. *BDNF* mRNA interaction with RNA binding proteins (RBPs). A) Graphical view of homology of BDNF coding regions and 3'UTR among Primates, Mammals and vertebrates. Similarity scores range from 0 (= no homology) to 1 (identical sequence). Numbers indicate the nucleotide position of BDNF gene on chromosome 11. B) Putative binding sites for RBPs indicated with different colors at the corresponding positions along *BDNF* mRNA. Positions of the short 3'UTR, long-mid 3'UTR and long-end sequences used in UV-CLIP assays in C) are also shown. C) (left panel) RT-PCR of BDNF mRNA immunoprecipitated with an antibody against the neuronal ELAV proteins (IP-16A11), or a control IgG antibody (IP-IgG) or no antibody (IP-beads). Total brain RNA (Input) and no sample (Blank) were used as a positive and a negative control, respectively. (right panel) UV-CLIP assay with an anti-neuronal ELAV proteins antibody (IP-16a11) to immunoprecipitate RNA-protein complexes formed in presence of murine brain protein lysate and radiolabeled BDNF CDS, 3'UTR short, or 3'UTR long-mid and 3'UTR long-end ribobrobes. As a negative control, UV-CLIP was performed using an anti-IgG antibody with a mix of all the *BDNF* riboprobes used.

D) Immunoblot assay to test specificity of the anti-FMRP antibody in inputs and immunoprecipitates from WT and Fmr1 knockout (KO) mice (left panel). RT-PCR of *BDNF* mRNA recovered from immunoprecipitates from WT and *Fmr1* knockout lysates upon CLIP assay (middle panel). *Map1b,* a known mRNA target of FMRP protein, was used as a positive control, while *Pgk1*, an unrelated mRNA, as a negative control. Blank, no sample in RT-PCR reaction.

E) Colocalization analysis of endogenous *BDNF* mRNA with different RBPs. Immunofluorescence signal from the different RBPs (green) and from endogenous *BDNF* mRNA (red) in proximal dendrites are shown separately (RBP, mRNA) and merged (MERGE). Scale bar: 1µm. F-G) Graphs report the Manders coefficient (Y-axis) of RBPs signal colocalized with endogenous BDNF mRNA (F) and BDNF mRNA signal colocalized with the different RBP (G) in proximal (black) and distal (gray) dendrites. Data are reported as mean ± S.E.M. Statistical significance of proximal vs.distal Manders coefficients of colocalization was evaluated performing *t*-test if the normality test was passed, or Mann–Whitney Rank-Sum test (* $p < 0.05$; ** $p < 0.01$; *** $p < 0.001$).

long, we performed a bioinformatics analysis to identify evolutionary conserved sequence among primates, mammals and vertebrates (see supplementary figure 1) The analysis was carried out in collaboration with Łukasz Gricman and prof. Alberto Pallavicini (University of Trieste, Italy). We used phastCons alignment software (Siepel et al., 2005) to analyze *BDNF* CDS and complete 3'UTR. The CDS resulted highly conserved in all the organisms considered, while the 3'UTR region contains three major hot spots of conservation (fig. 4A): the first consisted in the first 321 nucleotides of 3'UTR, corresponding to 3'UTR short isoform (short, nts 1-321). The other two hot spots were localized into 3'UTR long region, which display higher overall variability with respect to the short isoform. However, the central (mid, nts 890-1510) and terminal (end, nts 2339-2790) regions displayed high rates of conservation across vertebrates and mammals (fig. 4A). We focused our attention on these three conserved sequences to identify putative binding sites for RBPs involved in trafficking, mRNA stability and translation of *BDNF* mRNA: cytoplasmatic polyadenylation element binding proteins (CPEBs) (Oe and Yoneda, 2010), embryonic lethal abnormal vision like proteins (ELAVs) (Allen et al., 2013) and Fragile X mental retardation protein family (FMRP) (Louhivuori et al., 2011). The 3'UTR short presented two ELAVs binding sites and one CPEB binding element, followed by an "ELAV rich region" between the short and mid sequences (fig. 4B), potentially targeted by ELAV1 (HuR). The mid region contains another series of ELAV putative binding sites followed by a CPEB binding elements and G-quadruplex structure, known to be recognized by FMRP (Brown et al., 2001). Finally the end

region is preceded by a BC1 element (Rozhdestvensky et al., 2001) and contains a pattern of putative *cis*-element similar to those of 3'UTR short (fig. 4B).

CPEBs were previously demonstrated to interact with *BDNF* 3'UTR (Oe and Yoneda, 2010). In order to confirm the physical interaction of ELAVs to *BDNF* 3'UTR we performed RNA immunoprecipitation assays using a pan-neuronal ELAV (nELAV) antibody. Real-time PCR (RT-PCR) following RIP confirmed that *BDNF* is selectively recovered from mouse brain protein lysate precipitated with nELAV antibody and not with unspecific IgG (fig. 4C, RT-PCR). To test specificity of this binding we performed an UV cross-linking immunoprecipitation (UV-CLIP) assay using radiolabeled probe for CDS, 3'UTR short, mid and end regions (fig. 4C, IP). The CDS probe did not form any complex with nELAV, while all the three regions of the 3'UTR were specifically bound by nELAV, with a preference for mid sequence. FMRP binding was tested by RIP assay using a previously described polyclonal antibody (Davidovic et al., 2011) on wild type or FMR1 KO mouse brain protein lysates, which did not show any expression of FMR1 at protein level in western blot (fig. 4.D, WB). RT-PCR following RIP confirmed that *BDNF* mRNA was selectively recovered only from wild type lysates but not from FMR1 KO lysates (fig. 4D, RT-PCR left panel). *MAP2* and *Pgk1* mRNA were used as positive and negative control respectively of FMR1 binding (fig. 4D, RT-PCR, right panels). RIP and UV-CLIP experiments of with *BDNF* mRNA and ELAVLs were performed in collaboration with Claudia Colombrita and prof. Antonia Ratti (University of Milan, Italy). RIP experiments with Fmr1 were performed in collaboration with Laetitia Davidovic and prof. Barbara Bardoni (INSERM, Valbonne, France).

Finally, we investigated if *BDNF* mRNA and the identified RBPs were colocalized *in vitro*. To assess this, we performed double labeling experiments by coupling fluorescent *in situ* hybridization (FISH) to detect *BDNF* mRNA, to immunofluorescence (IF) for the different members of CPEB, ELAV and FMRP protein families. Tyramide amplification system was used in order to visualize endogenous *BDNF* mRNA due to its low level of expression in cultured neurons (Baj et al., 2013; Will et al., 2013). FISH signal using antisense probe against CDS is clearing visible in the soma and dendrites of stained rat hippocampal cultured neurons (fig. 4E). FISH using sense probe for CDS resulted in negligible signal (see

supplementary figure 2). IF staining highlighted a similar distribution along the dendrites for all the RBPs analyzed, suggesting that may be part of shared components of ribonucleoprotein particles (RNP) (fig.4E). CPEB1 and ELAV4 staining resulted undetectable after FISH process using two different antibodies therefore, the two proteins were excluded from the colocalization analysis. In unstimulated cultures, almost half of the staining spots of Translin, CPEB4, ELAV1, ELAV2, and FMRP were colocalized with endogenous *BDNF* mRNA (fig. 4F, black bars. Manders coefficient Translin 0.415±0.041, CPEB4 0,424±0.036, ELAV1 0.475 ± 0.040, ELAV2 0.465 ± 0.028, and FMRP 0.485 ± 0.023), while other transporting granules displayed lower Manders coefficient values ranging from 0.224 to 0.348. Similarly *BDNF* mRNA signal results to be more colocalized in the proximal compartment with Translin, ELAV1, ELAV2, ELAV3, and FMRP granules (fig. 4G, black bars. Manders coefficient Translin 0.417 ± 0.034, ELAV1 0,420 ± 0.041, ELAV2 0.440 ± 0.029, ELAV3 0.444 ± 0.031, and FMRP 0.423 ± 0.024). In distal compartments more than half of the transporting granules stained for Translin resulted to be colocalized with *BDNF* mRNA (fig. 4F, gray bars. Manders coefficient 0.579 ± 0.035), while other RBPs display similar colocalization degree with RNA, except for the less colocalized ELAV3 and FXR2 (fig. 4G, gray bars. Manders coefficient ELAV3 0.232 ± 0.026 and FXR2 0.240 ± 0.023). Moreover, BDNF mRNA displayed the highest colocalization rate with Translin protein (fig. 4G, gray bars. Manders coefficient 0.436 ± 0.032) confirming its involvement in this mRNA trafficking as previously demonstrated (Chiaruttini et al., 2009) while other RBPs displayed a heterogeneous colocalization rate (fig 4G, gray bars. Manders coefficient ranging from 0.152 to 0.304). The comparison of proximal versus distal compartments colocalization revealed that RBPs colocalization with *BDNF* mRNA was significantly higher in distal dendrites than in proximal dendrites for Translin, CPEB2, CPEB3, while it was higher in proximal than in distal for ELAV3 and FMRP, and was unchanged for CPEB4, ELAV1 and 2, and FXR2 (fig. 4F). Setting endogenous *BDNF* transcript as reference, we found that BDNF mRNA was significantly more localized with ELAV1, 2, 3, FMRP and FXR2 in proximal dendrites than in distal (fig 4G), suggesting that the different RBPs analyzed exert their regulation on *BDNF* mRNA in different dendritic compartments.

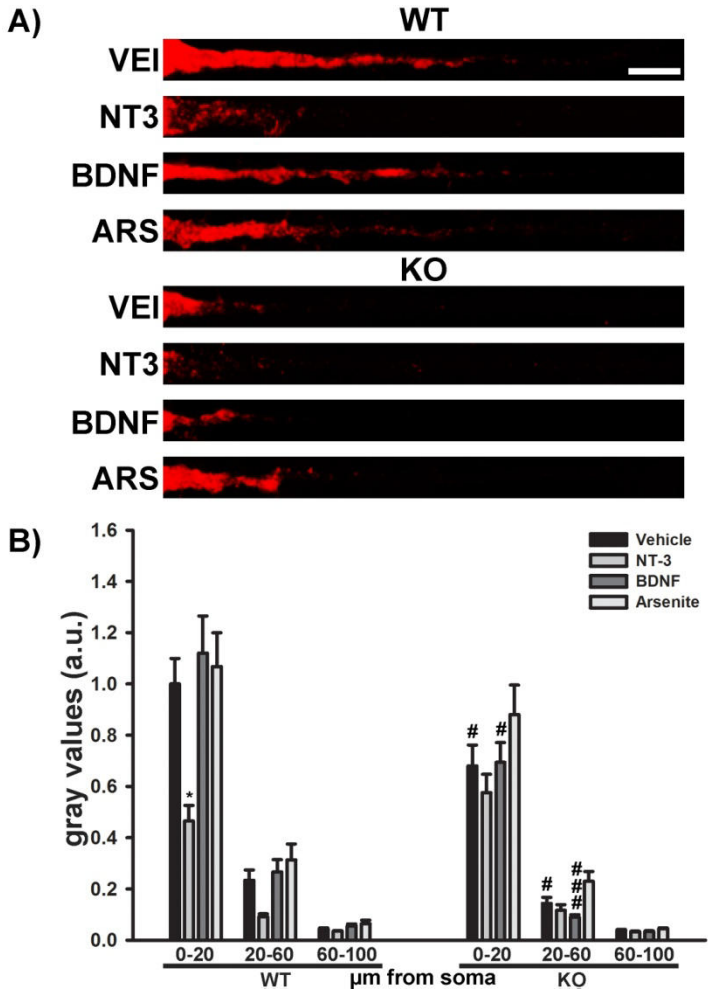

Figure 5. Endogenous *BDNF* mRNA expression along dendrites of MeCP2 hippocampal neurons A) Fluorescent *in situ* hybridization (FISH) for endogenous *BDNF* mRNA on apical dendrites of wild type (WT) and MeCP2 KO (KO) hippocampal neurons untreated (VEI) or treated with 50 ng/ml NT-3 (NT3) and BDNF (BDNF) or 0.5 mM sodium arsenite (ARS). Apical dendrites represented in figure A were straightened to line using ImageJ (NIH). Scale bar: 10 µm. B) Densitometric analysis of FISH signal. Data are expressed as mean±S.E.M. of the gray values normalized to the values of the first 20 µm of untreated WT neurons. *, p≤0.05 respect its own vehicle. #, p≤0.05, ###, p≤0.001, KO vs WT respect the same treatment.

3. Endogenous *BDNF* mRNA levels in dendrites of MeCP2$^{-/y}$ neurons

Rett syndrome (RTT) is characterized by extended neuronal atrophy in brain of RTT patients (Belichenko and Dahlstrom, 1995; Belichenko et al., 1997; Carter et al., 2008; Kaufmann et al., 1995; Kaufmann et al., 1997a; Subramaniam et al., 1997). These atrophic features were reproduced in the two major mouse models for these pathology: the MeCP2 Bird strain and the MeCP2 Jaenisch strain (Belichenko et al.,

2009; Kishi and Macklis, 2004). Moreover different studies highlighted deficits in BDNF mRNA and protein levels in RTT mouse models (Chang et al., 2006; Ogier et al., 2007; Wang et al., 2006). Indeed, BDNF is a key regulator of neuronal development and synaptic plasticity (Yoshii and Constantine-Paton, 2010).

We hypothesized that an incorrect localization of BDNF *mRNA* could be involved in the neuronal atrophy that occurs in MeCP2 KO mouse model. To verify this hypothesis we performed FISH against endogenous *BDNF* mRNA in hippocampal cultured neurons from MeCP2 KO mouse model and wild type mice and visualized the localization of this transcript into dendrites. We chose MeCP2$^{-/y}$ Bird male mice (see supplementary figure 3) because previous work from Baj et al. characterized the neuronal development deficits of hippocampal neurons *in vitro* from this strain. In particular, neurons were analyzed after 12 days in vitro (DIV12) because the neuronal development of MeCP2 KO neurons *in vitro* was mostly affected at this stage (Baj et al., 2014). FISH labeling in apical dendrites of wild-type neurons is clearly visible in proximal compartments and isolated mRNA granules were detectable until the first 40-50 µm from soma, as shown in representative straightened dendrites (fig. 5A, WT VEI). Conversely, mRNA labeling displayed a weaker signal in MeCP2 KO neurons both in proximal and distal compartments (fig. 5A, KO VEI). Densitometric analysis confirmed that *BDNF* mRNA is less abundant into MeCP2 KO neurons dendrites both in the first 20 µm of apical dendrites (fig. 5B, 0-20 µm black bars; wild type 1.0 ±0.1 vs. MeCP2 KO 0.68±0.082; #. $p<0.05$) and between 20 and 60 µm from soma (fig. 5B, 20-60 µm black bars; wild type 0.23 ±0.03 vs MeCP2 KO 0.14±0.04; #, $p<0.05$). Data are expressed as mean± S.E.M. of mean gray value normalized for the mean gray value of the first 20 µm of wild type. BDNF mRNA granules were not detected after 60 µm from soma.

Given these results, we investigated if neurotrophic stimulation, known to promote *BDNF* mRNA localization in dendrites (Vicario et al., 2015), was able to restore the normal dendritic distribution of BDNF mRNA. Neurons were treated with 50 ng/ml neurotrophin-3 (NT-3) or BDNF for one hour, then the levels of dendritic *BDNF* mRNA were evaluated. Surprisingly, NT-3 stimulation decreased dramatically the levels of *BDNF* transcripts along the whole apical dendrite in WT neurons (fig. 5B, 0-20 and 20-60 µm; 0.46 ± 0.06 and 0.09 ± 0.01 respectively. *, $p<0.05$ NT-3 vs vehicle

condition). In contrast, BDNF mRNA levels were not significantly altered in MeCP2 KO neurons treated with NT-3, with respect to untreated condition (fig. 5B, 0-20 and 20-60 µm; 0.57 ± 0.07 and 0.12 ± 0.02 respectively). One hour of BDNF treatment resulted not sufficient to increase *BDNF* mRNA in dendrites of wild type neurons (fig. 5B, 0-20 and 20-60 µm; 1.12 ± 0.14 and 0.27 ± 0.05 respectively). However, MeCP2 KO displayed less transcripts localized in proximal and distal dendritic compartments (fig. 5B, 0-20 and 20-60 µm; 0.69 ±0.08 and 0.09 ± 0.01 respectively. #, $p<0.05$ and ###, $p<0.001$ KO BDNF vs WT BDNF).

Finally, we evaluated if a stressful stimulus was able to alter dendritic sorting of *BDNF* mRNA. Previous evidence demonstrated that oxidative damage is present in the brain of human patients and of mouse models of RTT (De Felice et al., 2014; Leoncini et al., 2011). In order to induce oxidative stress in hippocampal cultured neurons we treated the cells with sodium arsenite. This compound is widely use to induce reactive oxygen species *in vitro* and a well characterized response to stress by the formation of stress granules, large RNP involved in mRNA homeostasis (Kedersha and Anderson, 2007). Moreover, central nervous system exposure to sodium arsenite lead to impaired spatial memory and synaptic structure of hippocampal neurons in rat (Jing et al., 2012) and lower BDNF protein level in mouse hippocampus (Sun et al., 2015), while *in vitro* arsenite decreased *BDNF* expression in SH-SY5Y neuroblastoma cell line (Chou et al., 2013). However no investigation were performed about the localization of *BDNF* transcript responding to this specific stressful condition.

After one hour of treatment with 0.5 mM sodium arsenite, BDNF *mRNA* localization was unaltered in dendrites of hippocampal wild type neurons (fig. 5B, 0-20 and 20-60 µm; 1.06 ± 0.13 and 0.31 ± 0.06 respectively), while MeCP2 KO neurons had lower level of mRNA although not statistically significant (fig. 5B, 0-20 and 20-60 µm; 0.94± 0.08 and 0.25 ± 0.04 respectively). Taken together, these results suggested that a basal deregulation of *BDNF* mRNA transport into dendrites could be one of the mechanisms underlying neuronal atrophy in RTT neurons.

4. Detection and isolation of RNPs in hippocampal neurons

The defective *BDNF* mRNA localization in dendrites of MeCP2 KO neurons suggested that RBPs underlying mechanisms of mRNA trafficking, translation and stability could be altered in RTT. Mutation in RNA binding protein machinery is the cause of Fragile-X syndrome, one of the most relevant neuronal developmental syndrome causing mental retardation and autism (Garber et al., 2008). In the mouse model of this syndrome, the lack of Fmr1 protein leads to an altered BDNF mRNA dendritic localization (Louhivuori et al., 2011). Moreover, protein translation was found dysregulated in presymptomatic and symptomatic brains of MeCP2$^{-/y}$ mouse model, with observed deficit in ribosomal protein S6 phosphorylation and AKT/mTOR pathway activation (Ricciardi et al., 2011). RBPs were involved in all these mechanisms, regulating mRNA trafficking and local protein synthesis (Liu-Yesucevitz et al., 2011), mTOR signaling transduction (Kedersha et al., 2013) and cellular response to oxidative stress (Wolozin, 2012). Accordingly, we focused our attention on three major classes of RNA granules: transporting granules, stress granules (SG) and processing bodies (P-bodies). We selected one representative RBP as marker for each class analyzed: Staufen1 (Stau1) for transporting granules, TIA-1 cytotoxic granule-associated RNA binding protein (TIA-1) for stress granules and mRNA-decapping enzyme 1A (Dcp1a) for processing bodies.

First, we evaluated the specificity of antibodies chosen for the visualization in immunofluorescence of the three markers. To avoid misleading results during RNP identification, images of immunostained neurons reported in figure 6 have been submitted to a deconvolution procedure that led to enhanced resolution and reduced signal to noise ratio. Staufen1 staining was strong in the somatic area, with bright and heterogeneous spots positive for Stau1 (fig. 6A, green) distributed along the whole apical dendrite of hippocampal neurons, in which the cytoskeleton was highlighted using antibody for microtubule associated protein 2 (Map2) (fig. 6A, cyan). Western blot using the same antibody on protein lysates of hippocampal cultured neurons revealed a band of the expected weight of 65 kDa (fig. 6B), confirming the specificity of the antibody. One representative hippocampal neuron treated with sodium arsenite and stained for TIA-1 protein is shown in figure 6C (green). TIA-1 was strongly expressed in nucleus, where it exerts its function in splicing and RNA stability. In cytoplasm, after arsenite treatment, TIA-1 spots

nucleated into large and dense SG that were mostly concentrated in the proximal segment of apical dendrites.

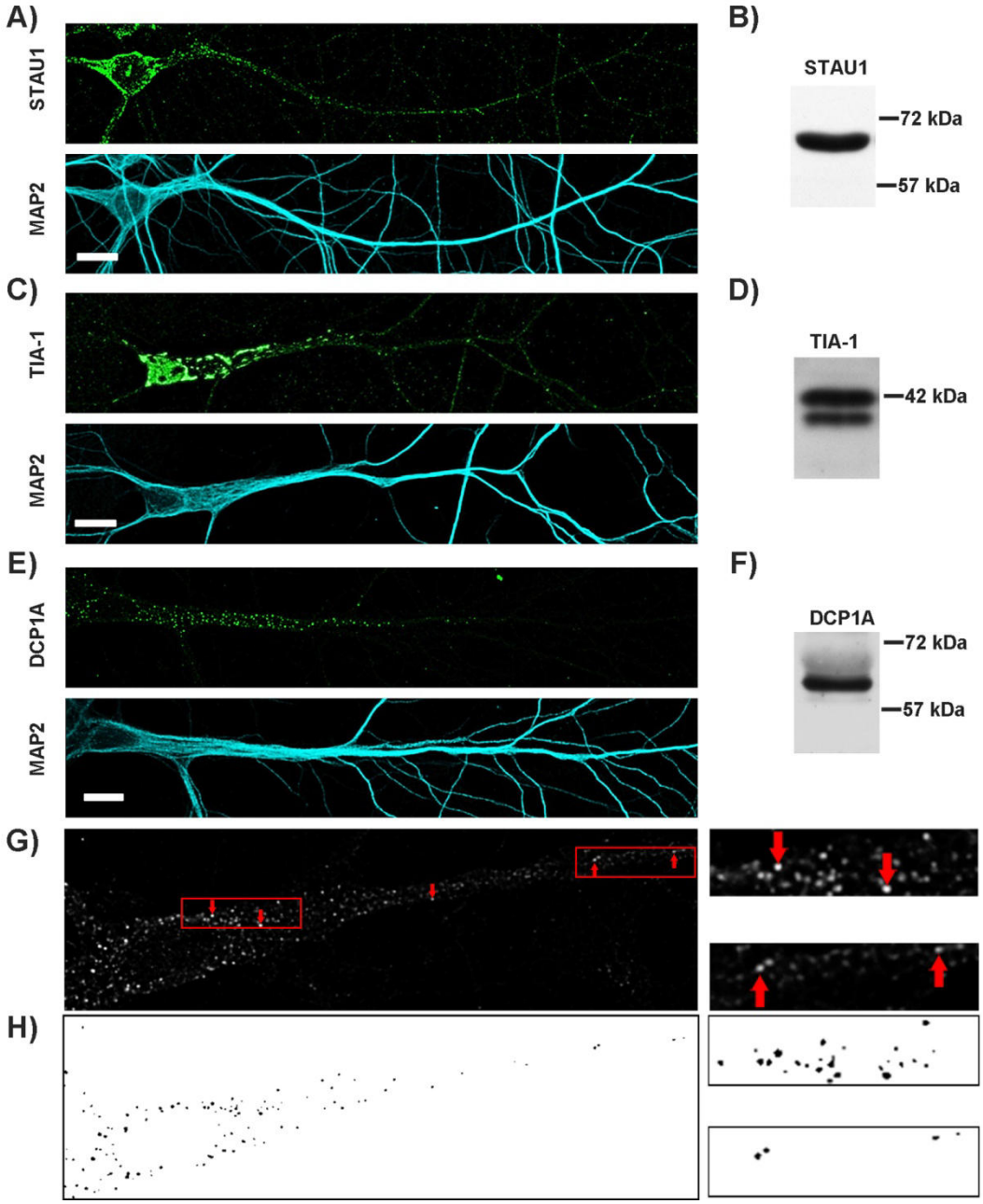

Figure 6 Detection and isolation of transporting granules, stress granules and processing bodies in hippocampal neurons. A, C, F) Representative image of immunofluorescence for Staufen1 (A, green), TIA-1 (C, green) and Dcp1a (E, green) in hippocampal cultured neuron along apical dendrite. Cell boundaries were highlighted through MAP2 immunostaining (A, C, E, cyan). B, D, E) Western blot on hippocampal neuron lysates for Staufen1 (B), TIA-1 (D) and Dcp1a (E) proteins. G) A detail of hippocampal neuron stained for DCP1a (left panel). Bright processing bodies were clearly visible in soma and dendrites of the cell. Red rectangular selection highlights the two magnification on the right in which bona-fide processing bodies (red arrows) were chosen for threshold evaluation. H) Binarized image of the same neuron (left panel the whole image, right panels the two insets) of panel G obtained by the application of the evaluated threshold. Granules chosen in panel G were still present after threshold application.

In order to confirm that the large spots visualized after arsenite administration were genuine SG, we treated Hek293T cells with 0.5 mM sodium arsenite alone or in the presence of 20 µg/ml cycloheximide, a drug known to stabilize polysomes and inhibit stress granules nucleation (Kedersha and Anderson, 2007). As expected, cells were positive for large SG staining after arsenite treatment alone, but SG were completely undetectable in the presence of cycloheximide (supplementary figure 4). Western blot analysis on neuronal culture lysates revealed two strong bands of 42 and 40 kDa of weight (fig. 6D), corresponding respectively to murine TIA-1a and TIA-1b isoforms generated by alternative splicing (Beck et al., 1996). P-bodies stained with Dcp1a antibody appeared as bright spots of approximately 300 nm of diameter that were distributed in the cytoplasm of soma and dendrites (fig. 6E, green). Western blot analysis confirmed the specificity of the antibody, which recognized a strong band of the expected weight of approximately 63 kDa (fig. 6F).

In order to characterize the RNP features in MeCP2$^{-/y}$ hippocampal neurons, we developed a method for processing of confocal images which allowed detection and analysis of single RNP in immunostained neurons. First, five *bona fide* stained granules were selected using dimension, localization and size parameters previously described in literature (see Introduction- RNA granules in neurons). An example of selection of five *bona fide* Dcp1a-positive P-bodies (red arrows) is shown in figure 6G (left panel). Magnification of the granules selected is reported in the two insets on the right. RNP were chosen uniformly, starting from soma and scanning the apical dendrite, ensuring to select a representative subpopulation of the RNPs analyzed. Once selected, spots were used to calculate an average threshold that was applied to each image. Thresholded images were then analyzed using ImageJ analyze particle function in order to create the mask for isolation of single RNPs (fig 6H) (see materials and methods). Masks were finally applied to raw images to measure different parameters: area and number of particles and intensity of labeling.

5. Staufen1, TIA-1 and Dcp1A protein levels in MeCP2 KO hippocampal cultured neurons

MeCP2 is a key regulator of transcription in neurons and its mutation could lead to dysregulation in the expression of several genes (Gabel et al., 2015). For this reason,

we investigated if Staufen1, TIA-1 and Dcp1a proteins levels in hippocampal MeCP2$^{-/y}$ neurons were altered. Western blot analysis was performed on protein lysates of DIV12 wild type and MeCP2 KO neurons (fig. 7A). The intensity of the specific bands of the three granule markers were normalized to the actin band, used as loading control. Immunoblots confirmed that all RBPs were expressed in MeCP2 KO neurons (fig. 7A, WT and KO lanes) and no alterations in protein levels could be appreciated in MeCP2 KO neurons with respect to wild type neurons for Staufen1 (Fig. 7B, Staufen1; 1 ± 0.12 vs 1.06 ±0.1 WT vs KO respectively), TIA-1 (Fig. 7B, TIA-1; 1 ± 0.03 vs 1.06 ±0.1 WT vs KO respectively) and Dcp1a (Fig. 7B, DCP1A; 1 ± 0.36 vs 1.33 ±0.11 WT vs KO respectively). Data were reported as mean of the protein ratio (protein band/actin band volume) ± S.E.M. normalized to the value of untreated wild type. Given the fact that systemic oxidative damage affects RTT mouse cells (De Felice et al., 2014), we wanted to asses if the response to oxidative damage induced by Arsenite is altered in RTT neurons. Western blot on protein lysates of wild type and MeCP2 KO neurons did not show any significant difference in the expression of Staufen1 (Fig. 7B, Staufen1, Arsenite +; 0.91 ± 0.1 vs 0.99 ±0.24 WT vs KO respectively), TIA-1 (Fig. 7B, TIA-1, Arsenite +; 1.02 ± 0.09 vs 1.07 ±0.03 WT vs KO respectively) and Dcp1a (Fig. 7B, DCP1A, Arsenite +; 1.04 ± 0.13 vs 1.14 ±0.12 WT vs KO respectively).

Since Staufen1, TIA-1 and Dcp1a protein levels in neuronal lysates resulted unaltered, we investigated how these three RNP markers were distributed along dendrites in MeCP2 KO neurons. DIV12 wild type and MeCP2$^{-/y}$ neurons were imaged as described above, then densitometric analysis was performed on apical dendrites of immunostained neurons. Data are shown in figure 7C, D and E as the mean ± S.E.M. of mean gray values for Staufen1, TIA-1 and Dcp1a signals normalized to the values measured in the first 20 µm of apical dendrites from untreated wild type neurons. Staufen1 distribution along dendrites was very similar in wild type and MeCP2 KO neurons (fig. 7C). In fact, both displayed a slight but not

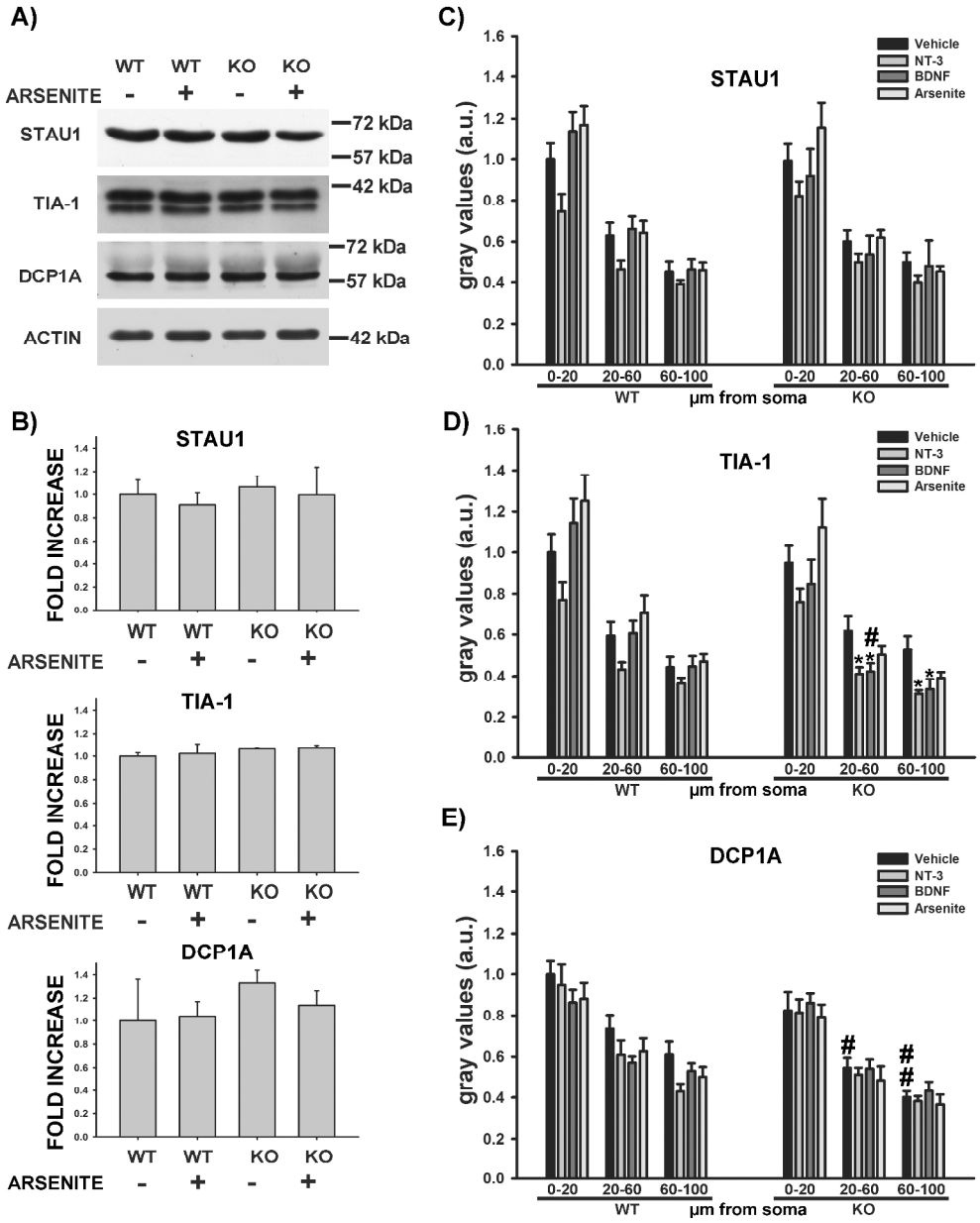

Figure 7. Analysis of Staufen1, TIA-1 and DCP1a protein level in wild type and MeCP2 KO cutlured neurons. A) Representative immunoblot of wild type (WT) or MeCP2 KO (KO) protein lysates of hippocampal cultured neurons untreated (-) or treated (+) with 0.5 mM Arsenite for one hour. Molecular weight are reported to the right of the immunoblots. B) Quantitative analysis of western blot as a ratio of the volume of Staufen1, TIA-1 and DCP1a bands normalized to actin bands used as loading control. Data were reported as mean ±S.E.M. normalized to untreated wild type.

C-E) Densitometric analysis of Staufen1 (C), TIA-1 (D) and DCP1a (E) expression along the first 100 µm of apical dendrites of hippocampal neurons of wild type (WT) or MeCP2 KO (KO) neurons untreated (black bars) or treated with or treated with 0.5 mM sodium arsenite, 50 ng/ml BDNF (BDNF) or NT-3 (NT3). Data are expressed as mean±S.E.M. of the gray values normalized to the values of the first 20 µm of untreated WT neurons. *, $p \leq 0.05$ respect its own vehicle. #, $p < 0.05$; ###, $p < 0.001$; KO vs WT respect the same treatment.

significant decrease of Staufen1 level in response to NT-3 stimulation in proximal and distal compartments, while other treatments did not change Staufen1 signal significantly with respect to untreated conditions. TIA-1 expression resulted similar to those of Staufen1 (fig. 7D) however, BDNF and NT-3 stimuli decreased its expression significantly with respect to untreated MeCP2 KO neurons (fig. 7 D; KO 20-60 µm; vehicle 0.62 ± 0.07, NT-3 0.41 ± 0.03, BDNF 0.42 ± 0.04; *, $p<0.05$ NT-3 and BDNF respect to vehicle) (fig. 7 D; KO 60-100 µm; vehicle 0.53 ± 0.06, NT-3 0.31 ± 0.02, BDNF 0.34 ± 0.05; *, $p<0.05$ NT-3 and BDNF respect to vehicle). Moreover, a slight decrease with respect to wild type levels was detected in distal dendritic compartments of MeCP2 KO neurons after BDNF treatment (fig. 7D; 20-60 µm; WT BDNF 0.6 ± 0.06, KO BDNF 0.43 ± 0.04; #, $p<0.05$ BDNF WT vs BDNF KO). Dcp1a resulted slightly, although not significantly, decreased in dendrites of wild type neurons both after neurotrophic or arsenite treatment in all the segments analyzed (fig. 7E). Interestingly, Dcp1a signal in resting conditions resulted systematically lower in dendrites of MeCP2 KO neurons, with significant changes between 20 and 60 µm (fig. 7E; 20-60 µm; WT vehicle 0.73 ± 0.07, KO vehicle 0.54 ± 0.05; #, $p<0.05$ WT vehicle vs KO vehicle) and between 60 and 100 µm from soma (fig. 7E; 60-100 µm; WT vehicle 0.61 ± 0.06, KO vehicle 0.40 ± 0.03; #, $p<0.05$ WT vehicle vs KO vehicle). Moreover, neurotrophic and arsenite treatment did not affect Dcp1a distribution along dendrites of MeCP2 KO neurons (fig. 4.7E).

These results suggest that general levels of RBPs marker were unaltered in MeCP2 KO neurons, however significant alterations, in particular in processing bodies, were present along dendrites of these neurons.

6. Characterization of RNA granules in dendrites of MeCP2$^{-/y}$ hippocampal neurons

Measurement of the Staufen1, TIA-1 and Dcp1a levels through western blot and densitometric analysis along apical dendrites did not provide exhaustive information about the composition of isolated RNA granules in dendrites. In fact, protein lysates retain also granule components from somatic area, while intensity measured in whole dendritic shaft did not discriminate between RBPs within granules and the cytoplasmic diffused pool. For example, in resting conditions TIA-1 protein is

organized in diffuse pools and small granules that after stressful stimuli, nucleate in large, dense and intensely stained stress granules (Kedersha et al., 2008).

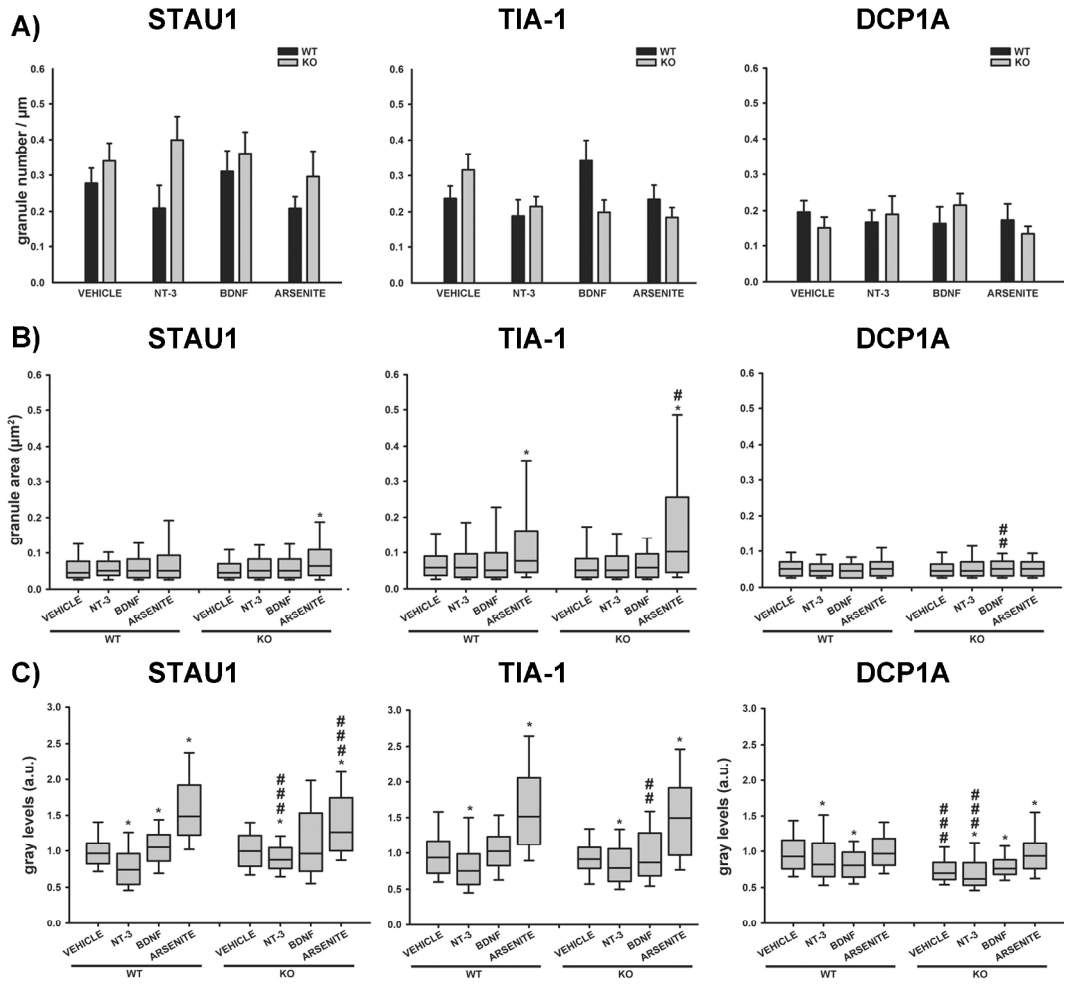

Figure 8. Granule analysis of RNP containing Staufen1, Tia-1 and DCP1a in apical dendrites of wild type and MeCP2 KO hippocampal neurons. A) Measurement of the density of transporting granules (Stau1), stress granules (TIA-1) and processing bodies (DCP1A) along the first 100 microns of apical dendrites in wild type (WT) and MeCP2 KO (KO) neurons untreated (vehicle) or treated with 0.5 mM sodium arsenite, 50 ng/ml BDNF (BDNF) or NT-3 (NT3) . Data are expressed as mean±S.E.M. of the number of granules counted for micron. B) Measurement of dimension of the granule classes in the same experimental condition. Data are reported as the distribution of the area (μm^2) of each granule detected. *, $p \leq 0.05$ respect its own vehicle. C) Measurement of intensity of the granule classes in the same experimental condition. Data are reported as the distribution of the intensity (gray scale) of each granule detected normalized to the average value of granule intensity of untreated wild type neurons. *, $p \leq 0.05$ respect its own vehicle. #, $p \leq 0.05$ KO vs WT respect the same treatment.

Accordingly, we decided to analyze individual transporting granules (Staufen1), stress granules (TIA-1) and processing bodies (Dcp1a) from apical dendrites of wild type and MeCP2 KO hippocampal neurons at DIV12 following the image processing

procedure described (see materials and methods and results chapter 4). We measured the number of granules along dendrites, expressed as n° of granules/µm, the area of granules, expressed in μm^2, and the labeling intensity, expressed as the mean of gray values normalized to the intensity of the granules in untreated wild type neurons. Analyses were performed in untreated neurons, after one hour of neurotrophic stimulation with NT-3 and BDNF, and after one hour of sodium oxidative stress induction by arsenite, to observe nucleation of stress granules and their interaction with other RNPs.

Regarding the number of granules detected per µm, no significant differences were highlighted between untreated wild type and MeCP2 KO neurons (fig. 8A, vehicle) in all the three classes of RNA granules. Moreover, we did not notice a clear pattern of re-localization of the RNP after neurotrophic stimulation or oxidative stress induction (fig. 8A, NT-3, BDNF and Arsenite), suggesting that the dynamic changes in the number of RNA granules were possibly detectable in a shorter or longer period of stimulation.

Transporting granules dimensions in resting neurons resulted similar between wild type and MeCP2 KO neurons, and were constant after the different treatments (fig. 8B, Stau1). However, an increase in the size of transporting particles were measured in MeCP2 KO neurons responding to oxidative stress induction (fig. 8B, Stau1 KO, *, $p<0.05$ Arsenite respect its own vehicle).

TIA-1 granules dimensions in resting condition and after neurotrophic stimulation displayed similar values to those of transporting particles in both wild type and MeCP2 KO population (fig. 8B, TIA-1). However, as expected, size of TIA-1 particles dramatically increased after sodium arsenite administration indicating the correct formation of stress granules (fig. 8B, TIA-1 WT and KO, *, $p<0.05$ arsenite respect its own vehicle). Of note, MeCP2 KO neurons nucleated larger stress granules with respect to wild type (fig. 4.8B, TIA-1 WT vs KO arsenite, #, $p<0.05$ WT vs KO after Arsenite treatment).

P-bodies presented less heterogeneous dimensions in comparison to transporting granules and stress granules, according to their constant round shaped structure along all the segment of dendrite (fig. 8B, Dcp1a). However, BDNF stimulation

promoted an enlarged size of Dcp1a granules in MeCP2 KO neurons with respect to wild type (fig. 8B, DCP1A WT vs KO BDNF, ##, $p<0.01$ WT vs KO after BDNF treatment).

RNA granules displayed heterogeneous RBP composition within the same type of particles, therefore granules of similar type and dimension could differ in the composition and quantity of RBPs that they contain. Moreover, it has been hypothesized that RNPs could exchange their components and RNA content by direct or indirect interactions (Buchan, 2014; Kedersha et al., 2005; Zeitelhofer et al., 2008). For these reasons, we decided to measure also the intensity of Staufen1, TIA-1 and Dcp1a within individual RNPs upon stimulation in order to identify possible patterns of interaction between them.

Transporting granules stained for Staufen1 showed comparable intensity in untreated wild type and MeCP2 KO neurons (fig. 8C, Stau1). After NT-3 stimulation, transporting granules where significantly depleted by their Staufen1 component in all neurons analyzed (fig. 8C, Stau1,WT and KO; *, $p<0.05$ NT3 respect its own vehicle), with a less extent in MeCP2 KO neurons (fig. 8C, Stau1,WT vs KO; ##, $p<0.01$ KO NT3 vs WT NT3). Previous studies demonstrated that synaptic activation lead to increased translation and RNP disassembly in neuronal dendrites (Mikl et al., 2011; Park et al., 2014). This suggested that a partially disassembly of Staufen1 RNP could occur after NT-3 stimulus, and this process is partially impaired in MeCP KO neurons. Conversely BDNF stimulation lead to an increase in wild type, but not in MeCP2 KO, neurons of the intensity of Staufen1 particles (fig. 8C, Stau1,WT; *, $p<0.05$ BDNF respect its own vehicle). Arsenite stimulation greatly increased intensity of Staufen1 granules in both wild type and MeCP2 KO neurons (fig. 8C, Stau1, WT and KO; *, $p<0.05$ arsenite respect its own vehicle). Staufen1 was previously found to be a component of stress granules, although it is not necessary for their nucleation (Thomas et al., 2009). However, in our experiments we did not notice an important increase in dendritic Staufen1 particles size after Arsenite treatment (fig. 8B, Staufen), confirming that after induction of oxidative stress we were still able to detect transporting particles individually. However, large stress granules in which Staufen1 particles were included were occasionally detected in soma.

TIA-1 granules intensity displayed a pattern similar to those of Staufen1 particles. In fact, basal levels were similar between wild type and MeCP2 KO neurons, and both displayed decreased levels after NT-3 stimulus (fig. 8C, TIA-1,WT and KO; *, $p<0.05$ NT3 respect its own vehicle). TIA-1 levels after BDNF treatment were slightly decreased in KO neurons respect to wild type (fig. 8C, TIA-1,WT vs KO; ##, $p<0.01$ BDNF KO respect BDNF wt), although no significant differences were found respect to resting condition. As expected, sodium arsenite treatment induced a dramatic enrichment of TIA-1 protein in newly formed stress granules (fig. 8C, TIA-1,WT and KO; *, $p<0.05$ arsenite respect its own vehicle). Remarkably, intensity were not changed in MeCP2 KO neurons despite the increased size.

Finally we evaluated Dcp1a labeling intensity in processing bodies. Intensity of processing bodies was significantly decreased after both neurotrophic stimuli respect untreated condition in wild type neurons (fig. 8C, Dcp1a, WT; *, $p<0.05$ NT3 and BDNF respect its own vehicle), in accordance to previous work that demonstrated how processing bodies were disassembled in response to synaptic activation (Zeitelhofer et al., 2008). Arsenite treatment did not affect Dcp1a intensity in wild type neurons. MeCP2 KO neurons displayed significantly less intense granules respect to those of wild type in resting condtion (fig. 8C, DCP1a,WT vs KO; ###, $p<0.01$ vehicle KO respect vehicle WT). NT-3 stimulus disassembled processing bodies also in MeCP2 KO neurons (fig. 8C, DCP1A, KO; *, $p<0.05$ NT3 respect its own vehicle), keeping the level of protein lower respect of NT-3 treated wild type neurons (fig. 8C, DCP1A, WT vs KO; ###, $p<0.01$ NT-3 KO respect NT-3 WT). Conversely BDNF and arsenite treatment had the opposite effect to raise Dcp1a level in processing bodies (fig. 8C, DCP1A, KO; *, $p<0.05$ BDNF and arsenite respect its own vehicle).

7. Interaction of stress granules with transporting granules and processing bodies in dendrites

Analysis of RNP intensity revealed that the larger size of stress granules observed in MeCP2 KO, as compared to wild type, neurons was not coupled to an increased content of TIA-1 protein. Moreover, transporting particles displayed reduced Staufen1 content respect to wild type, despite a slight increase in dimensions. Finally, processing bodies of KO neurons were enriched in Dcp1a protein during oxidative stress stimulus. Taken together, these observations suggest an altered interaction of

stress granules, known to be a site of RNP remodeling, with both transporting granules and processing bodies (Aulas et al., 2015; Kedersha et al., 2005).

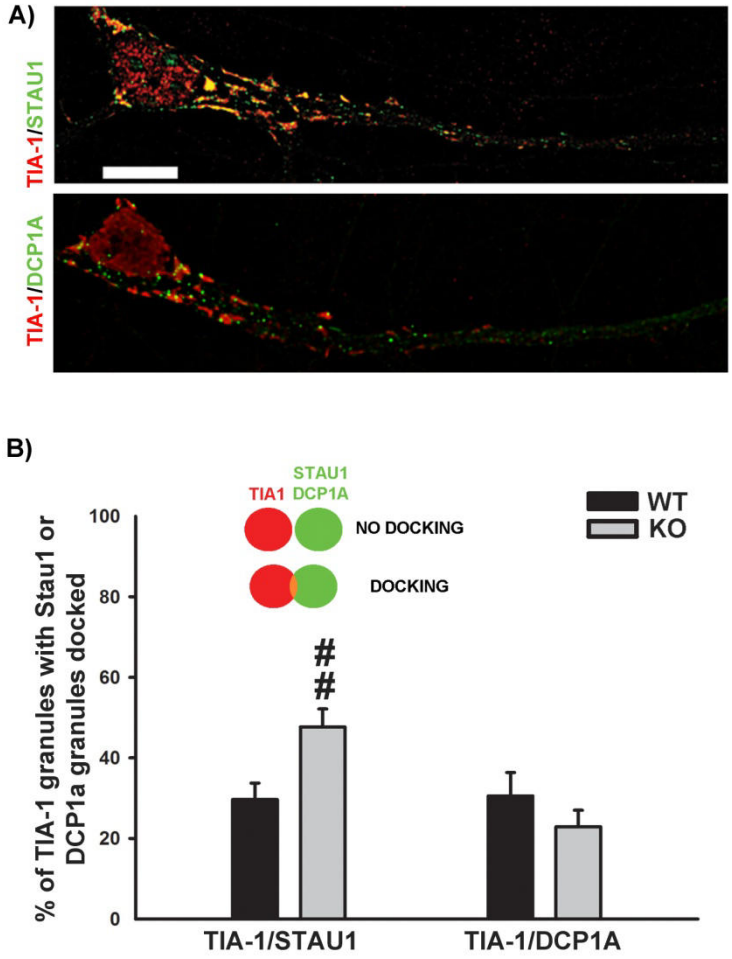

Figure 9. Docking of transporting granules and processing bodies on stress granules A) Representative images of hippocampal neurons stained for marker of stress granules TIA-1 (Red, both panels) and for marker of transporting granules Staufen1 (green, upper panel) and DCP1a (green, bottom panel). Scale bar: 10 µm. B) Docking analysis representing the percentage of TIA-1 positive granules that were partially or totally overlapped with Staufen1 or DCP1a granules (red and green circles) in wild type (WT, black bars) and MeCP2 KO (gray bars) neurons. Data are expressed as mean± S.E.M. ##, $p<0.01$ KO vs WT.

To asses this hypothesis we evaluated the percentage of stress granules presenting transporting particles or processing bodies "docked" on their surface. In figure 9A, representative images of hippocampal neurons treated with sodium arsenite and double-stained for TIA-1 (red) and Staufen1 or TIA-1 (red) Dcp1a (green) were reported. Stress granules of MeCP2 KO neurons resulted to be more engaged with transporting particles than in wild type neurons (fig. 9B, TIA-1/STAU1; wild type

29.65 % ± 4.1, MeCP2 KO 47.69 ±4.45; ##, p<0.01 KO respect to WT). No significant difference was found in the percentage of stress granules engaged with processing bodies (fig. 9B, TIA-1/DCP1a; wild type 30.56 % ± 5.8, MeCP2 KO 22.9 % ±4.11). Taken together, these findings show that the mechanism for stress response in which RNP are involved is altered in MeCP2 KO neurons, with exacerbated interaction between stress granules and transporting particles. In addition, these results point out to an unbalance in processing bodies composition and disassembly in response to BDNF stimulation.

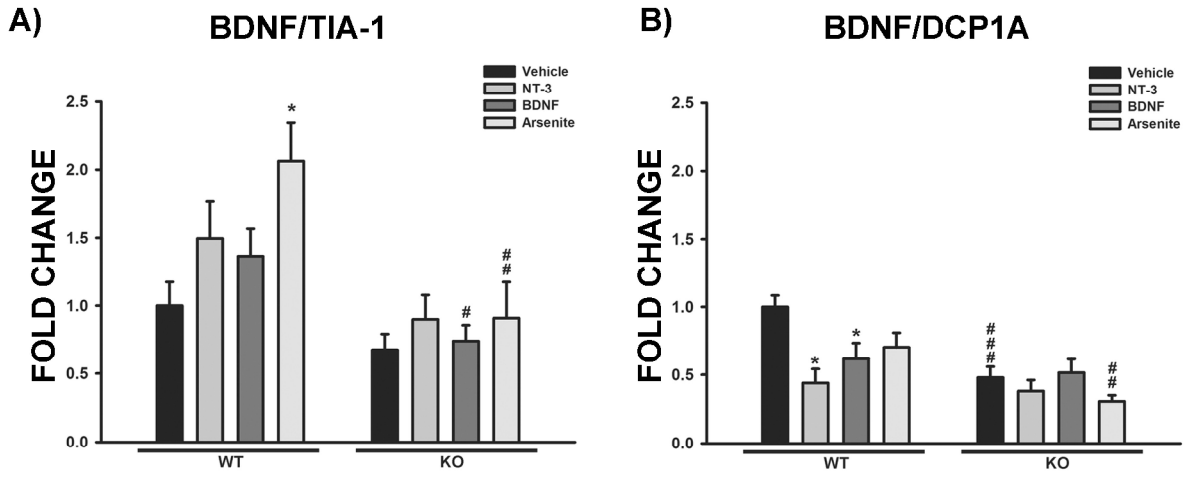

Figure 10. Colocalization of endogenous *BDNF* mRNA with stress granules and processing bodies in hippocampal neurons. Colocalization analysis of fluorescent *in situ* hybridization for endogenous *BDNF* mRNA in wild type (WT) and MeCP2 KO (KO) neurons untreated (vehicle) or treated with 0.5 mM sodium arsenite, 50 ng/ml BDNF (BDNF) or NT-3 (NT3) . Data are expressed as mean±SEM of the % of mRNA volume colocalized with TIA-1 protein (A) or DCP1a protein (B) normalized to the value of untreated wild type. *, p≤0.05 respect its own vehicle. #, p≤0.05, ##, p≤0.01, ###, p≤0.001, KO vs WT respect the same treatment.

8. Colocalization of BDNF mRNA with stress granules and processing bodies

In this set of experiments, we wanted to assess if the decreased amount of *BDNF* mRNA in MeCP2$^{-/y}$ dendrites was caused by an altered association of this transcript with stress granules or processing bodies. We then performed FISH against endogenous *BDNF* mRNA coupled to immunofluorescence for TIA-1 and Dcp1a, and evaluated the colocalization between RNA and these two proteins.

BDNF mRNA resulted poorly associated with TIA-1 granules (10.53 % ± 2.18 of mRNA volume colocalized) and Dcp1a (23.92 % ± 2.2) in untreated wild type neurons. Therefore, we decided to investigate if neurotrophic stimulation or oxidative damage were able to change the quantity of transcript localized in these granules. In wild type neurons, *BDNF* mRNA association with TIA-1 in resting condition and after BDNF and NT-3 neurotrophic stimulation (fig. 10A) did not differ significantly (fig. 10A). However, during oxidative stress, association was increased by two fold (fig. 10A, WT; vehicle 1 ± 0.18, arsenite 2.06 ±0.28; *,$p<0.05$ arsenite respect vehicle). In MeCP2 KO neurons, *BDNF* mRNA association to TIA-1 resulted systematically lower with respect to wild type, with a significant decrease after BDNF (fig. 10A, WT vs KO; BDNF WT 1.36 ± 0.2, BDNF KO 0.74 ± 0.12; ## ,$p<0.05$ WT BDNF vs KO BDNF) and sodium arsenite treatment (fig. 10A, arsenite WT 2.06 ±0.28 vs arsenite KO 0.91 ±0.27; ##, $p<0.01$).

In wild type neurons, *BDNF* mRNA reduced its colocalization with Dcp1a, suggesting it was released from processing bodies, after stimulation with NT-3 (fig. 10B, NT-3 WT 0.44 ± 0.1 vs vehicle WT 1.0 ± 0.09; *, $p<0.05$), or BDNF (fig. 10B, BDNF WT 0.62 ± 0.12 vs vehicle WT 1.0 ± 0.09; *, $p<0.05$) and in part, also after arsenite treatment, although statistically not significant (fig. 10B, arsenite WT 0.70 ± 0.11 vs vehicle WT 1.0 ± 0.09). In contrast, MeCP2 KO neurons did not display any significant change in the pattern of association between *BDNF* mRNA and Dcp1a in response to stimuli (fig. 10B KO). Moreover, *BDNF* mRNA resulted less associated with P-bodies in basal condition (fig. 10B, vehicle WT 1.0 ± 0.09 vs vehicle KO 0.48 ± 0.08; ###, $p<0.001$) and during oxidative stress (fig. 10B, arsenite WT 0.7 ± 0.11 vs vehicle KO 0.31 ±0.04; ##, $p<0.01$).

The general poor association in MeCP2 KO neurons of *BDNF* mRNA with stress granules or processing bodies could be caused by the general lower level of transcript and, in the case of P-bodies Dcp1a proteins in dendrites of mutated neurons.

9. Pharmacological treatment for rescue of neuronal atrophy in Rett syndrome hippocampal neurons *in vitro*

Previous *in vitro* and *ex-vivo* studies showed that MeCP2 mutation was associated to reduced total dendritic length, branching and spine density (Chapleau et al., 2009; Larimore et al., 2009).

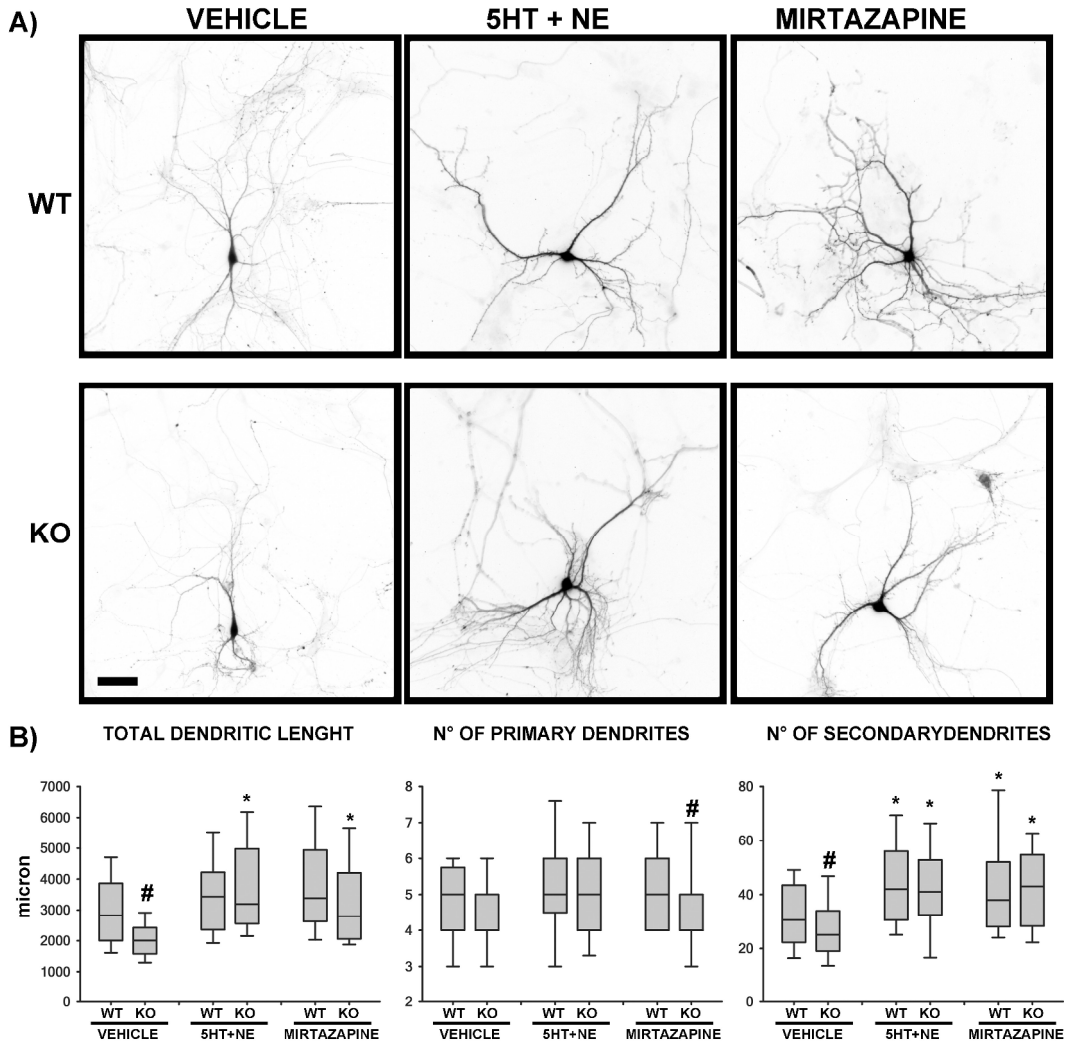

Figure 11. Chronic pharmacological treatment of MeCP2$^{-/y}$ Bird hippocampal neurons *in vitro*. A) Representative images of pEGFP-N1 transfected hippocampal neurons from wild type (WT, upper row) and MeCP$^{-/y}$ (KO, lower row) mice untreated (vehicle) or treated with 50 µM serotonin + 50 µM Norepinephrine (5HT + NE) or 10 µM Mirtazapine for 9 days. Scale bars: 20 µm. B) Measurements of morphological parameters analyzed. Total dendritic length is expressed in micron; box plots represent the distribution of the total dendritic length, the number of primary and secondary dendrites of all neuron analyzed. *, $p<0.05$ respect its own vehicle. #, $p<0.05$ KO vs WT respect the same treatment.

An *in vitro* staging system for the study of neuronal development, consisting in a detailed morphometric quantification of axons, dendrites, spines and synapses development from days-in-vitro (DIV) 1 to 15 of murine hippocampal cultured neurons was developed. Using this tool it was demonstrated that RTT neurons displayed both a developmental delay and a phenotype maintenance failure regarding dendritic arborization and spine development in hippocampal neurons (Baj et al., 2014).

Treatment of MeCP2-null Bird mice with Mirtazapine, an anti-depressant that enhances serotoninergic and noradrenergic transmission and raises BDNF levels (Holm and Markham, 1999; Rogoz et al., 2005; Vaghi et al., 2014), recovered most of the neuronal atrophy features affecting total cortical thickness, brain weight, cortical neuron soma size and dendritic arborization (Bittolo et al., 2016). However the mechanisms involved in this rescue are still poorly understood. We took advantage of the *in vitro* staging system described by Baj and colleagues to evaluate if the developmental delay of hippocampal Mecp2$^{-/y}$ neurons could be rescued also *in vitro* by chronic or acute treatment with Mirtazapine. Hippocampal neuronal cultures were obtained from p0 wild type and MeCP2$^{-/y}$ Bird C57/BL6 male mice. Starting from DIV3 cultures were treated in parallel with 10 µM Mirtazapine or 50 µM serotonin (5HT) + 50 µM Norepinephrine (NE) for 9 days.

Neurons were transfected at DIV9 with pEGFP-N1 vector to allow the visualization of neuronal morphology in isolated cells. Neurons were imaged at DIV12, which represented the development stage in which major morphological deficits were reported (Baj et al., 2014), and morphological parameters (total dendritic length, number of primary and secondary dendrites) were measured in order to evaluate if a rescue occurred.

As previously described, MeCP2 KO neurons displayed lower dendritic complexity (fig. 11A, vehicle), with reduced length of total dendritic arborization (fig. 11B, total dendritic length; WT vehicle vs KO vehicle; #, $p<0.05$) and reduced number of secondary dendrites (fig. 11B, n° of secondary dendrites; WT vehicle vs KO vehicle; #, $p<0.05$). Number of primary dendrites resulted unaltered. After 9 days of treatment, Mirtazapine or combined 5HT+NE administration were able to rescue total dendritic length (fig. 11B, total dendritic length; KO 5HT+NE and KO mirtazapine vs KO vehicle; *, $p<0.05$) and the secondary branches (fig. 11B, n° of secondary

dendrites; KO 5HT+NE and KO mirtazapine vs KO vehicle; *, p<0.05) to wild type levels. Antidepressant and 5HT+NE treatment did not affect significantly the total length of dendrites in wild type neurons, although they increased the number of secondary dendrites (fig. 11B, n° of secondary dendrites; WT 5HT+NE and WT mirtazapine vs WT vehicle; *, p<0.05). These results show that Mirtazapine retains *in vitro* the ability to rescue neuronal atrophy similar to the *in vivo* situation.

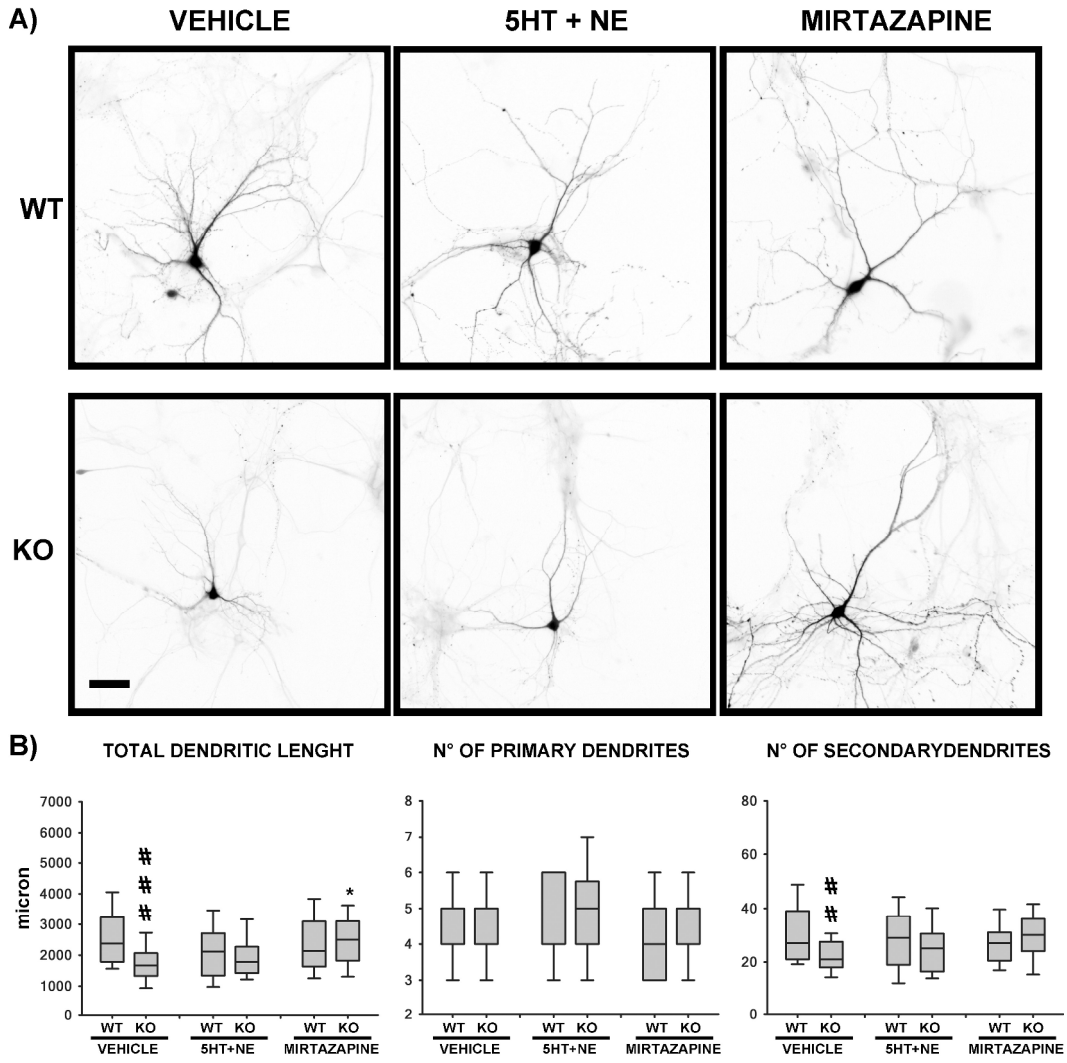

Figure 12. Acute pharmacological treatment of MeCP2$^{-/y}$ Bird hippocampal neurons *in vitro*. A) Representative images of pEGFP-N1 transfected hippocampal neurons from wild type (WT, upper row) and MeCP$^{-/y}$ (KO, lower row) mice untreated (vehicle) or treated with 50 µM serotonin + 50 µM Norepinephrine (5HT + NE) or 10 µM Mirtazapine for 3 days. Scale bars: 20 µm. B) Measurements of morphological parameters analyzed. Total dendritic length is expressed in micron; box plots represent the distribution of the total dendritic length, the number of primary and secondary dendrites of all neuron analyzed. *, p<0.05 respect its own vehicle. ##, p<0.01; ### p<0.01, KO vs WT respect the same treatment.

We then decided to investigate if a shorter treatment with the same drugs were still able to recover morphological deficits. To test this hypothesis, we performed a rescue experiment by treating cultured neurons for only 3 days, starting treatments at DIV9. In fact, at the stage between 9 and 12 DIV, MeCP2 KO neurons display the highest atrophy along all *in vitro* development. Shortened treatment with 5HT+NE resulted ineffective to rescue morphological deficits in MeCP2 KO neurons (fig. 12A and B), and also wild type neurons morphology resulted unaltered (fig. 12A and B). In contrast, shortened Mirtazapine treatment was still able to increase total dendritic length in MeCP2 KO neurons (fig. 12B, total dendritic length; KO 5HT+NE and KO mirtazapine vs KO vehicle; *, $p<0.05$) to similar levels of wild type. However, the number of secondary dendrites resulted not fully recovered.

In conclusion, chronic administration and, to a lesser extent, acute administration of Mirtazapine were able to rescue neuronal atrophy features in MeCP2 KO neurons. This model may allow to dissect out the molecular mechanisms underlying neuronal atrophy and its pharmacological rescue.

DISCUSSION

In the first part of this work we elucidated unrevealed mechanisms for the regulation of *BDNF* mRNA localization into dendrites. Recent studies suggested that trafficking of a specific group of mRNA into dendrites is a key mechanism of spinogenesis, synaptic plasticity and neurites outgrowth (Liu-Yesucevitz et al., 2011). *Brain-derived neurotrophic factor (BDNF)* mRNA is expressed in dendrites of cortical and hippocampal neurons (Eberwine et al., 2002) and its translation is required during long term potentiation (LTP) (Pang and Lu, 2004; Santi et al., 2006). Recently, *BDNF* mRNA transport in dendrites has been deeply investigated in order to discover which mechanisms regulate its trafficking. *BDNF* mRNA is transported in dendrites upon activity dependent stimulation both *in vitro* (Righi et al., 2000; Tongiorgi et al., 1997) and *in vivo* (Baj et al., 2013; Tongiorgi et al., 2004), where it has been found associated to polyribosomes of dendritic shaft and spines (Tongiorgi et al., 2004). Moreover, the eleven splicing variants in rodents (Aid et al., 2007) were found to be differentially expressed in brain areas (Maynard et al., 2015) and dendritic compartments of hippocampus (Baj et al., 2013; Baj et al., 2011; Chiaruttini et al., 2008; Chiaruttini et al., 2009). Interestingly, the work of Chiaruttini and colleagues on rat hippocampal cultured neurons clearly demonstrated that BDNF coding sequence (CDS) encodes a signal for constitutive dendritic targeting which required Translin RNA binding protein (RBP). However, dendritic targeting is abolished in BDNF transcripts harboring 5'UTR exon1 and, partially, exon4, while it is not affected by exon2B, 2C and 6 (Chiaruttini et al., 2009).

Despite these findings, one important question remained unanswered: do the different 5'UTR splice variants contain targeting signals able to regulate sorting of a reporter mRNA?

In order to answer this question we used the same approach of the above cited work, evaluating the ability of *BDNF* 5'UTR to affect the sorting of *green fluorescent protein* (GFP) reporter mRNA. We found that exon1 and 4 did not affect significantly *GFP* localization, and so did exon 6. Differently, all exon2 splicing isoforms (2a, 2b and 2c) induced a general re-localization of reporter mRNA along distal segments of dendritic shafts. Furthermore none of this exon affected mRNA sorting upon depolarization induced by KCl. The remaining isoforms (3, 5, 7 and 8) have not been previously investigated *in vitro* regarding their influence on *BDNF* CDS targeting. Exon 3, 5 and

7 resembled the same distribution of *GFP* alone in basal condition and after depolarization, although exon 3 was weakly targeted into dendrites after KCl. Exon 8 resulted weakly expressed in all dendrites with lower levels respect to GFP. Taken together, these results suggested that all the 5'UTR variants, except those of exon2, have no signals that directly regulate mRNA trafficking. Bioinformatic analysis of these sequences did not identify putative binding sites for RNA binding proteins (RBPs) involved in mRNA trafficking. As expected most of isolated *cis*-elements have been previously described to be involved in mRNA alternative splicing, stability and translation. This confirmed previous evidence that placed most of the regulatory sequences for mRNA trafficking in 3'UTR (Andreassi and Riccio, 2009). However, some important exception for 5'UTR were reported in literature. 5'UTR of BC1 untranslated RNA retains a dendritic targeting element (DTE) organized in a stem loop structure bound by hnRNP A2 protein (Muslimov et al., 2006). Stem loop formation and complex secondary structure have been reported to be required for mRNA localization mediated by *trans*-acting factor (Martin and Ephrussi, 2009). Staufen1 is a perfect example for this purpose. This RBP is a key regulator of mRNA trafficking and translation in dendrites and binds to several heterogeneous double strand RNA (dsRNA) structures to regulate mRNA fate (Heraud-Farlow and Kiebler, 2014; Sugimoto et al., 2015). For these reasons, possible secondary structures in the exon 2a sequence, shared by all exon 2 isoforms, have to be further investigated. Bioinformatic analysis of exon2 highlighted the presence of several AU-rich regions, possibly bound by ELAVLs proteins, known to regulate *BDNF* mRNA stability through the binding of its 3'UTR (Allen et al., 2013). This let us speculate about the possibility that binding of ELVALs to 5'UTR may differentially regulate mRNA stability of *BDNF* variants and consequently, their localization.

However, it is worth noting that *BDNF* 5'UTR variants have been characterized as regulator of *BDNF* CDS induced constitutive trafficking, acting as selectors for subcellular localization of this transcript (Baj et al., 2011; Chiaruttini et al., 2009). Moreover, the systematic analysis carried out by Baj and colleagues about the localization of 5'UTR variants in hippocampus upon pilocarpine-treatment demonstrated that the same variant could be enriched following *status epilepticus* in proximal or distal dendrites depending on the hippocampus region (Baj et al., 2013), suggesting that factors recruited on *BDNF* transcript may affect differently transcription variants. These studies strongly suggested that an interaction between

5'UTRs and CDS or 3'UTR of *BDNF* could be required for regulation of endogenous *BDNF* mRNA trafficking.

In the past years, we have deeply characterized mechanisms of activity dependent *BDNF* mRNA trafficking mediated by the two 3'UTRs (Vicario et al., 2015). In this context we described the interaction of different RBPs with *BDNF* transcript required for the targeting into dendrites. Using an *in silico* approach we identified sequence clusters highly conserved during evolution in the CDS and 3'UTRs of *BDNF*. The short 3'UTR (nts 1-321) resulted almost identical in vertebrates, while the long isoform displayed two hotspots of conservation: the mid (nts 890-1515) and the end (nts 2339-2790) regions. Within these high conserved sequences we identified several putative binding sites for RBPs involved in *BDNF* mRNA trafficking, stability and translatability: CPEBs, ELAVLs and FMRPs. CPEB1 is required for both short (Oe and Yoneda, 2010) and long 3'UTR dendritic trafficking (Vicario et al., 2015). ELAVL4/HuD enhances stabilization and translation of long 3'UTR transcripts (Allen et al., 2013). Fmr1 knock-out mice display increased *BDNF* mRNA level in dendrites (Louhivuori et al., 2011), suggesting a role for this protein in *BDNF* mRNA localization. In this work we demonstrated by IP assay that neuronal ELAVLs bound exclusively to both isoforms of 3'UTR and no to CDS. UV-CLIP using radiolabeled probes for 3'UTRs region demonstrated a marked affinity of nELAVLs for AU-rich mid region. Further IP assay demonstrated that *BDNF* mRNA was specifically bound from Fmr1. Interaction with CPEBs has been previously described by Oe and Yoneda (Oe and Yoneda, 2010). Then we characterized *in vitro* the colocalization grade of RBPs and *BDNF* mRNA by visualization of endogenous mRNA using FISH and by immunofluorescence for the different RBPs, including Translin (Chiaruttini et al., 2009). As expected, Translin was highly associated to *BDNF* mRNA and vice versa, both in proximal and distal compartments, confirming the previous role in the trafficking of this transcript (Chiaruttini et al., 2009). *BDNF* mRNA displayed a similar pattern of colocalization with ELAVLs and FMRP, with high level of association in proximal compartments that dropped down in distal dendrites. This is in accordance with different features displayed by this RBPs: first they represent the only subset of proteins negatively affecting mRNA dendritic trafficking (Louhivuori et al., 2011; Vicario et al., 2015), therefore they are strongly associated in proximal compartment, keeping *BDNF* mRNA anchored near soma, but are less present in mRNA granules

targeted to dendrites. However, a basal association was detectable in dendrites, in accordance with their role of mRNA stabilizer for ELAVLs (Allen et al., 2013), and of translational repressor for Fmr1 (Castren and Castren, 2014). Conversely, CPEBs association resulted generally lower respect to other RBPs in the proximal compartment, with a slight increase in distal dendrites. However, it should be noted that unfortunately CPEB1, the most involved member in trafficking mechanism, was not detectable after FISH processing. CPEB2 mediates the trafficking of short 3'UTR mRNA, that represent approximately half of the endogenous *BDNF* mRNA in hippocampus (An et al., 2008) thus, low levels of association were expected. Accordingly, its association increased in distal compartments, suggesting that BDNF mRNA granules were enriched of CPEB2.

In conclusion, we characterized the association of different families of RBPs to *BDNF* mRNA, highlighting an heterogeneous pattern of association. However, the dynamic interaction of RBPs and mRNA during synaptic activation are still unclear. Live imaging studies would be very helpful to elucidate which are the dynamics of *BDNF* mRNA transporting granules harboring the different subset of RBPs responding to KCl depolarization or neurotrophic stimuli.

In the second part of the work we investigated the mechanisms underlying neuronal atrophy in Rett Syndrome. This postnatal neurodevelopmental disorder is mainly caused by mutations on X chromosome in *MECP2* gene, that encodes for MeCP2 protein, a methylated CpG binding protein considered one of the most important transcriptional regulator during brain development (Chahrour and Zoghbi, 2007). Brains of RTT patients are characterized by a general neuronal atrophy concerning the dimension of neuronal soma, the dendritic arborization, spine density and maturation (Armstrong et al., 1995; Armstrong, 1995; Chapleau et al., 2009; Kaufmann et al., 1995; Kaufmann et al., 1997a; Kaufmann et al., 1997b; Subramaniam et al., 1997). These atrophic features are present in different mouse models for this pathology both *in vivo* (Belichenko et al., 2009; Fukuda et al., 2005) and *in vitro* (Baj et al., 2014; Larimore et al., 2009). Actually, many hypothesis have been proposed about the altered mechanisms that could cause this atrophic development. First, BDNF expression, both mRNA and protein, is decreased in different brain region, including hippocampus (Li and Pozzo-Miller, 2014), and

treatments that raise BDNF levels results in amelioration of symptoms (Ogier et al., 2007; Tropea et al., 2009) and reversion of atrophic neuronal phenotypes (Larimore et al., 2009). Despite these findings, possible deficits in *BDNF* mRNA levels in dendrites has not been clearly characterized. For this reason, we investigated if *BDNF* mRNA was not correctly localized in apical dendrites of RTT hippocampal cultured neurons. It was previously demonstrated that major deficits of *in vitro* neuronal development in RTT neurons were detectable at DIV12 (Baj et al., 2014). Accordingly, we chose this time point for our analysis. We found that *BDNF* mRNA was basally decreased along all apical dendrites of RTT neurons comparing to wild type, suggesting that an altered mechanism in mRNA localization may be involved. Accordingly, we treated neurons with NT-3 and BDNF to induce *BDNF* mRNA trafficking (Righi et al., 2000; Vicario et al., 2015). Surprisingly, we observed a dramatic decrease of *BDNF* transcripts in dendrites after NT-3 stimulation and no significant alteration after BDNF treatment. NT-3 treatment has been described to rapidly increase translation in neurons (Krichevsky and Kosik, 2001) and to induce dendritic trafficking of short 3'UTR transcript after 3 hours (Vicario et al., 2015). It is worth noting that mRNA with short *BDNF* 3'UTR display higher translatability with respect to those with long 3'UTR (Vaghi et al., 2014). Thus, we hypothesized that one hour of NT-3 treatment could rapidly induce the translation of *BDNF* mRNA and its degradation, but was not sufficient to increase the transport of *BDNF* mRNA as changes in trafficking probably require longer stimulations (Vicario et al., 2015). Similarly, one hour of BDNF stimulation was not sufficient to induce an increase in *BDNF* mRNA trafficking. *BDNF* transcripts display low expression in distal dendrites both in basal and after neuronal stimulation (An et al., 2008; Tongiorgi et al., 1997; Will et al., 2013). The transport induced by BDNF itself displays a significantly lower speed rate (2.5 µm/h) (Righi et al., 2000) respect those induced by KCl (8 µm/h) (Tongiorgi et al., 1997) and needs at least three hours to be exerted, independently from the duration of the triggering stimulus (Righi et al., 2000). Furthermore, trafficking of *BDNF* mRNA harboring long 3'UTR is constitutively repressed by ELAVLs and FMRPs, and dendritic localization is achieved only upon relief of repressors factor by BDNF (Vicario et al., 2015). Finally, BDNF mRNAs with the long 3'UTR display lower translatability respect to short one (Vaghi et al., 2014). According to this evidence, increments of *BDNF* mRNA levels after only one hour of BDNF stimulation could not be detectable. *BDNF* mRNA levels in dendrites of

MeCP2$^{-/y}$ neurons did not decrease after NT-3 stimulation, displaying comparable level of unstimulated MeCP2$^{-/y}$ neurons. Additionally, BDNF stimulation was not able to rescue mRNA levels to those of wild type. Together, these findings demonstrated a general alteration in *BDNF* mRNA localization in MeCP2$^{-/y}$ neurons.

We hypothesized that deficits in RBP machinery could be the cause of low levels of *BDNF* mRNA in dendrites. Other evidence indirectly suggests that alteration in RNA granules could represent a pathogenic mechanism in RTT. Recent studies reported high levels of oxidative stress in RTT patients (De Felice et al., 2009; Durand et al., 2013) that are reported also in two different RTT mouse models (De Felice et al., 2014). Indeed, nucleation of stress granules represents a well characterized cellular response to oxidative stress (Kedersha and Anderson, 2007). Furthermore, severe alterations in mTOR/PI3K signaling pathway are associated to a decreased general protein synthesis in RTT mouse brain (Ricciardi et al., 2011). This is in accordance with several recent studies that are converging on the hypothesis that dysregulated mTOR pathway could be a common mechanism leading to altered local protein synthesis in dendrites and consequently altered spines and synapses development (Phillips and Pozzo-Miller, 2015). Fragile-X syndrome represent the most explanatory case that connected alteration of RBPs and dysregulated local protein synthesis (Bassell and Warren, 2008). According to our hypothesis, we chose representative markers for the three most representative classes of mRNA granules in neurons: Staufen1 for transporting granules, TIA-1 for stress granules and Dcp1a for P-bodies. We found no significant alterations of general protein levels of the three markers in lysates of hippocampal cultured neurons. Conversely, the densitometric analysis along apical dendrites highlighted lower levels of Dcp1a protein along dendrites. We decided to characterize dendritic mRNA granules individually in order to get a most refined analysis of their number, dimensions and density of RBP content. Regarding the number, we did not notice any significant change in RNPs number in the whole apical dendrites. It should be noted that this parameter was often found variable in literature, depending on the cellular system, duration and extent of stimulation (Cougot et al., 2008; Krichevsky and Kosik, 2001; Zeitelhofer et al., 2008). Moreover, live imaging studies demonstrated that activity dependent stimuli results in a switch from oscillatory to straightforward dynamic followed by a fine positional adjustment of RNA granules, without affecting their total number (Rook et al., 2000).

Granules dimensions and RBP content revealed several alterations. Neurotrophic stimuli did not alter dimension of transporting particles or TIA-1 granules, while P-bodies were slightly enlarged after BDNF treatment in MeCP2$^{-/y}$ neurons. NT-3 stimulation dramatically decreased Staufen1 and TIA-1 content from their respective granules. This is in accordance with dynamics of *BDNF* mRNA observed in apical dendrites of wild type neurons. Previous works demonstrated that NT-3 stimulus is able to open the dense structure of transporting granules to release mRNA, ribosomes and Staufen1 RNPs (Krichevsky and Kosik, 2001). Furthermore, live imaging studies shown how transporting granules may gradually disassemble in response to activity dependent stimulation (Mikl et al., 2011; Park et al., 2014). Our findings suggest that NT-3 generally increased the translation of dendritic mRNA by inducing the disassembly of transporting granules. This is further confirmed by the fact that TIA-1, a general repressor of translation (Lopez de Silanes et al., 2005), was decreased in dendritic RNPs following NT-3 treatment. MeCP2$^{-/y}$ neurons displayed only a partial transporting granule disassembly upon NT-3 stimulation, suggesting a decreased release of mRNAs from transporting particles. This is in line with previous observations regarding lower *BDNF* mRNA level in MeCP2$^{-/y}$ neurons. Differently from NT-3, BDNF stimulation did not affect significantly the RBP content of transporting granules and TIA-1 particles. The analysis of Dcp1a content in P-bodies confirmed the lower density of MeCP2$^{-/y}$ p-bodies respect to wild type. Neurotrophic stimulation induced a decrease in Dcp1a levels, in accordance to previous studies that observed a general disassembly of p-bodies after synaptic activation (Zeitelhofer et al., 2008). This mechanism was partially impaired in MeCP2$^{-/y}$ neurons, where BDNF stimulation even increases the density of Dcp1a in P-Bodies, suggesting an increased mRNA degradation. However, it is important to note that Dcp1a levels were constitutively lower in MeCP2$^{-/y}$ dendrites, despite comparable total protein levels from the western blot analysis. Together, these findings suggest that dendrites of MeCP2$^{-/y}$ neurons are characterized by a dysregulation of RBPs regulating mRNA dynamics in particular, in their response to neurotrophic stimuli.

Concerning oxidative damage response, stress granules nucleated in MeCP2$^{-/y}$ neurons were larger than wild type but their TIA-1 average intensity remained stable. Transporting particles instead, displayed a slight increase of size in MeCP2$^{-/y}$ neurons but their content in Staufen1 resulted significantly lower. Given this we

investigated the interaction of mRNA granules with stress granules, considered a docking station for dynamic RNP remodeling (Kedersha et al., 2000; Kedersha et al., 2005). We found an exacerbated docking of transporting particles on stress granules of MeCP2$^{-/y}$ neurons, suggesting that mRNA could be shunt and repressed into these RNPs during stressful condition, contributing to increased oxidative damage previously observed (De Felice et al., 2014).

We finally investigated if lower dendritic levels of *BDNF* mRNA in MeCP2$^{-/y}$ neurons were caused by an aberrant association with stress granules or processing bodies. *BDNF* transcripts resulted poorly associated with these two classes of RNPs in all conditions, suggesting that degradation of this mRNA is regulated in other ways. Interestingly this transcript was released from p-bodies upon neurotrophic stimuli, allowing its presumable translation. In MeCP2$^{-/y}$ neurons *BDNF* were generally less associated respect to wild type with both stress granules and p-bodies. This was probably caused by the basal lower level of *BDNF* mRNA in dendrites.

In conclusion, the lower levels of *BDNF* mRNA, together with the altered RNPs regulation during neuronal activity and oxidative stress, suggested possible pathogenic mechanisms involving mRNA homeostasis in dendrites of MeCP2$^{-/y}$ neurons. Some major issues remained unresolved and will be investigated in the next future: first, the general level of dendritic mRNA could directly influence RNA granules assembly and dynamics, and should be investigated. Secondly, this last aspect, together with the reported RBP alteration, should be monitored during *in vitro* development to possibly reveal a critical point in which the RBP machinery displays the major deficits. Thirdly, shorter or longer times of neurotrophic and arsenite stimulation should be investigated due to the high dynamism of RNPs. Finally, the dynamics of the different RNPs should be investigated in living neurons using fluorescent markers. This will better elucidate the mechanism behind the aberrant interaction between RNPs, reported here.

In the last part of this work, we performed an *in vitro* pharmacological rescue in MeCP2$^{-/y}$ hippocampal neurons. Many efforts were made to develop a therapy for the cure of RTT (Pozzo-Miller et al., 2015). MeCP2 mutations do not cause neuronal degeneration in RTT brains (Akbarian, 2003) and reintroduction of normal levels of

expression of MeCP2 results in a complete reversion of atrophic phenotypes (Guy et al., 2007). The actual therapeutic strategies for curing RTT used different approaches, from the reintroduction of MeCP2 through gene therapy to the targeting of downstream effectors of MeCP2 (Pozzo-Miller et al., 2015). Treatment with the anti-depressant Desipramine, an inhibitor of serotonin reuptake, to restore monoaminergic pathway improves lifespan and respiratory dysfunction in a mouse model of RTT (Roux et al., 2007). However, heart failure occurred during a clinical trial on RTT patients. Recently, our laboratory developed a promising treatment with Mirtazapine, a selective antagonist of α2-adrenergic autoreceptors and heterorecepetors and blocker of 5-HT2 and 5-HT3 receptors. Mirtazapine, rescued general brain atrophy of MeCP2$^{-/y}$ mice (Bittolo et al., 2016). The characterization of the molecular mechanisms promoting this rescue could improve therapeutic strategies using ADs for the cure of RTT. It is worth noting that RTT neuronal atrophic features are resembled in different *in vitro* models (Baj et al., 2014; Larimore et al., 2009). In our laboratory, Baj and colleagues developed an *in vitro* staging system for the study of neuronal development from murine hippocampal cultures. Moreover, they demonstrated that MeCP2$^{-/y}$ neurons display a delayed development of dendritic arborization, with major deficits reported between 9 and 12 days of *in vitro* (Baj et al., 2014). According to these findings, we decided to use this staging system in order to investigate if Mirtazapine treatment could rescue atrophic phenotype of MeCP2$^{-/y}$ neurons *in vitro*. We found that chronic treatment with Mirtazapine completely rescued dendritic arborization deficits of MeCP2$^{-/y}$ neurons, increasing also the secondary dendritic branches in wild type neurons. Shorter treatment performed in the critical staging step between DIV 9 and 12 partially rescued the length of dendrites in MeCP2$^{-/y}$ neurons, but was not able to increase dendritic branches. Interestingly also MeCP2$^{-/y}$ neurons chronically treated in parallel with serotonin and norepinephrine rescued to wild type level. Accordingly, acute treatment with both neurotransmitters had no significant effects on dendritic arborization.

In conclusion, we found that both Mirtazapine and combined treatment with serotonin and norepinephrine were able to rescue neuronal atrophy in MeCP2$^{-/y}$ neurons *in vitro.* The striking parallelism between *in vivo* and *in vitro* effects of Mirtazapine opened new perspective to dissect molecular mechanisms underlying neuronal

atrophy in RTT. In the next future we are planning to use selective inhibitors of BDNF signaling in order to evaluate if its pathway is involved for the rescue mediated by Mirtazapine and monoamines. Finally this model could be useful for high throughput screening of different compounds for possible therapies of RTT.

CONCLUDING REMARKS

In the first part of this work we investigated unrevealed mechanisms of 5'UTR and 3'UTR *BDNF* mRNA trafficking in hippocampal neurons. We found that:

- exon 2a, 2b and 2c 5'UTR splicing isoforms contained a constitutive dendritic targeting element that induced the trafficking of *GFP* reporter mRNA
- 5'UTR sequences do not encode *cis*-element for activity dependent mRNA trafficking
- *BDNF* mRNA displayed hot spots of evolutionary conservation in its 3'UTR sequence. In these regions, several putative binding sites for CPEBs, ELAVLs and FMRPs were detected
- Neuronal ELAVLs and Fmr1 bind to the central region of 3'UTR
- *BDNF* mRNA was strongly colocalized with Translin *in vitro*, and displayed heterogeneous colocalization patterns with other RBPs

In the second part of the work, we investigated possible mechanisms involved in neuronal atrophy of Rett Syndrome hippocampal neurons. We found that:

- *BDNF* mRNA levels were significantly lower in dendrites of MeCP2$^{-/y}$ neurons
- General levels of marker for transporting granules, stress granules and processing bodies were unaltered in protein lysates of MeCP2$^{-/y}$ neurons
- Processing bodies of MeCP2$^{-/y}$ neurons were significantly less dense and did not disassemble upon BDNF stimulation
- Transporting granules disassembly upon NT-3 stimulation is partially impaired in MeCP2$^{-/y}$ neurons
- MeCP2$^{-/y}$ neurons nucleated larger stress granules than wild type neurons during oxidative stress, resulting in exacerbate recruiting of transporting particles on their surface
- *BDNF* mRNA was poorly associated to stress granules and p-bodies

Finally, we performed a pharmacological rescue of MeCP2$^{-/y}$ neurons *in vitro* using Mirtazapine antidepressant. We found that:

- Chronic (9 days) but no acute (3 days) treatment with Mirtazapine fully rescued atrophic phenotype of MeCP2$^{-/y}$ dendritic arborization

- Chronic (9 days) but no acute (3 days) treatment with serotonin and norepinephrine fully rescued atrophic phenotype of MeCP2$^{-/y}$ dendritic arborization

SUPPLEMENTARY FIGURES

Supplementary Figure 1. Bioinformatic analysis using phastCons showing the degree of consensus on *BDNF* coding regions and 3'UTR among Primates (top), Mammals (middle) and vertebrates (bottom). Similarity scores range from 0 (= no homology) to 1 (identical sequence). Numbers at the top of the figure indicate the nucleotide position along the *BDNF* gene along chromosome 11.

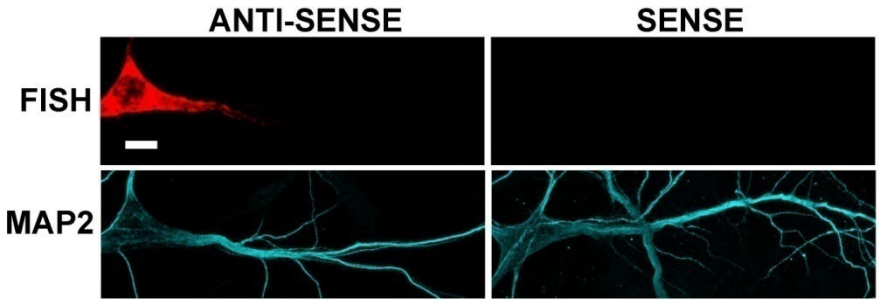

Supplementary Figure 2. Representative images of fluorescent *in sity* hybridization signal (F.I.S.H., red) using an anti-sense or a sense probe against *BDNF* coding sequence. Hippocampal neurons were stained with anti-MAP2 antibody (MAP2, cyan) to highlight cell boundaries. Scale bar: 10 µm.

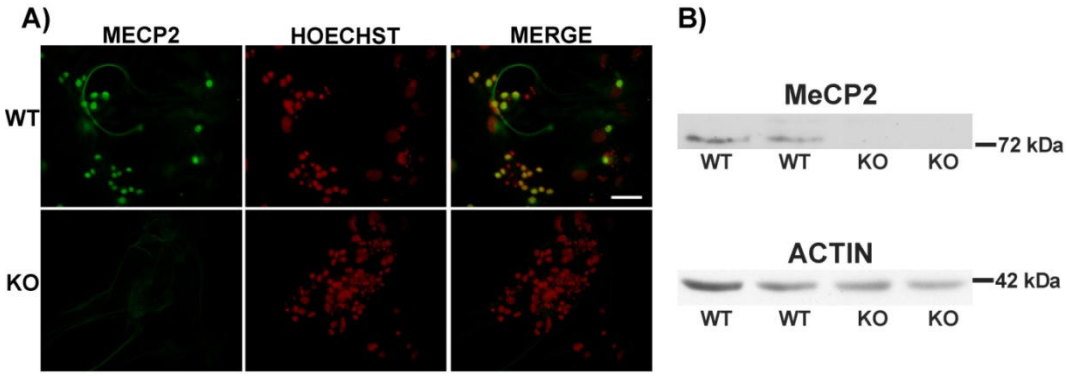

Supplementary Figure 3. MeCP2 expression in MeCP2 KO hippocampal cultured neurons A) Representative images of MeCP2 immunofluorescence (green, left column) in wild type (WT) and MeCP2$^{-/y}$ neurons (KO) . Cell nuclei were stained with Hoechst (red, central column). MeCP2 signal and stained nuclei were merged (merge, right column) to highlight the expression of MeCP2 protein in neurons (yellow staining). Scale bar: 50 µm. B) Western blot on lysates of wild type and MeCP2$^{-/y}$ cultured neurons using a monoclonal anti-MeCP2 Antibody (MeCP2, upper blot). Actin (Actin, bottom blot) was used as loading control.

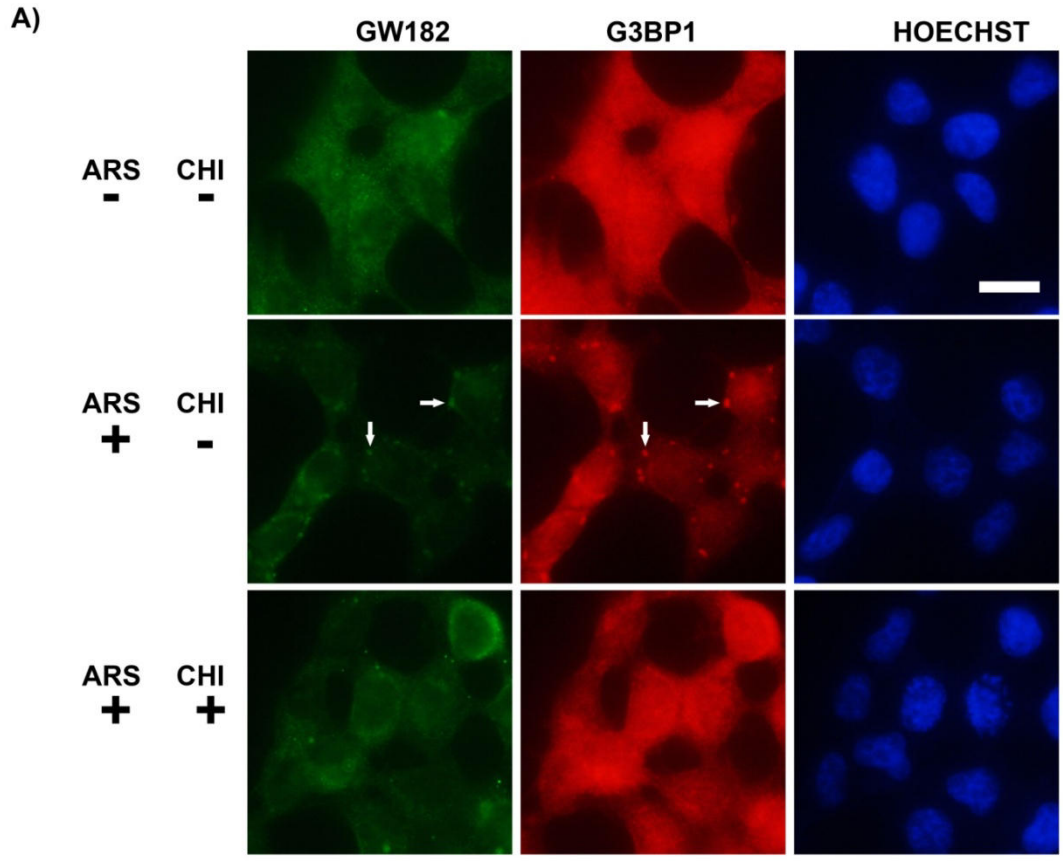

Supplementary Figure 4. Arsenite induction of stress granules A) HEK293T cells immunostained for GW182 (left column, green), a marker of both stress granules and processing bodies, and G3BP1, a specific marker for stress granules (central column, red). Nuclei were stained with hoechst (right column, blue). Diffuse staining was detected in untreated cells (first row, ars - chi -), while large stress granules were clearly visible in cells treated with 0.5 mM sodium arsenite (central row, ars + chi -, white arrows). Stress granules were not detectable after sodium arsenite treatment in the presence of 20 µg/ml cycloheximide (lower row, ars + chi +). Scale bar: 20 µm

BIBLIOGRAPHY

Abuhatzira, L., Makedonski, K., Kaufman, Y., Razin, A., and Shemer, R. (2007). MeCP2 deficiency in the brain decreases BDNF levels by REST/CoREST-mediated repression and increases TRKB production. Epigenetics *2*, 214-222.

Aid, T., Kazantseva, A., Piirsoo, M., Palm, K., and Timmusk, T. (2007). Mouse and rat BDNF gene structure and expression revisited. J Neurosci Res *85*, 525-535.

Ainger, K., Avossa, D., Diana, A.S., Barry, C., Barbarese, E., and Carson, J.H. (1997). Transport and localization elements in myelin basic protein mRNA. J Cell Biol *138*, 1077-1087.

Ainger, K., Avossa, D., Morgan, F., Hill, S.J., Barry, C., Barbarese, E., and Carson, J.H. (1993). Transport and localization of exogenous myelin basic protein mRNA microinjected into oligodendrocytes. J Cell Biol *123*, 431-441.

Aizer, A., Brody, Y., Ler, L.W., Sonenberg, N., Singer, R.H., and Shav-Tal, Y. (2008). The dynamics of mammalian P body transport, assembly, and disassembly in vivo. Mol Biol Cell *19*, 4154-4166.

Akbarian, S. (2003). The neurobiology of Rett syndrome. Neuroscientist *9*, 57-63.

Allen, M., Bird, C., Feng, W., Liu, G., Li, W., Perrone-Bizzozero, N.I., and Feng, Y. (2013). HuD promotes BDNF expression in brain neurons via selective stabilization of the BDNF long 3'UTR mRNA. PLoS One *8*, e55718.

Amir, R.E., Van den Veyver, I.B., Wan, M., Tran, C.Q., Francke, U., and Zoghbi, H.Y. (1999). Rett syndrome is caused by mutations in X-linked MECP2, encoding methyl-CpG-binding protein 2. Nat Genet *23*, 185-188.

An, J.J., Gharami, K., Liao, G.Y., Woo, N.H., Lau, A.G., Vanevski, F., Torre, E.R., Jones, K.R., Feng, Y., Lu, B., *et al.* (2008). Distinct role of long 3' UTR BDNF mRNA in spine morphology and synaptic plasticity in hippocampal neurons. Cell *134*, 175-187.

Anderson, P., and Kedersha, N. (2008). Stress granules: the Tao of RNA triage. Trends Biochem Sci *33*, 141-150.

Anderson, P., Kedersha, N., and Ivanov, P. (2015). Stress granules, P-bodies and cancer. Biochim Biophys Acta *1849*, 861-870.

Andreassi, C., and Riccio, A. (2009). To localize or not to localize: mRNA fate is in 3'UTR ends. Trends Cell Biol *19*, 465-474.

Antar, L.N., Afroz, R., Dictenberg, J.B., Carroll, R.C., and Bassell, G.J. (2004). Metabotropic glutamate receptor activation regulates fragile x mental retardation protein and FMR1 mRNA localization differentially in dendrites and at synapses. J Neurosci *24*, 2648-2655.

Antic, D., Lu, N., and Keene, J.D. (1999). ELAV tumor antigen, Hel-N1, increases translation of neurofilament M mRNA and induces formation of neurites in human teratocarcinoma cells. Genes Dev *13*, 449-461.

Arevalo, J.C., and Wu, S.H. (2006). Neurotrophin signaling: many exciting surprises! Cell Mol Life Sci *63*, 1523-1537.

Armstrong, D., Dunn, J.K., Antalffy, B., and Trivedi, R. (1995). Selective dendritic alterations in the cortex of Rett syndrome. J Neuropathol Exp Neurol *54*, 195-201.

Armstrong, D.D. (1995). The neuropathology of Rett syndrome--overview 1994. Neuropediatrics *26*, 100-104.

Atkins, C.M., Nozaki, N., Shigeri, Y., and Soderling, T.R. (2004). Cytoplasmic polyadenylation element binding protein-dependent protein synthesis is regulated by calcium/calmodulin-dependent protein kinase II. J Neurosci *24*, 5193-5201.

Aulas, A., Caron, G., Gkogkas, C.G., Mohamed, N.V., Destroismaisons, L., Sonenberg, N., Leclerc, N., Parker, J.A., and Vande Velde, C. (2015). G3BP1 promotes stress-induced RNA granule interactions to preserve polyadenylated mRNA. J Cell Biol *209*, 73-84.
Baj, G., Del Turco, D., Schlaudraff, J., Torelli, L., Deller, T., and Tongiorgi, E. (2013). Regulation of the spatial code for BDNF mRNA isoforms in the rat hippocampus following pilocarpine-treatment: a systematic analysis using laser microdissection and quantitative real-time PCR. Hippocampus *23*, 413-423.
Baj, G., Leone, E., Chao, M.V., and Tongiorgi, E. (2011). Spatial segregation of BDNF transcripts enables BDNF to differentially shape distinct dendritic compartments. Proc Natl Acad Sci U S A *108*, 16813-16818.
Baj, G., Patrizio, A., Montalbano, A., Sciancalepore, M., and Tongiorgi, E. (2014). Developmental and maintenance defects in Rett syndrome neurons identified by a new mouse staging system in vitro. Front Cell Neurosci *8*, 18.
Barde, Y.A., Edgar, D., and Thoenen, H. (1982). Purification of a new neurotrophic factor from mammalian brain. EMBO J *1*, 549-553.
Bassell, G.J., and Kelic, S. (2004). Binding proteins for mRNA localization and local translation, and their dysfunction in genetic neurological disease. Curr Opin Neurobiol *14*, 574-581.
Bassell, G.J., and Warren, S.T. (2008). Fragile X syndrome: loss of local mRNA regulation alters synaptic development and function. Neuron *60*, 201-214.
Bear, M.F., Huber, K.M., and Warren, S.T. (2004). The mGluR theory of fragile X mental retardation. Trends Neurosci *27*, 370-377.
Beck, A.R., Medley, Q.G., O'Brien, S., Anderson, P., and Streuli, M. (1996). Structure, tissue distribution and genomic organization of the murine RRM-type RNA binding proteins TIA-1 and TIAR. Nucleic Acids Res *24*, 3829-3835.
Belichenko, P.V., and Dahlstrom, A. (1995). Studies on the 3-dimensional architecture of dendritic spines and varicosities in human cortex by confocal laser scanning microscopy and Lucifer yellow microinjections. J Neurosci Methods *57*, 55-61.
Belichenko, P.V., Hagberg, B., and Dahlstrom, A. (1997). Morphological study of neocortical areas in Rett syndrome. Acta Neuropathol *93*, 50-61.
Belichenko, P.V., Wright, E.E., Belichenko, N.P., Masliah, E., Li, H.H., Mobley, W.C., and Francke, U. (2009). Widespread changes in dendritic and axonal morphology in Mecp2-mutant mouse models of Rett syndrome: evidence for disruption of neuronal networks. J Comp Neurol *514*, 240-258.
Bittolo, T., Raminelli, C.A., Deiana, C., Baj, G., Vaghi, V., Ferrazzo, S., Bernareggi, A., and Tongiorgi, E. (2016). Pharmacological treatment with mirtazapine rescues cortical atrophy and respiratory deficits in MeCP2 null mice. Sci Rep *6*, 19796.
Blichenberg, A., Rehbein, M., Muller, R., Garner, C.C., Richter, D., and Kindler, S. (2001). Identification of a cis-acting dendritic targeting element in the mRNA encoding the alpha subunit of Ca2+/calmodulin-dependent protein kinase II. Eur J Neurosci *13*, 1881-1888.
Bramham, C.R., and Wells, D.G. (2007). Dendritic mRNA: transport, translation and function. Nat Rev Neurosci *8*, 776-789.
Brengues, M., Teixeira, D., and Parker, R. (2005). Movement of eukaryotic mRNAs between polysomes and cytoplasmic processing bodies. Science *310*, 486-489.
Brown, V., Jin, P., Ceman, S., Darnell, J.C., O'Donnell, W.T., Tenenbaum, S.A., Jin, X., Feng, Y., Wilkinson, K.D., Keene, J.D., *et al.* (2001). Microarray identification of FMRP-associated brain mRNAs and altered mRNA translational profiles in fragile X syndrome. Cell *107*, 477-487.
Buchan, J.R. (2014). mRNP granules. Assembly, function, and connections with disease. RNA Biol *11*, 1019-1030.

Buchan, J.R., and Parker, R. (2009). Eukaryotic stress granules: the ins and outs of translation. Mol Cell *36*, 932-941.
Buratti, E., and Baralle, F.E. (2012). TDP-43: gumming up neurons through protein-protein and protein-RNA interactions. Trends Biochem Sci *37*, 237-247.
Burrows, G.D., and Kremer, C.M. (1997). Mirtazapine: clinical advantages in the treatment of depression. J Clin Psychopharmacol *17 Suppl 1*, 34S-39S.
Cajigas, I.J., Tushev, G., Will, T.J., tom Dieck, S., Fuerst, N., and Schuman, E.M. (2012). The local transcriptome in the synaptic neuropil revealed by deep sequencing and high-resolution imaging. Neuron *74*, 453-466.
Cartegni, L., Maconi, M., Morandi, E., Cobianchi, F., Riva, S., and Biamonti, G. (1996). hnRNP A1 selectively interacts through its Gly-rich domain with different RNA-binding proteins. J Mol Biol *259*, 337-348.
Carter, J.C., Lanham, D.C., Pham, D., Bibat, G., Naidu, S., and Kaufmann, W.E. (2008). Selective cerebral volume reduction in Rett syndrome: a multiple-approach MR imaging study. AJNR Am J Neuroradiol *29*, 436-441.
Casanova, M.F., Naidu, S., Goldberg, T.E., Moser, H.W., Khoromi, S., Kumar, A., Kleinman, J.E., and Weinberger, D.R. (1991). Quantitative magnetic resonance imaging in Rett syndrome. J Neuropsychiatry Clin Neurosci *3*, 66-72.
Castren, E., Voikar, V., and Rantamaki, T. (2007). Role of neurotrophic factors in depression. Curr Opin Pharmacol *7*, 18-21.
Castren, M.L., and Castren, E. (2014). BDNF in fragile X syndrome. Neuropharmacology *76 Pt C*, 729-736.
Chahrour, M., Jung, S.Y., Shaw, C., Zhou, X., Wong, S.T., Qin, J., and Zoghbi, H.Y. (2008). MeCP2, a key contributor to neurological disease, activates and represses transcription. Science *320*, 1224-1229.
Chahrour, M., and Zoghbi, H.Y. (2007). The story of Rett syndrome: from clinic to neurobiology. Neuron *56*, 422-437.
Chang, Q., Khare, G., Dani, V., Nelson, S., and Jaenisch, R. (2006). The disease progression of Mecp2 mutant mice is affected by the level of BDNF expression. Neuron *49*, 341-348.
Chao, M.V., Rajagopal, R., and Lee, F.S. (2006). Neurotrophin signalling in health and disease. Clin Sci (Lond) *110*, 167-173.
Chapleau, C.A., Calfa, G.D., Lane, M.C., Albertson, A.J., Larimore, J.L., Kudo, S., Armstrong, D.L., Percy, A.K., and Pozzo-Miller, L. (2009). Dendritic spine pathologies in hippocampal pyramidal neurons from Rett syndrome brain and after expression of Rett-associated MECP2 mutations. Neurobiol Dis *35*, 219-233.
Chartrand, P., Meng, X.H., Huttelmaier, S., Donato, D., and Singer, R.H. (2002). Asymmetric sorting of ash1p in yeast results from inhibition of translation by localization elements in the mRNA. Mol Cell *10*, 1319-1330.
Chen, C.Y., Xu, N., and Shyu, A.B. (2002). Highly selective actions of HuR in antagonizing AU-rich element-mediated mRNA destabilization. Mol Cell Biol *22*, 7268-7278.
Chen, W.G., Chang, Q., Lin, Y., Meissner, A., West, A.E., Griffith, E.C., Jaenisch, R., and Greenberg, M.E. (2003). Derepression of BDNF transcription involves calcium-dependent phosphorylation of MeCP2. Science *302*, 885-889.
Chiaruttini, C., Sonego, M., Baj, G., Simonato, M., and Tongiorgi, E. (2008). BDNF mRNA splice variants display activity-dependent targeting to distinct hippocampal laminae. Mol Cell Neurosci *37*, 11-19.
Chiaruttini, C., Vicario, A., Li, Z., Baj, G., Braiuca, P., Wu, Y., Lee, F.S., Gardossi, L., Baraban, J.M., and Tongiorgi, E. (2009). Dendritic trafficking of BDNF mRNA is mediated by translin and blocked by the G196A (Val66Met) mutation. Proc Natl Acad Sci U S A *106*, 16481-16486.

Chotiner, J.K., Khorasani, H., Nairn, A.C., O'Dell, T.J., and Watson, J.B. (2003). Adenylyl cyclase-dependent form of chemical long-term potentiation triggers translational regulation at the elongation step. Neuroscience *116*, 743-752.
Chou, C.T., Lin, W.F., Kong, Z.L., Chen, S.Y., and Hwang, D.F. (2013). Taurine prevented cell cycle arrest and restored neurotrophic gene expression in arsenite-treated SH-SY5Y cells. Amino Acids *45*, 811-819.
Cohen, S., Levi-Montalcini, R., and Hamburger, V. (1954). A Nerve Growth-Stimulating Factor Isolated from Sarcom as 37 and 180. Proc Natl Acad Sci U S A *40*, 1014-1018.
Colombrita, C., Zennaro, E., Fallini, C., Weber, M., Sommacal, A., Buratti, E., Silani, V., and Ratti, A. (2009). TDP-43 is recruited to stress granules in conditions of oxidative insult. J Neurochem *111*, 1051-1061.
Coppell, A.L., Pei, Q., and Zetterstrom, T.S. (2003). Bi-phasic change in BDNF gene expression following antidepressant drug treatment. Neuropharmacology *44*, 903-910.
Costa-Mattioli, M., and Monteggia, L.M. (2013). mTOR complexes in neurodevelopmental and neuropsychiatric disorders. Nat Neurosci *16*, 1537-1543.
Cougot, N., Bhattacharyya, S.N., Tapia-Arancibia, L., Bordonne, R., Filipowicz, W., Bertrand, E., and Rage, F. (2008). Dendrites of mammalian neurons contain specialized P-body-like structures that respond to neuronal activation. J Neurosci *28*, 13793-13804.
Cougot, N., van Dijk, E., Babajko, S., and Seraphin, B. (2004). 'Cap-tabolism'. Trends Biochem Sci *29*, 436-444.
Cunha, C., Brambilla, R., and Thomas, K.L. (2010). A simple role for BDNF in learning and memory? Front Mol Neurosci *3*, 1.
Davidovic, L., Jaglin, X.H., Lepagnol-Bestel, A.M., Tremblay, S., Simonneau, M., Bardoni, B., and Khandjian, E.W. (2007). The fragile X mental retardation protein is a molecular adaptor between the neurospecific KIF3C kinesin and dendritic RNA granules. Hum Mol Genet *16*, 3047-3058.
Davidovic, L., Navratil, V., Bonaccorso, C.M., Catania, M.V., Bardoni, B., and Dumas, M.E. (2011). A metabolomic and systems biology perspective on the brain of the fragile X syndrome mouse model. Genome Res *21*, 2190-2202.
De Felice, C., Ciccoli, L., Leoncini, S., Signorini, C., Rossi, M., Vannuccini, L., Guazzi, G., Latini, G., Comporti, M., Valacchi, G., *et al.* (2009). Systemic oxidative stress in classic Rett syndrome. Free Radic Biol Med *47*, 440-448.
De Felice, C., Cortelazzo, A., Signorini, C., Guerranti, R., Leoncini, S., Pecorelli, A., Durand, T., Galano, J.M., Oger, C., Zollo, G., *et al.* (2013). Effects of omega-3 polyunsaturated fatty acids on plasma proteome in Rett syndrome. Mediators Inflamm *2013*, 723269.
De Felice, C., Della Ragione, F., Signorini, C., Leoncini, S., Pecorelli, A., Ciccoli, L., Scalabri, F., Marracino, F., Madonna, M., Belmonte, G., *et al.* (2014). Oxidative brain damage in Mecp2-mutant murine models of Rett syndrome. Neurobiol Dis *68*, 66-77.
De Felice, C., Signorini, C., Leoncini, S., Pecorelli, A., Durand, T., Valacchi, G., Ciccoli, L., and Hayek, J. (2012). The role of oxidative stress in Rett syndrome: an overview. Ann N Y Acad Sci *1259*, 121-135.
Decker, C.J., and Parker, R. (2012). P-bodies and stress granules: possible roles in the control of translation and mRNA degradation. Cold Spring Harb Perspect Biol *4*, a012286.
Deng, V., Matagne, V., Banine, F., Frerking, M., Ohliger, P., Budden, S., Pevsner, J., Dissen, G.A., Sherman, L.S., and Ojeda, S.R. (2007). FXYD1 is an MeCP2 target gene overexpressed in the brains of Rett syndrome patients and Mecp2-null mice. Hum Mol Genet *16*, 640-650.
Dias, B.G., Banerjee, S.B., Duman, R.S., and Vaidya, V.A. (2003). Differential regulation of brain derived neurotrophic factor transcripts by antidepressant treatments in the adult rat brain. Neuropharmacology *45*, 553-563.

Didiot, M.C., Subramanian, M., Flatter, E., Mandel, J.L., and Moine, H. (2009). Cells lacking the fragile X mental retardation protein (FMRP) have normal RISC activity but exhibit altered stress granule assembly. Mol Biol Cell *20*, 428-437.
Doyle, M., and Kiebler, M.A. (2011). Mechanisms of dendritic mRNA transport and its role in synaptic tagging. EMBO J *30*, 3540-3552.
Dragich, J.M., Kim, Y.H., Arnold, A.P., and Schanen, N.C. (2007). Differential distribution of the MeCP2 splice variants in the postnatal mouse brain. J Comp Neurol *501*, 526-542.
Duchaine, T.F., Hemraj, I., Furic, L., Deitinghoff, A., Kiebler, M.A., and DesGroseillers, L. (2002). Staufen2 isoforms localize to the somatodendritic domain of neurons and interact with different organelles. J Cell Sci *115*, 3285-3295.
Durand, T., De Felice, C., Signorini, C., Oger, C., Bultel-Ponce, V., Guy, A., Galano, J.M., Leoncini, S., Ciccoli, L., Pecorelli, A., *et al.* (2013). F(2)-Dihomo-isoprostanes and brain white matter damage in stage 1 Rett syndrome. Biochimie *95*, 86-90.
Dynes, J.L., and Steward, O. (2007). Dynamics of bidirectional transport of Arc mRNA in neuronal dendrites. J Comp Neurol *500*, 433-447.
Eberwine, J., Belt, B., Kacharmina, J.E., and Miyashiro, K. (2002). Analysis of subcellularly localized mRNAs using in situ hybridization, mRNA amplification, and expression profiling. Neurochem Res *27*, 1065-1077.
Edbauer, D., Neilson, J.R., Foster, K.A., Wang, C.F., Seeburg, D.P., Batterton, M.N., Tada, T., Dolan, B.M., Sharp, P.A., and Sheng, M. (2010). Regulation of synaptic structure and function by FMRP-associated microRNAs miR-125b and miR-132. Neuron *65*, 373-384.
Elvira, G., Wasiak, S., Blandford, V., Tong, X.K., Serrano, A., Fan, X., del Rayo Sanchez-Carbente, M., Servant, F., Bell, A.W., Boismenu, D., *et al.* (2006). Characterization of an RNA granule from developing brain. Mol Cell Proteomics *5*, 635-651.
Eom, T., Antar, L.N., Singer, R.H., and Bassell, G.J. (2003). Localization of a beta-actin messenger ribonucleoprotein complex with zipcode-binding protein modulates the density of dendritic filopodia and filopodial synapses. J Neurosci *23*, 10433-10444.
Erickson, S.L., and Lykke-Andersen, J. (2011). Cytoplasmic mRNP granules at a glance. J Cell Sci *124*, 293-297.
Eulalio, A., Behm-Ansmant, I., Schweizer, D., and Izaurralde, E. (2007). P-body formation is a consequence, not the cause, of RNA-mediated gene silencing. Mol Cell Biol *27*, 3970-3981.
Ferrandon, D., Koch, I., Westhof, E., and Nusslein-Volhard, C. (1997). RNA-RNA interaction is required for the formation of specific bicoid mRNA 3' UTR-STAUFEN ribonucleoprotein particles. EMBO J *16*, 1751-1758.
Friedman, W.J., Ernfors, P., and Persson, H. (1991a). Transient and persistent expression of NT-3/HDNF mRNA in the rat brain during postnatal development. J Neurosci *11*, 1577-1584.
Friedman, W.J., Olson, L., and Persson, H. (1991b). Cells that Express Brain-Derived Neurotrophic Factor mRNA in the Developing Postnatal Rat Brain. Eur J Neurosci *3*, 688-697.
Fukuda, T., Itoh, M., Ichikawa, T., Washiyama, K., and Goto, Y. (2005). Delayed maturation of neuronal architecture and synaptogenesis in cerebral cortex of Mecp2-deficient mice. J Neuropathol Exp Neurol *64*, 537-544.
Furic, L., Maher-Laporte, M., and DesGroseillers, L. (2008). A genome-wide approach identifies distinct but overlapping subsets of cellular mRNAs associated with Staufen1- and Staufen2-containing ribonucleoprotein complexes. RNA *14*, 324-335.
Gabel, H.W., Kinde, B., Stroud, H., Gilbert, C.S., Harmin, D.A., Kastan, N.R., Hemberg, M., Ebert, D.H., and Greenberg, M.E. (2015). Disruption of DNA-methylation-dependent long gene repression in Rett syndrome. Nature *522*, 89-93.
Gadalla, K.K., Bailey, M.E., and Cobb, S.R. (2011). MeCP2 and Rett syndrome: reversibility and potential avenues for therapy. Biochem J *439*, 1-14.

Gao, Y., Su, J., Guo, W., Polich, E.D., Magyar, D.P., Xing, Y., Li, H., Smrt, R.D., Chang, Q., and Zhao, X. (2015). Inhibition of miR-15a Promotes BDNF Expression and Rescues Dendritic Maturation Deficits in MeCP2-Deficient Neurons. Stem Cells *33*, 1618-1629.
Gao, Y., Tatavarty, V., Korza, G., Levin, M.K., and Carson, J.H. (2008). Multiplexed dendritic targeting of alpha calcium calmodulin-dependent protein kinase II, neurogranin, and activity-regulated cytoskeleton-associated protein RNAs by the A2 pathway. Mol Biol Cell *19*, 2311-2327.
Garber, K.B., Visootsak, J., and Warren, S.T. (2008). Fragile X syndrome. Eur J Hum Genet *16*, 666-672.
Giacometti, E., Luikenhuis, S., Beard, C., and Jaenisch, R. (2007). Partial rescue of MeCP2 deficiency by postnatal activation of MeCP2. Proc Natl Acad Sci U S A *104*, 1931-1936.
Goetze, B., Tuebing, F., Xie, Y., Dorostkar, M.M., Thomas, S., Pehl, U., Boehm, S., Macchi, P., and Kiebler, M.A. (2006). The brain-specific double-stranded RNA-binding protein Staufen2 is required for dendritic spine morphogenesis. J Cell Biol *172*, 221-231.
Gonzales, M.L., Adams, S., Dunaway, K.W., and LaSalle, J.M. (2012). Phosphorylation of distinct sites in MeCP2 modifies cofactor associations and the dynamics of transcriptional regulation. Mol Cell Biol *32*, 2894-2903.
Gonzales, M.L., and LaSalle, J.M. (2010). The role of MeCP2 in brain development and neurodevelopmental disorders. Curr Psychiatry Rep *12*, 127-134.
Good, P.J. (1995). A conserved family of elav-like genes in vertebrates. Proc Natl Acad Sci U S A *92*, 4557-4561.
Greenberg, M.E., Xu, B., Lu, B., and Hempstead, B.L. (2009). New insights in the biology of BDNF synthesis and release: implications in CNS function. J Neurosci *29*, 12764-12767.
Gumy, L.F., Yeo, G.S., Tung, Y.C., Zivraj, K.H., Willis, D., Coppola, G., Lam, B.Y., Twiss, J.L., Holt, C.E., and Fawcett, J.W. (2011). Transcriptome analysis of embryonic and adult sensory axons reveals changes in mRNA repertoire localization. RNA *17*, 85-98.
Guy, J., Gan, J., Selfridge, J., Cobb, S., and Bird, A. (2007). Reversal of neurological defects in a mouse model of Rett syndrome. Science *315*, 1143-1147.
Guy, J., Hendrich, B., Holmes, M., Martin, J.E., and Bird, A. (2001). A mouse Mecp2-null mutation causes neurological symptoms that mimic Rett syndrome. Nat Genet *27*, 322-326.
Han, J.R., Yiu, G.K., and Hecht, N.B. (1995). Testis/brain RNA-binding protein attaches translationally repressed and transported mRNAs to microtubules. Proc Natl Acad Sci U S A *92*, 9550-9554.
Han, S.P., Friend, L.R., Carson, J.H., Korza, G., Barbarese, E., Maggipinto, M., Hatfield, J.T., Rothnagel, J.A., and Smith, R. (2010). Differential subcellular distributions and trafficking functions of hnRNP A2/B1 spliceoforms. Traffic *11*, 886-898.
Harikrishnan, K.N., Chow, M.Z., Baker, E.K., Pal, S., Bassal, S., Brasacchio, D., Wang, L., Craig, J.M., Jones, P.L., Sif, S., *et al.* (2005). Brahma links the SWI/SNF chromatin-remodeling complex with MeCP2-dependent transcriptional silencing. Nat Genet *37*, 254-264.
Hartmann, P.M. (1999). Mirtazapine: a newer antidepressant. Am Fam Physician *59*, 159-161.
He, Y., and Smith, R. (2009). Nuclear functions of heterogeneous nuclear ribonucleoproteins A/B. Cell Mol Life Sci *66*, 1239-1256.
Hecht, N.B. (1998). Molecular mechanisms of male germ cell differentiation. Bioessays *20*, 555-561.
Heraud-Farlow, J.E., and Kiebler, M.A. (2014). The multifunctional Staufen proteins: conserved roles from neurogenesis to synaptic plasticity. Trends Neurosci *37*, 470-479.
Hoeffer, C.A., and Klann, E. (2010). mTOR signaling: at the crossroads of plasticity, memory and disease. Trends Neurosci *33*, 67-75.

Holm, K.J., and Markham, A. (1999). Mirtazapine: a review of its use in major depression. Drugs *57*, 607-631.
Huang, E.J., and Reichardt, L.F. (2003). Trk receptors: roles in neuronal signal transduction. Annu Rev Biochem *72*, 609-642.
Huang, Y.S., Carson, J.H., Barbarese, E., and Richter, J.D. (2003). Facilitation of dendritic mRNA transport by CPEB. Genes Dev *17*, 638-653.
Huang, Y.S., Jung, M.Y., Sarkissian, M., and Richter, J.D. (2002). N-methyl-D-aspartate receptor signaling results in Aurora kinase-catalyzed CPEB phosphorylation and alpha CaMKII mRNA polyadenylation at synapses. EMBO J *21*, 2139-2148.
Huang, Y.S., Kan, M.C., Lin, C.L., and Richter, J.D. (2006). CPEB3 and CPEB4 in neurons: analysis of RNA-binding specificity and translational control of AMPA receptor GluR2 mRNA. EMBO J *25*, 4865-4876.
Huang, Y.W., Ruiz, C.R., Eyler, E.C., Lin, K., and Meffert, M.K. (2012). Dual regulation of miRNA biogenesis generates target specificity in neurotrophin-induced protein synthesis. Cell *148*, 933-946.
Huttelmaier, S., Zenklusen, D., Lederer, M., Dictenberg, J., Lorenz, M., Meng, X., Bassell, G.J., Condeelis, J., and Singer, R.H. (2005). Spatial regulation of beta-actin translation by Src-dependent phosphorylation of ZBP1. Nature *438*, 512-515.
Jacobsen, J.P., and Mork, A. (2004). The effect of escitalopram, desipramine, electroconvulsive seizures and lithium on brain-derived neurotrophic factor mRNA and protein expression in the rat brain and the correlation to 5-HT and 5-HIAA levels. Brain Res *1024*, 183-192.
Jiang, C., and Schuman, E.M. (2002). Regulation and function of local protein synthesis in neuronal dendrites. Trends Biochem Sci *27*, 506-513.
Jin, P., Alisch, R.S., and Warren, S.T. (2004). RNA and microRNAs in fragile X mental retardation. Nat Cell Biol *6*, 1048-1053.
Jing, J., Zheng, G., Liu, M., Shen, X., Zhao, F., Wang, J., Zhang, J., Huang, G., Dai, P., Chen, Y., *et al.* (2012). Changes in the synaptic structure of hippocampal neurons and impairment of spatial memory in a rat model caused by chronic arsenite exposure. Neurotoxicology *33*, 1230-1238.
Johnson, R.A., Lam, M., Punzo, A.M., Li, H., Lin, B.R., Ye, K., Mitchell, G.S., and Chang, Q. (2012). 7,8-dihydroxyflavone exhibits therapeutic efficacy in a mouse model of Rett syndrome. J Appl Physiol (1985) *112*, 704-710.
Johnstone, O., and Lasko, P. (2001). Translational regulation and RNA localization in Drosophila oocytes and embryos. Annu Rev Genet *35*, 365-406.
Jung, B.P., Jugloff, D.G., Zhang, G., Logan, R., Brown, S., and Eubanks, J.H. (2003). The expression of methyl CpG binding factor MeCP2 correlates with cellular differentiation in the developing rat brain and in cultured cells. J Neurobiol *55*, 86-96.
Kaludov, N.K., and Wolffe, A.P. (2000). MeCP2 driven transcriptional repression in vitro: selectivity for methylated DNA, action at a distance and contacts with the basal transcription machinery. Nucleic Acids Res *28*, 1921-1928.
Kanai, Y., Dohmae, N., and Hirokawa, N. (2004). Kinesin transports RNA: isolation and characterization of an RNA-transporting granule. Neuron *43*, 513-525.
Kang, H., and Schuman, E.M. (1995a). Long-lasting neurotrophin-induced enhancement of synaptic transmission in the adult hippocampus. Science *267*, 1658-1662.
Kang, H., and Schuman, E.M. (1996). A requirement for local protein synthesis in neurotrophin-induced hippocampal synaptic plasticity. Science *273*, 1402-1406.
Kang, H.J., and Schuman, E.M. (1995b). Neurotrophin-induced modulation of synaptic transmission in the adult hippocampus. J Physiol Paris *89*, 11-22.
Kanhema, T., Dagestad, G., Panja, D., Tiron, A., Messaoudi, E., Havik, B., Ying, S.W., Nairn, A.C., Sonenberg, N., and Bramham, C.R. (2006). Dual regulation of translation

initiation and peptide chain elongation during BDNF-induced LTP in vivo: evidence for compartment-specific translation control. J Neurochem *99*, 1328-1337.
Katoh-Semba, R., Semba, R., Takeuchi, I.K., and Kato, K. (1998). Age-related changes in levels of brain-derived neurotrophic factor in selected brain regions of rats, normal mice and senescence-accelerated mice: a comparison to those of nerve growth factor and neurotrophin-3. Neurosci Res *31*, 227-234.
Katz, D.M., Berger-Sweeney, J.E., Eubanks, J.H., Justice, M.J., Neul, J.L., Pozzo-Miller, L., Blue, M.E., Christian, D., Crawley, J.N., Giustetto, M., *et al.* (2012). Preclinical research in Rett syndrome: setting the foundation for translational success. Dis Model Mech *5*, 733-745.
Kaufmann, W.E., and Moser, H.W. (2000). Dendritic anomalies in disorders associated with mental retardation. Cereb Cortex *10*, 981-991.
Kaufmann, W.E., Naidu, S., and Budden, S. (1995). Abnormal expression of microtubule-associated protein 2 (MAP-2) in neocortex in Rett syndrome. Neuropediatrics *26*, 109-113.
Kaufmann, W.E., Taylor, C.V., Hohmann, C.F., Sanwal, I.B., and Naidu, S. (1997a). Abnormalities in neuronal maturation in Rett syndrome neocortex: preliminary molecular correlates. Eur Child Adolesc Psychiatry *6 Suppl 1*, 75-77.
Kaufmann, W.E., Worley, P.F., Taylor, C.V., Bremer, M., and Isakson, P.C. (1997b). Cyclooxygenase-2 expression during rat neocortical development and in Rett syndrome. Brain Dev *19*, 25-34.
Kedersha, N., and Anderson, P. (2007). Mammalian stress granules and processing bodies. Methods Enzymol *431*, 61-81.
Kedersha, N., Cho, M.R., Li, W., Yacono, P.W., Chen, S., Gilks, N., Golan, D.E., and Anderson, P. (2000). Dynamic shuttling of TIA-1 accompanies the recruitment of mRNA to mammalian stress granules. J Cell Biol *151*, 1257-1268.
Kedersha, N., Ivanov, P., and Anderson, P. (2013). Stress granules and cell signaling: more than just a passing phase? Trends Biochem Sci *38*, 494-506.
Kedersha, N., Stoecklin, G., Ayodele, M., Yacono, P., Lykke-Andersen, J., Fritzler, M.J., Scheuner, D., Kaufman, R.J., Golan, D.E., and Anderson, P. (2005). Stress granules and processing bodies are dynamically linked sites of mRNP remodeling. J Cell Biol *169*, 871-884.
Kedersha, N., Tisdale, S., Hickman, T., and Anderson, P. (2008). Real-time and quantitative imaging of mammalian stress granules and processing bodies. Methods Enzymol *448*, 521-552.
Kedersha, N.L., Gupta, M., Li, W., Miller, I., and Anderson, P. (1999). RNA-binding proteins TIA-1 and TIAR link the phosphorylation of eIF-2 alpha to the assembly of mammalian stress granules. J Cell Biol *147*, 1431-1442.
Kiebler, M.A., and Bassell, G.J. (2006). Neuronal RNA granules: movers and makers. Neuron *51*, 685-690.
Kim, H.J., Kim, N.C., Wang, Y.D., Scarborough, E.A., Moore, J., Diaz, Z., MacLea, K.S., Freibaum, B., Li, S., Molliex, A., *et al.* (2013). Mutations in prion-like domains in hnRNPA2B1 and hnRNPA1 cause multisystem proteinopathy and ALS. Nature *495*, 467-473.
Kim, J.H., and Richter, J.D. (2006). Opposing polymerase-deadenylase activities regulate cytoplasmic polyadenylation. Mol Cell *24*, 173-183.
Kim, Y.K., Furic, L., Desgroseillers, L., and Maquat, L.E. (2005). Mammalian Staufen1 recruits Upf1 to specific mRNA 3'UTRs so as to elicit mRNA decay. Cell *120*, 195-208.
King, M.L., Messitt, T.J., and Mowry, K.L. (2005). Putting RNAs in the right place at the right time: RNA localization in the frog oocyte. Biol Cell *97*, 19-33.
Kishi, N., and Macklis, J.D. (2004). MECP2 is progressively expressed in post-migratory neurons and is involved in neuronal maturation rather than cell fate decisions. Mol Cell Neurosci *27*, 306-321.

Kislauskis, E.H., Zhu, X., and Singer, R.H. (1994). Sequences responsible for intracellular localization of beta-actin messenger RNA also affect cell phenotype. J Cell Biol *127*, 441-451.
Klein, M.E., Lioy, D.T., Ma, L., Impey, S., Mandel, G., and Goodman, R.H. (2007). Homeostatic regulation of MeCP2 expression by a CREB-induced microRNA. Nat Neurosci *10*, 1513-1514.
Kline, D.D., Ogier, M., Kunze, D.L., and Katz, D.M. (2010). Exogenous brain-derived neurotrophic factor rescues synaptic dysfunction in Mecp2-null mice. J Neurosci *30*, 5303-5310.
Klose, R.J., Sarraf, S.A., Schmiedeberg, L., McDermott, S.M., Stancheva, I., and Bird, A.P. (2005). DNA binding selectivity of MeCP2 due to a requirement for A/T sequences adjacent to methyl-CpG. Mol Cell *19*, 667-678.
Knowles, R.B., Sabry, J.H., Martone, M.E., Deerinck, T.J., Ellisman, M.H., Bassell, G.J., and Kosik, K.S. (1996). Translocation of RNA granules in living neurons. J Neurosci *16*, 7812-7820.
Kobayashi, S., Takashima, A., and Anzai, K. (1998). The dendritic translocation of translin protein in the form of BC1 RNA protein particles in developing rat hippocampal neurons in primary culture. Biochem Biophys Res Commun *253*, 448-453.
Kohrmann, M., Luo, M., Kaether, C., DesGroseillers, L., Dotti, C.G., and Kiebler, M.A. (1999). Microtubule-dependent recruitment of Staufen-green fluorescent protein into large RNA-containing granules and subsequent dendritic transport in living hippocampal neurons. Mol Biol Cell *10*, 2945-2953.
Kokura, K., Kaul, S.C., Wadhwa, R., Nomura, T., Khan, M.M., Shinagawa, T., Yasukawa, T., Colmenares, C., and Ishii, S. (2001). The Ski protein family is required for MeCP2-mediated transcriptional repression. J Biol Chem *276*, 34115-34121.
Kolbeck, R., Bartke, I., Eberle, W., and Barde, Y.A. (1999). Brain-derived neurotrophic factor levels in the nervous system of wild-type and neurotrophin gene mutant mice. J Neurochem *72*, 1930-1938.
Koushika, S.P., Soller, M., and White, K. (2000). The neuron-enriched splicing pattern of Drosophila erect wing is dependent on the presence of ELAV protein. Mol Cell Biol *20*, 1836-1845.
Krichevsky, A.M., and Kosik, K.S. (2001). Neuronal RNA granules: a link between RNA localization and stimulation-dependent translation. Neuron *32*, 683-696.
Larimore, J.L., Chapleau, C.A., Kudo, S., Theibert, A., Percy, A.K., and Pozzo-Miller, L. (2009). Bdnf overexpression in hippocampal neurons prevents dendritic atrophy caused by Rett-associated MECP2 mutations. Neurobiol Dis *34*, 199-211.
Lebeau, G., Maher-Laporte, M., Topolnik, L., Laurent, C.E., Sossin, W., Desgroseillers, L., and Lacaille, J.C. (2008). Staufen1 regulation of protein synthesis-dependent long-term potentiation and synaptic function in hippocampal pyramidal cells. Mol Cell Biol *28*, 2896-2907.
Lecuyer, E., Yoshida, H., Parthasarathy, N., Alm, C., Babak, T., Cerovina, T., Hughes, T.R., Tomancak, P., and Krause, H.M. (2007). Global analysis of mRNA localization reveals a prominent role in organizing cellular architecture and function. Cell *131*, 174-187.
Leoncini, S., De Felice, C., Signorini, C., Pecorelli, A., Durand, T., Valacchi, G., Ciccoli, L., and Hayek, J. (2011). Oxidative stress in Rett syndrome: natural history, genotype, and variants. Redox Rep *16*, 145-153.
Lessmann, V., Gottmann, K., and Malcangio, M. (2003). Neurotrophin secretion: current facts and future prospects. Prog Neurobiol *69*, 341-374.
Levine, T.D., Gao, F., King, P.H., Andrews, L.G., and Keene, J.D. (1993). Hel-N1: an autoimmune RNA-binding protein with specificity for 3' uridylate-rich untranslated regions of growth factor mRNAs. Mol Cell Biol *13*, 3494-3504.

Li, H., Zhong, X., Chau, K.F., Williams, E.C., and Chang, Q. (2011). Loss of activity-induced phosphorylation of MeCP2 enhances synaptogenesis, LTP and spatial memory. Nat Neurosci *14*, 1001-1008.
Li, W., Calfa, G., Larimore, J., and Pozzo-Miller, L. (2012). Activity-dependent BDNF release and TRPC signaling is impaired in hippocampal neurons of Mecp2 mutant mice. Proc Natl Acad Sci U S A *109*, 17087-17092.
Li, W., and Pozzo-Miller, L. (2014). BDNF deregulation in Rett syndrome. Neuropharmacology *76 Pt C*, 737-746.
Li, Y., Wang, H., Muffat, J., Cheng, A.W., Orlando, D.A., Loven, J., Kwok, S.M., Feldman, D.A., Bateup, H.S., Gao, Q., *et al.* (2013a). Global transcriptional and translational repression in human-embryonic-stem-cell-derived Rett syndrome neurons. Cell Stem Cell *13*, 446-458.
Li, Y.R., King, O.D., Shorter, J., and Gitler, A.D. (2013b). Stress granules as crucibles of ALS pathogenesis. J Cell Biol *201*, 361-372.
Lin, A.C., and Holt, C.E. (2007). Local translation and directional steering in axons. EMBO J *26*, 3729-3736.
Litman, P., Barg, J., Rindzoonski, L., and Ginzburg, I. (1993). Subcellular localization of tau mRNA in differentiating neuronal cell culture: implications for neuronal polarity. Neuron *10*, 627-638.
Liu-Yesucevitz, L., Bassell, G.J., Gitler, A.D., Hart, A.C., Klann, E., Richter, J.D., Warren, S.T., and Wolozin, B. (2011). Local RNA translation at the synapse and in disease. J Neurosci *31*, 16086-16093.
Liu, J., Dalmau, J., Szabo, A., Rosenfeld, M., Huber, J., and Furneaux, H. (1995). Paraneoplastic encephalomyelitis antigens bind to the AU-rich elements of mRNA. Neurology *45*, 544-550.
Lloyd, R.E. (2013). Regulation of stress granules and P-bodies during RNA virus infection. Wiley Interdiscip Rev RNA *4*, 317-331.
Lonetti, G., Angelucci, A., Morando, L., Boggio, E.M., Giustetto, M., and Pizzorusso, T. (2010). Early environmental enrichment moderates the behavioral and synaptic phenotype of MeCP2 null mice. Biol Psychiatry *67*, 657-665.
Long, R.M., Singer, R.H., Meng, X., Gonzalez, I., Nasmyth, K., and Jansen, R.P. (1997). Mating type switching in yeast controlled by asymmetric localization of ASH1 mRNA. Science *277*, 383-387.
Lopez de Silanes, I., Galban, S., Martindale, J.L., Yang, X., Mazan-Mamczarz, K., Indig, F.E., Falco, G., Zhan, M., and Gorospe, M. (2005). Identification and functional outcome of mRNAs associated with RNA-binding protein TIA-1. Mol Cell Biol *25*, 9520-9531.
Loschi, M., Leishman, C.C., Berardone, N., and Boccaccio, G.L. (2009). Dynein and kinesin regulate stress-granule and P-body dynamics. J Cell Sci *122*, 3973-3982.
Louhivuori, V., Vicario, A., Uutela, M., Rantamaki, T., Louhivuori, L.M., Castren, E., Tongiorgi, E., Akerman, K.E., and Castren, M.L. (2011). BDNF and TrkB in neuronal differentiation of Fmr1-knockout mouse. Neurobiol Dis *41*, 469-480.
Luikenhuis, S., Giacometti, E., Beard, C.F., and Jaenisch, R. (2004). Expression of MeCP2 in postmitotic neurons rescues Rett syndrome in mice. Proc Natl Acad Sci U S A *101*, 6033-6038.
Lukong, K.E., Chang, K.W., Khandjian, E.W., and Richard, S. (2008). RNA-binding proteins in human genetic disease. Trends Genet *24*, 416-425.
Lunde, B.M., Moore, C., and Varani, G. (2007). RNA-binding proteins: modular design for efficient function. Nat Rev Mol Cell Biol *8*, 479-490.
Macdonald, P.M., Kerr, K., Smith, J.L., and Leask, A. (1993). RNA regulatory element BLE1 directs the early steps of bicoid mRNA localization. Development *118*, 1233-1243.

Maisonpierre, P.C., Belluscio, L., Friedman, B., Alderson, R.F., Wiegand, S.J., Furth, M.E., Lindsay, R.M., and Yancopoulos, G.D. (1990). NT-3, BDNF, and NGF in the developing rat nervous system: parallel as well as reciprocal patterns of expression. Neuron *5*, 501-509.
Mallardo, M., Deitinghoff, A., Muller, J., Goetze, B., Macchi, P., Peters, C., and Kiebler, M.A. (2003). Isolation and characterization of Staufen-containing ribonucleoprotein particles from rat brain. Proc Natl Acad Sci U S A *100*, 2100-2105.
Martel, C., Dugre-Brisson, S., Boulay, K., Breton, B., Lapointe, G., Armando, S., Trepanier, V., Duchaine, T., Bouvier, M., and Desgroseillers, L. (2010). Multimerization of Staufen1 in live cells. RNA *16*, 585-597.
Martin, K.C., and Ephrussi, A. (2009). mRNA localization: gene expression in the spatial dimension. Cell *136*, 719-730.
Martin, K.C., and Zukin, R.S. (2006). RNA trafficking and local protein synthesis in dendrites: an overview. J Neurosci *26*, 7131-7134.
Martinowich, K., Hattori, D., Wu, H., Fouse, S., He, F., Hu, Y., Fan, G., and Sun, Y.E. (2003). DNA methylation-related chromatin remodeling in activity-dependent BDNF gene regulation. Science *302*, 890-893.
Maynard, K.R., Hill, J.L., Calcaterra, N.E., Palko, M.E., Kardian, A., Paredes, D., Sukumar, M., Adler, B.D., Jimenez, D.V., Schloesser, R.J., *et al.* (2015). Functional Role of BDNF Production from Unique Promoters in Aggression and Serotonin Signaling. Neuropsychopharmacology.
McAllister, A.K., Katz, L.C., and Lo, D.C. (1997). Opposing roles for endogenous BDNF and NT-3 in regulating cortical dendritic growth. Neuron *18*, 767-778.
Mendez, R., and Richter, J.D. (2001). Translational control by CPEB: a means to the end. Nat Rev Mol Cell Biol *2*, 521-529.
Messaoudi, E., Kanhema, T., Soule, J., Tiron, A., Dagyte, G., da Silva, B., and Bramham, C.R. (2007). Sustained Arc/Arg3.1 synthesis controls long-term potentiation consolidation through regulation of local actin polymerization in the dentate gyrus in vivo. J Neurosci *27*, 10445-10455.
Mikl, M., Vendra, G., and Kiebler, M.A. (2011). Independent localization of MAP2, CaMKIIalpha and beta-actin RNAs in low copy numbers. EMBO Rep *12*, 1077-1084.
Miller, S., Yasuda, M., Coats, J.K., Jones, Y., Martone, M.E., and Mayford, M. (2002). Disruption of dendritic translation of CaMKIIalpha impairs stabilization of synaptic plasticity and memory consolidation. Neuron *36*, 507-519.
Minichiello, L., Calella, A.M., Medina, D.L., Bonhoeffer, T., Klein, R., and Korte, M. (2002). Mechanism of TrkB-mediated hippocampal long-term potentiation. Neuron *36*, 121-137.
Minichiello, L., Korte, M., Wolfer, D., Kuhn, R., Unsicker, K., Cestari, V., Rossi-Arnaud, C., Lipp, H.P., Bonhoeffer, T., and Klein, R. (1999). Essential role for TrkB receptors in hippocampus-mediated learning. Neuron *24*, 401-414.
Monshausen, M., Putz, U., Rehbein, M., Schweizer, M., DesGroseillers, L., Kuhl, D., Richter, D., and Kindler, S. (2001). Two rat brain staufen isoforms differentially bind RNA. J Neurochem *76*, 155-165.
Morales, C.R., Wu, X.Q., and Hecht, N.B. (1998). The DNA/RNA-binding protein, TB-RBP, moves from the nucleus to the cytoplasm and through intercellular bridges in male germ cells. Dev Biol *201*, 113-123.
Mori, Y., Imaizumi, K., Katayama, T., Yoneda, T., and Tohyama, M. (2000). Two cis-acting elements in the 3' untranslated region of alpha-CaMKII regulate its dendritic targeting. Nat Neurosci *3*, 1079-1084.
Muddashetty, R.S., Nalavadi, V.C., Gross, C., Yao, X., Xing, L., Laur, O., Warren, S.T., and Bassell, G.J. (2011). Reversible inhibition of PSD-95 mRNA translation by miR-125a, FMRP phosphorylation, and mGluR signaling. Mol Cell *42*, 673-688.

Muramatsu, T., Ohmae, A., and Anzai, K. (1998). BC1 RNA protein particles in mouse brain contain two y-,h-element-binding proteins, translin and a 37 kDa protein. Biochem Biophys Res Commun *247*, 7-11.
Muslimov, I.A., Iacoangeli, A., Brosius, J., and Tiedge, H. (2006). Spatial codes in dendritic BC1 RNA. J Cell Biol *175*, 427-439.
Nan, X., Ng, H.H., Johnson, C.A., Laherty, C.D., Turner, B.M., Eisenman, R.N., and Bird, A. (1998). Transcriptional repression by the methyl-CpG-binding protein MeCP2 involves a histone deacetylase complex. Nature *393*, 386-389.
Nan, X., Tate, P., Li, E., and Bird, A. (1996). DNA methylation specifies chromosomal localization of MeCP2. Mol Cell Biol *16*, 414-421.
Nikitina, T., Ghosh, R.P., Horowitz-Scherer, R.A., Hansen, J.C., Grigoryev, S.A., and Woodcock, C.L. (2007). MeCP2-chromatin interactions include the formation of chromatosome-like structures and are altered in mutations causing Rett syndrome. J Biol Chem *282*, 28237-28245.
Oe, S., and Yoneda, Y. (2010). Cytoplasmic polyadenylation element-like sequences are involved in dendritic targeting of BDNF mRNA in hippocampal neurons. FEBS Lett *584*, 3424-3430.
Ogier, M., Wang, H., Hong, E., Wang, Q., Greenberg, M.E., and Katz, D.M. (2007). Brain-derived neurotrophic factor expression and respiratory function improve after ampakine treatment in a mouse model of Rett syndrome. J Neurosci *27*, 10912-10917.
Oh, J.Y., Kwon, A., Jo, A., Kim, H., Goo, Y.S., Lee, J.A., and Kim, H.K. (2013). Activity-dependent synaptic localization of processing bodies and their role in dendritic structural plasticity. J Cell Sci *126*, 2114-2123.
Pang, P.T., and Lu, B. (2004). Regulation of late-phase LTP and long-term memory in normal and aging hippocampus: role of secreted proteins tPA and BDNF. Ageing Res Rev *3*, 407-430.
Park, H.Y., Lim, H., Yoon, Y.J., Follenzi, A., Nwokafor, C., Lopez-Jones, M., Meng, X., and Singer, R.H. (2014). Visualization of dynamics of single endogenous mRNA labeled in live mouse. Science *343*, 422-424.
Perycz, M., Urbanska, A.S., Krawczyk, P.S., Parobczak, K., and Jaworski, J. (2011). Zipcode binding protein 1 regulates the development of dendritic arbors in hippocampal neurons. J Neurosci *31*, 5271-5285.
Phillips, M., and Pozzo-Miller, L. (2015). Dendritic spine dysgenesis in autism related disorders. Neurosci Lett *601*, 30-40.
Plath, N., Ohana, O., Dammermann, B., Errington, M.L., Schmitz, D., Gross, C., Mao, X., Engelsberg, A., Mahlke, C., Welzl, H., *et al.* (2006). Arc/Arg3.1 is essential for the consolidation of synaptic plasticity and memories. Neuron *52*, 437-444.
Pozzo-Miller, L., Pati, S., and Percy, A.K. (2015). Rett Syndrome: Reaching for Clinical Trials. Neurotherapeutics *12*, 631-640.
Ramaswami, M., Taylor, J.P., and Parker, R. (2013). Altered ribostasis: RNA-protein granules in degenerative disorders. Cell *154*, 727-736.
Ratti, A., Fallini, C., Cova, L., Fantozzi, R., Calzarossa, C., Zennaro, E., Pascale, A., Quattrone, A., and Silani, V. (2006). A role for the ELAV RNA-binding proteins in neural stem cells: stabilization of Msi1 mRNA. J Cell Sci *119*, 1442-1452.
Reiss, A.L., Faruque, F., Naidu, S., Abrams, M., Beaty, T., Bryan, R.N., and Moser, H. (1993). Neuroanatomy of Rett syndrome: a volumetric imaging study. Ann Neurol *34*, 227-234.
Ricciardi, S., Boggio, E.M., Grosso, S., Lonetti, G., Forlani, G., Stefanelli, G., Calcagno, E., Morello, N., Landsberger, N., Biffo, S., *et al.* (2011). Reduced AKT/mTOR signaling and protein synthesis dysregulation in a Rett syndrome animal model. Hum Mol Genet *20*, 1182-1196.

Richter, J.D., and Sonenberg, N. (2005). Regulation of cap-dependent translation by eIF4E inhibitory proteins. Nature *433*, 477-480.
Righi, M., Tongiorgi, E., and Cattaneo, A. (2000). Brain-derived neurotrophic factor (BDNF) induces dendritic targeting of BDNF and tyrosine kinase B mRNAs in hippocampal neurons through a phosphatidylinositol-3 kinase-dependent pathway. J Neurosci *20*, 3165-3174.
Riikonen, R. (2003). Neurotrophic factors in the pathogenesis of Rett syndrome. J Child Neurol *18*, 693-697.
Rogoz, Z., Skuza, G., and Legutko, B. (2005). Repeated treatment with mirtazepine induces brain-derived neurotrophic factor gene expression in rats. J Physiol Pharmacol *56*, 661-671.
Rook, M.S., Lu, M., and Kosik, K.S. (2000). CaMKIIalpha 3' untranslated region-directed mRNA translocation in living neurons: visualization by GFP linkage. J Neurosci *20*, 6385-6393.
Ross, A.F., Oleynikov, Y., Kislauskis, E.H., Taneja, K.L., and Singer, R.H. (1997). Characterization of a beta-actin mRNA zipcode-binding protein. Mol Cell Biol *17*, 2158-2165.
Roux, J.C., Dura, E., Moncla, A., Mancini, J., and Villard, L. (2007). Treatment with desipramine improves breathing and survival in a mouse model for Rett syndrome. Eur J Neurosci *25*, 1915-1922.
Rozhdestvensky, T.S., Kopylov, A.M., Brosius, J., and Huttenhofer, A. (2001). Neuronal BC1 RNA structure: evolutionary conversion of a tRNA(Ala) domain into an extended stem-loop structure. RNA *7*, 722-730.
Sama, R.R., Ward, C.L., and Bosco, D.A. (2014). Functions of FUS/TLS from DNA repair to stress response: implications for ALS. ASN Neuro *6*.
Santi, S., Cappello, S., Riccio, M., Bergami, M., Aicardi, G., Schenk, U., Matteoli, M., and Canossa, M. (2006). Hippocampal neurons recycle BDNF for activity-dependent secretion and LTP maintenance. EMBO J *25*, 4372-4380.
Santos, M., Summavielle, T., Teixeira-Castro, A., Silva-Fernandes, A., Duarte-Silva, S., Marques, F., Martins, L., Dierssen, M., Oliveira, P., Sousa, N., *et al.* (2010). Monoamine deficits in the brain of methyl-CpG binding protein 2 null mice suggest the involvement of the cerebral cortex in early stages of Rett syndrome. Neuroscience *170*, 453-467.
Schaeffer, C., Bardoni, B., Mandel, J.L., Ehresmann, B., Ehresmann, C., and Moine, H. (2001). The fragile X mental retardation protein binds specifically to its mRNA via a purine quartet motif. EMBO J *20*, 4803-4813.
Schmid, D.A., Yang, T., Ogier, M., Adams, I., Mirakhur, Y., Wang, Q., Massa, S.M., Longo, F.M., and Katz, D.M. (2012). A TrkB small molecule partial agonist rescues TrkB phosphorylation deficits and improves respiratory function in a mouse model of Rett syndrome. J Neurosci *32*, 1803-1810.
Severt, W.L., Biber, T.U., Wu, X., Hecht, N.B., DeLorenzo, R.J., and Jakoi, E.R. (1999). The suppression of testis-brain RNA binding protein and kinesin heavy chain disrupts mRNA sorting in dendrites. J Cell Sci *112 (Pt 21)*, 3691-3702.
Shahbazian, M.D., Antalffy, B., Armstrong, D.L., and Zoghbi, H.Y. (2002). Insight into Rett syndrome: MeCP2 levels display tissue- and cell-specific differences and correlate with neuronal maturation. Hum Mol Genet *11*, 115-124.
Siepel, A., Bejerano, G., Pedersen, J.S., Hinrichs, A.S., Hou, M., Rosenbloom, K., Clawson, H., Spieth, J., Hillier, L.W., Richards, S., *et al.* (2005). Evolutionarily conserved elements in vertebrate, insect, worm, and yeast genomes. Genome Res *15*, 1034-1050.
Sirianni, N., Naidu, S., Pereira, J., Pillotto, R.F., and Hoffman, E.P. (1998). Rett syndrome: confirmation of X-linked dominant inheritance, and localization of the gene to Xq28. Am J Hum Genet *63*, 1552-1558.
Sossin, W.S., and DesGroseillers, L. (2006). Intracellular trafficking of RNA in neurons. Traffic *7*, 1581-1589.

Souquere, S., Mollet, S., Kress, M., Dautry, F., Pierron, G., and Weil, D. (2009). Unravelling the ultrastructure of stress granules and associated P-bodies in human cells. J Cell Sci *122*, 3619-3626.
Spacek, J. (1985). Three-dimensional analysis of dendritic spines. II. Spine apparatus and other cytoplasmic components. Anat Embryol (Berl) *171*, 235-243.
St Johnston, D., Beuchle, D., and Nusslein-Volhard, C. (1991). Staufen, a gene required to localize maternal RNAs in the Drosophila egg. Cell *66*, 51-63.
Stalder, L., and Muhlemann, O. (2009). Processing bodies are not required for mammalian nonsense-mediated mRNA decay. RNA *15*, 1265-1273.
Steward, O., and Falk, P.M. (1986). Protein-synthetic machinery at postsynaptic sites during synaptogenesis: a quantitative study of the association between polyribosomes and developing synapses. J Neurosci *6*, 412-423.
Steward, O., Falk, P.M., and Torre, E.R. (1996). Ultrastructural basis for gene expression at the synapse: synapse-associated polyribosome complexes. J Neurocytol *25*, 717-734.
Steward, O., and Levy, W.B. (1982). Preferential localization of polyribosomes under the base of dendritic spines in granule cells of the dentate gyrus. J Neurosci *2*, 284-291.
Steward, O., and Schuman, E.M. (2001). Protein synthesis at synaptic sites on dendrites. Annu Rev Neurosci *24*, 299-325.
Subramaniam, B., Naidu, S., and Reiss, A.L. (1997). Neuroanatomy in Rett syndrome: cerebral cortex and posterior fossa. Neurology *48*, 399-407.
Sugimoto, Y., Vigilante, A., Darbo, E., Zirra, A., Militti, C., D'Ambrogio, A., Luscombe, N.M., and Ule, J. (2015). hiCLIP reveals the in vivo atlas of mRNA secondary structures recognized by Staufen 1. Nature *519*, 491-494.
Sun, B.F., Wang, Q.Q., Yu, Z.J., Yu, Y., Xiao, C.L., Kang, C.S., Ge, G., Linghu, Y., Zhu, J.D., Li, Y.M., *et al.* (2015). Exercise Prevents Memory Impairment Induced by Arsenic Exposure in Mice: Implication of Hippocampal BDNF and CREB. PLoS One *10*, e0137810.
Sweet, T.J., Boyer, B., Hu, W., Baker, K.E., and Coller, J. (2007). Microtubule disruption stimulates P-body formation. RNA *13*, 493-502.
Takahara, T., and Maeda, T. (2012). Transient sequestration of TORC1 into stress granules during heat stress. Mol Cell *47*, 242-252.
Taylor, A.M., Berchtold, N.C., Perreau, V.M., Tu, C.H., Li Jeon, N., and Cotman, C.W. (2009). Axonal mRNA in uninjured and regenerating cortical mammalian axons. J Neurosci *29*, 4697-4707.
Teixeira, D., Sheth, U., Valencia-Sanchez, M.A., Brengues, M., and Parker, R. (2005). Processing bodies require RNA for assembly and contain nontranslating mRNAs. RNA *11*, 371-382.
Thomas, M.G., Loschi, M., Desbats, M.A., and Boccaccio, G.L. (2011). RNA granules: the good, the bad and the ugly. Cell Signal *23*, 324-334.
Thomas, M.G., Martinez Tosar, L.J., Desbats, M.A., Leishman, C.C., and Boccaccio, G.L. (2009). Mammalian Staufen 1 is recruited to stress granules and impairs their assembly. J Cell Sci *122*, 563-573.
Thomas, M.G., Martinez Tosar, L.J., Loschi, M., Pasquini, J.M., Correale, J., Kindler, S., and Boccaccio, G.L. (2005). Staufen recruitment into stress granules does not affect early mRNA transport in oligodendrocytes. Mol Biol Cell *16*, 405-420.
Tiedge, H., and Brosius, J. (1996). Translational machinery in dendrites of hippocampal neurons in culture. J Neurosci *16*, 7171-7181.
Tiruchinapalli, D.M., Oleynikov, Y., Kelic, S., Shenoy, S.M., Hartley, A., Stanton, P.K., Singer, R.H., and Bassell, G.J. (2003). Activity-dependent trafficking and dynamic localization of zipcode binding protein 1 and beta-actin mRNA in dendrites and spines of hippocampal neurons. J Neurosci *23*, 3251-3261.

Tongiorgi, E. (2008). Activity-dependent expression of brain-derived neurotrophic factor in dendrites: facts and open questions. Neurosci Res *61*, 335-346.
Tongiorgi, E., Armellin, M., Giulianini, P.G., Bregola, G., Zucchini, S., Paradiso, B., Steward, O., Cattaneo, A., and Simonato, M. (2004). Brain-derived neurotrophic factor mRNA and protein are targeted to discrete dendritic laminas by events that trigger epileptogenesis. J Neurosci *24*, 6842-6852.
Tongiorgi, E., Righi, M., and Cattaneo, A. (1997). Activity-dependent dendritic targeting of BDNF and TrkB mRNAs in hippocampal neurons. J Neurosci *17*, 9492-9505.
Torre, E.R., and Steward, O. (1996). Protein synthesis within dendrites: glycosylation of newly synthesized proteins in dendrites of hippocampal neurons in culture. J Neurosci *16*, 5967-5978.
Tourriere, H., Chebli, K., Zekri, L., Courselaud, B., Blanchard, J.M., Bertrand, E., and Tazi, J. (2003). The RasGAP-associated endoribonuclease G3BP assembles stress granules. J Cell Biol *160*, 823-831.
Tropea, D., Giacometti, E., Wilson, N.R., Beard, C., McCurry, C., Fu, D.D., Flannery, R., Jaenisch, R., and Sur, M. (2009). Partial reversal of Rett Syndrome-like symptoms in MeCP2 mutant mice. Proc Natl Acad Sci U S A *106*, 2029-2034.
Tubing, F., Vendra, G., Mikl, M., Macchi, P., Thomas, S., and Kiebler, M.A. (2010). Dendritically localized transcripts are sorted into distinct ribonucleoprotein particles that display fast directional motility along dendrites of hippocampal neurons. J Neurosci *30*, 4160-4170.
Tudor, M., Akbarian, S., Chen, R.Z., and Jaenisch, R. (2002). Transcriptional profiling of a mouse model for Rett syndrome reveals subtle transcriptional changes in the brain. Proc Natl Acad Sci U S A *99*, 15536-15541.
Tyler, W.J., and Pozzo-Miller, L. (2003). Miniature synaptic transmission and BDNF modulate dendritic spine growth and form in rat CA1 neurones. J Physiol *553*, 497-509.
Vaghi, V., Polacchini, A., Baj, G., Pinheiro, V.L., Vicario, A., and Tongiorgi, E. (2014). Pharmacological profile of brain-derived neurotrophic factor (BDNF) splice variant translation using a novel drug screening assay: a "quantitative code". J Biol Chem *289*, 27702-27713.
Vanevski, F., and Xu, B. (2015). HuD interacts with Bdnf mRNA and is essential for activity-induced BDNF synthesis in dendrites. PLoS One *10*, e0117264.
Vessey, J.P., Macchi, P., Stein, J.M., Mikl, M., Hawker, K.N., Vogelsang, P., Wieczorek, K., Vendra, G., Riefler, J., Tubing, F., *et al.* (2008). A loss of function allele for murine Staufen1 leads to impairment of dendritic Staufen1-RNP delivery and dendritic spine morphogenesis. Proc Natl Acad Sci U S A *105*, 16374-16379.
Vicario, A., Colliva, A., Ratti, A., Davidovic, L., Baj, G., Gricman, L., Colombrita, C., Pallavicini, A., Jones, K.R., Bardoni, B., *et al.* (2015). Dendritic targeting of short and long 3' UTR BDNF mRNA is regulated by BDNF or NT-3 and distinct sets of RNA-binding proteins. Front Mol Neurosci *8*, 62.
Wang, H., Chan, S.A., Ogier, M., Hellard, D., Wang, Q., Smith, C., and Katz, D.M. (2006). Dysregulation of brain-derived neurotrophic factor expression and neurosecretory function in Mecp2 null mice. J Neurosci *26*, 10911-10915.
Waung, M.W., Pfeiffer, B.E., Nosyreva, E.D., Ronesi, J.A., and Huber, K.M. (2008). Rapid translation of Arc/Arg3.1 selectively mediates mGluR-dependent LTD through persistent increases in AMPAR endocytosis rate. Neuron *59*, 84-97.
Wickens, M., Bernstein, D.S., Kimble, J., and Parker, R. (2002). A PUF family portrait: 3'UTR regulation as a way of life. Trends Genet *18*, 150-157.
Will, T.J., Tushev, G., Kochen, L., Nassim-Assir, B., Cajigas, I.J., Tom Dieck, S., and Schuman, E.M. (2013). Deep sequencing and high-resolution imaging reveal compartment-specific localization of Bdnf mRNA in hippocampal neurons. Sci Signal *6*, rs16.

Williamson, S.L., and Christodoulou, J. (2006). Rett syndrome: new clinical and molecular insights. Eur J Hum Genet *14*, 896-903.
Wolozin, B. (2012). Regulated protein aggregation: stress granules and neurodegeneration. Mol Neurodegener *7*, 56.
Wu, H., Tao, J., Chen, P.J., Shahab, A., Ge, W., Hart, R.P., Ruan, X., Ruan, Y., and Sun, Y.E. (2010). Genome-wide analysis reveals methyl-CpG-binding protein 2-dependent regulation of microRNAs in a mouse model of Rett syndrome. Proc Natl Acad Sci U S A *107*, 18161-18166.
Wu, X.Q., Lefrancois, S., Morales, C.R., and Hecht, N.B. (1999). Protein-protein interactions between the testis brain RNA-binding protein and the transitional endoplasmic reticulum ATPase, a cytoskeletal gamma actin and Trax in male germ cells and the brain. Biochemistry *38*, 11261-11270.
Xing, L., and Bassell, G.J. (2013). mRNA localization: an orchestration of assembly, traffic and synthesis. Traffic *14*, 2-14.
Yisraeli, J.K., and Melton, D.A. (1988). The material mRNA Vg1 is correctly localized following injection into Xenopus oocytes. Nature *336*, 592-595.
Yoshii, A., and Constantine-Paton, M. (2010). Postsynaptic BDNF-TrkB signaling in synapse maturation, plasticity, and disease. Dev Neurobiol *70*, 304-322.
Young, J.I., Hong, E.P., Castle, J.C., Crespo-Barreto, J., Bowman, A.B., Rose, M.F., Kang, D., Richman, R., Johnson, J.M., Berget, S., *et al.* (2005). Regulation of RNA splicing by the methylation-dependent transcriptional repressor methyl-CpG binding protein 2. Proc Natl Acad Sci U S A *102*, 17551-17558.
Zachariah, R.M., and Rastegar, M. (2012). Linking epigenetics to human disease and Rett syndrome: the emerging novel and challenging concepts in MeCP2 research. Neural Plast *2012*, 415825.
Zalfa, F., Achsel, T., and Bagni, C. (2006). mRNPs, polysomes or granules: FMRP in neuronal protein synthesis. Curr Opin Neurobiol *16*, 265-269.
Zeitelhofer, M., Karra, D., Macchi, P., Tolino, M., Thomas, S., Schwarz, M., Kiebler, M., and Dahm, R. (2008). Dynamic interaction between P-bodies and transport ribonucleoprotein particles in dendrites of mature hippocampal neurons. J Neurosci *28*, 7555-7562.
Zhang, H.L., Eom, T., Oleynikov, Y., Shenoy, S.M., Liebelt, D.A., Dictenberg, J.B., Singer, R.H., and Bassell, G.J. (2001). Neurotrophin-induced transport of a beta-actin mRNP complex increases beta-actin levels and stimulates growth cone motility. Neuron *31*, 261-275.
Zhou, Z., Hong, E.J., Cohen, S., Zhao, W.N., Ho, H.Y., Schmidt, L., Chen, W.G., Lin, Y., Savner, E., Griffith, E.C., *et al.* (2006). Brain-specific phosphorylation of MeCP2 regulates activity-dependent Bdnf transcription, dendritic growth, and spine maturation. Neuron *52*, 255-269.
Zivraj, K.H., Tung, Y.C., Piper, M., Gumy, L., Fawcett, J.W., Yeo, G.S., and Holt, C.E. (2010). Subcellular profiling reveals distinct and developmentally regulated repertoire of growth cone mRNAs. J Neurosci *30*, 15464-15478.
Zoghbi, H. (1988). Genetic aspects of Rett syndrome. J Child Neurol *3 Suppl*, S76-78.